ELECTRON PARAMAGNETIC RESONANCE MEASUREMENTS ON THE BACTERIAL GLUTAMATE TRANSPORTER HOMOLOG GLT_{Ph} IN DISTINCT STATES

By

Paul J. Focke

A THESIS DISSERTATION

Presented to the Department of Neuroscience and the
Oregon Health & Science University
School of Medicine
in fulfillment of the requirements for
the degree of

Doctor of Philosophy

December, 2009

School of Medicine
Oregon Health & Science University

CERTIFICATE OF APPROVAL

This is to certify that the Ph.D. dissertation of
PAUL JOSEPH FOCKE
has been approved

Advisor: Hans Peter Larsson, Ph.D.

Member: Eric Gouaux, Ph.D.

Member: John Adelman, Ph.D.

Member: Craig Jahr, Ph.D.

Member: David Farrens, Ph.D.

Member: Pierre Moenne-Loccoz, Ph.D.

Table of Contents

List of Illustrations

III. Results

IV. Summary and Conclusions

ACKNOWLEDGEMENTS

I would like to first thank Dr. Hans Peter Larsson for being an extremely good mentor during my years as a graduate student. I am confident that had I not joined his lab my experience would have been nowhere near as positive as it was. I'd also like to thank the other members of my committee for providing a good environment in which to discuss my project. They ultimately helped me down a path to success in my research career as a graduate student and I could not have done it without them. Specifically, Dr. Eric Gouaux, Dr. Craig Jahr, Dr. John Adelman, Dr. David Farrens, and Dr. Pierre Moenne-Loccoz.

I would also like to thank the sources of funding that made my research possible, specifically the OHSU Tarter Trust for providing me with two separate grants while in grad school, and the NIH/NINDS for awarding me a predoctoral NRSA.

Finally, thanks to all my family and friends who has made life in Portland a wonderful experience!

ABSTRACT

The remarkable ability to maintain low levels of glutamate in the extracellular space following signaling events is achieved mainly by excitatory amino acid transporters (EAATs) located in the plasma membranes of both glial cells and neurons. Abnormal glutamate transporter function is implicated in Parkinson's disease, Alzheimer's disease, cerebral ischemia, epilepsy, and amyotrophic lateral sclerosis, underscoring the importance of understanding how these transporters function. Our research is centered on elucidating the structural and functional properties of glutamate transporters to reveal novel (i.e. small-molecule) approaches for treating these neuropathological conditions. To this end, we have developed a technique of using double site-directed spin labeling (DSDSL) electron paramagnetic spectroscopy (EPR) on a bacterial glutamate transporter homolog from *Pyrococcus horikoshii*, Glt_{Ph}. Briefly, this technique provides the ability to make distance measurements in the ~8-25 Å range between two spin labels, based on the extent of the dipolar interactions between them. This thus allows us to monitor conformational changes in Glt_{Ph} in response to events such as ion, substrate, and inhibitor-binding. In our current work, we have utilized this technique specifically to examine regions of the Glt_{Ph} transporter proposed to contribute to the extracellular gating mechanism. Our research validates the conclusions from previous electrophysiological studies and crystal structures, as well as provides new insight into previously undescribed conformational changes in the extracellular gate of GltPh that occur in response to the binding of ions to the apo-state of the transporter.

I. Chapter 1

Introduction

1. Overview

The human brain consists of a network of over 100 billion individual nerve cells, connected into a highly orchestrated bioelectrical signaling system of which emerges our ability to perceive and interact with the external world. The task of neural science is to understand how simple electrical signals generated by neurons are translated into everything from thoughts and emotions to movements and instincts. To study something this complex, first the fundamental aspects of communication between neurons must be established. To this end, much progress has been made. We now understand in great detail the mechanisms whereby the stimulated release of neurotransmitter from one cell and subsequent detection and interpretation of that signal by other cells coordinates the electrical communication between neurons, and thereby networks of neurons.

Excitatory neurotransmission is a form of neuronal signaling in which the release of neurotransmitter by a presynaptic cell and subsequent detection by postsynaptic cells results in a high probability of postsynaptic action potential generation and electrical signal propagation. The principle mediator of excitatory neurotransmission is the amino acid neurotransmitter $_{L}$-glutamate, and synapses in which $_{L}$-glutamate acts as the primary neurotransmitter are known as glutamatergic synapses (Mayer and Westbrook, 1987). These synapses are essential for normal development, are critical for learning and memory, and

importantly, the dysfunction of these synapses is implicated in a wide range of nervous system diseases (Hinoi et al., 2005).

At normal glutamatergic synapses, $_{L}$-glutamate is released into the synaptic cleft and binds to postsynaptic glutamate receptors consisting of ionotropic (ion channel coupled) and metabotropic (second messenger coupled) subtypes (Dingledine et al., 1999) (Fig. 1). To ensure a postsynaptic cell will respond properly to a given stimulus, high concentrations of $_{L}$-glutamate are released into the synapse, as it is the $_{L}$-glutamate concentration in the extracellular fluid that determines the extent of receptor stimulation. There is a fine balance to this method of receptor stimulation, however, as it is well documented that excessive activation of glutamate receptors is harmful, with prolonged glutamate receptor stimulation resulting in cell death through a process termed excitotoxicity (Olney and Sharpe, 1969).

Not only is excessive glutamate receptor stimulation toxic, but in addition prolonged high glutamate concentrations would considerably distort the synaptic signal to noise ratio in response to subsequent incoming neural activity. For these two reasons, it is imperative that excess glutamate in the synapse is rapidly cleared after a signaling event. To put this in perspective, recent work has shown that immediately after neurotransmitter release into the synaptic cleft, the concentration of glutamate rises about 10^5-fold from resting concentrations to reach millimolar concentrations (Wadiche and Jahr, 2001), while the resting or basal concentration of glutamate is held to approximately 25 nM (Herman and Jahr, 2007).

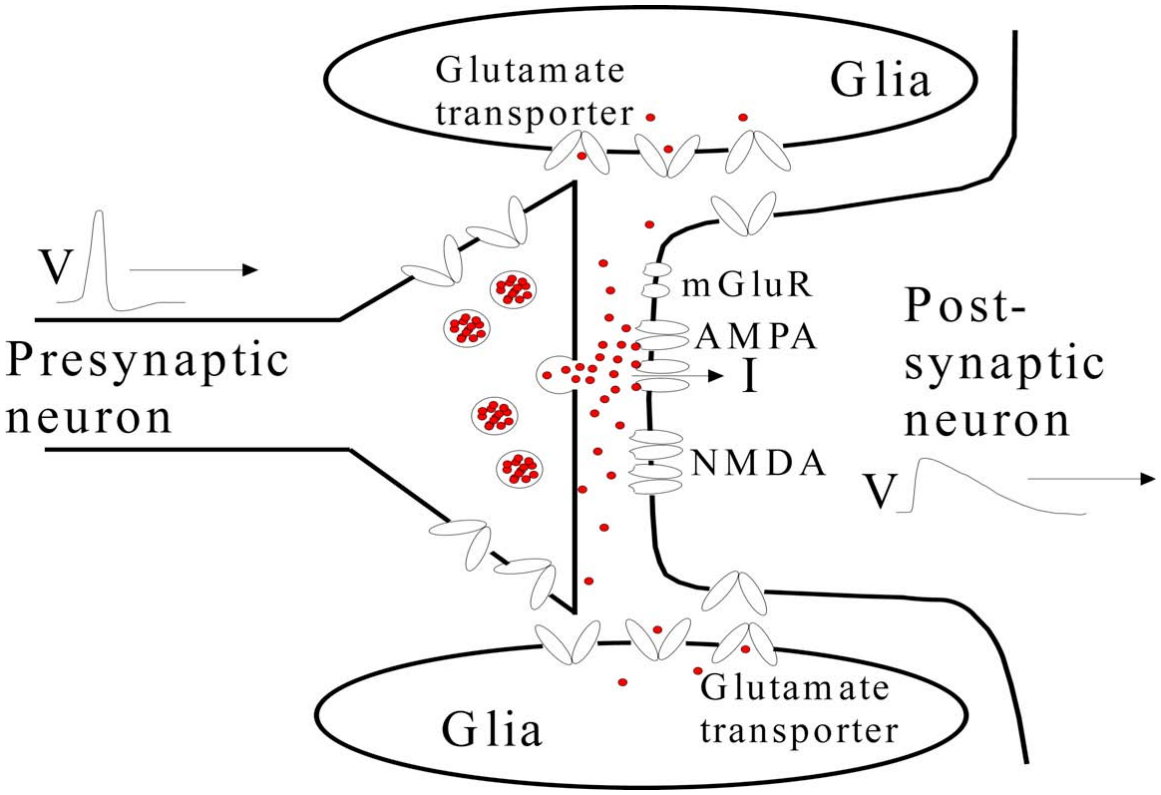

Figure 1. Overview of the glutamatergic system. Glutamate is concentrated into vesicles in synaptic terminals of glutamatergic neurons, where it is released at a high concentration into the synaptic cleft following presynaptic depolarization. Glutamate released into the synaptic cleft activates both ionotropic (AMPA, NMDA, and kainate) and metabotropic (mGluR) glutamate receptors, leading to electrical responses in the postsynaptic cell. Glutamate transporters situated near the synaptic cleft function to remove excess glutamate, thereby preventing excitotoxicity, as well as readying the synapse for subsequent neural activity (Danbolt, 2001).

The remarkable ability to maintain low levels of glutamate in the extracellular space following signaling events is achieved mainly by sophisticated proteins known as excitatory amino acid transporters (EAATs), located in the plasma membranes of both glial cells and neurons (Danbolt, 2001) (Fig. 1). By utilizing the free energy stored in ion gradients across cell membranes, these transporters are able to maintain a 10,000-fold gradient of intracellular glutamate to extracellular glutamate that is necessary for proper glutamatergic signaling.

How EAATs structurally accomplish the task of maintaining low extracellular glutamate concentrations, is a current research topic of high interest. Given the enormous importance of glutamatergic signaling in the development, maintenance, and function of the adult brain, and the central role that the EAATs play in glutamatergic signaling, it is of great importance to understand the structural biophysical mechanisms by which EAATs operate. Because many neurodegenerative diseases such as Parkinson's, Alzheimer's, cerebral ischemia, epilepsy, and amyotrophic lateral sclerosis (ALS) are linked to abnormal glutamate homeostasis, this is a very active area of research. Previous efforts to treat these diseases focused on glutamate receptors, rather than glutamate transporter proteins, and have yielded little success (Hinoi et al., 2005). This suggests the need for alternative approaches to treat the large number of neuropathological conditions associated with abnormal glutamate homeostasis. Novel small molecule approaches for treating these various diseases are likely to emerge from scientific study surrounding the biophysical properties of glutamate transporters. Indeed, this is certainly a credible

alternative based on the broad spectrum of drugs that target various neurotransmitter transporter proteins, including drugs used to treat depression, anxiety, obesity, and epilepsy. Therefore, research into the structural mechanisms of glutamate transport will likely provide insight toward the development of novel compounds with clinical applications for the treatment of neurodegenerative disorders. This introduction will focus on the physiological, pharmacological, and structural aspects of glutamate transporters, and set the stage for our current work on these transporters described in later chapters.

2. The SLC 1 family: Physiological aspects

2.1. Overview

Termination of all synaptic neurotransmitter signaling is determined in part by solute transporters of two families. Transporters for the excitatory amino acids glutamate/aspartate (excitatory amino acid transporters, or EAATs), as well as the neutral amino acids (alanine, serine, cysteine, threonine, or ASCT transporters) are members of the SLC1 family (solute carrier 1 family). Transporters for the inhibitory transmitters glycine and γ-amino butyric acid (GABA), along with the biogenic amines (serotonin, noradrenalin, dopamine) are classified into the SLC6 family (solute carrier family 6), also known as neurotransmitter sodium symporters (NSS) (Kanai and Hediger, 2004). Interestingly, members of both families also have intrinsic channel-like properties that are activated by their substrates, and which in some cases may play a

physiological role (Picaud et al., 1995a). As our research is focused on elucidating the biomechanical properties of glutamate transporter proteins (members of the SLC1 family), this introduction centers on the SLC1 family of glutamate transporter proteins and their prokaryotic orthologues. Nonetheless, it is important to note that by comparing and contrasting the structural and functional mechanisms by which both transporter families operate, much can be learned in terms of each family's role in synaptic physiology.

2.2. Cloning of the SLC1 family

Molecular identification of the SLC1 family began in 1992. At this time, three distinct isoforms of glutamate transporters (EAAC1, GLT1, and GLAST) were identified by independent groups all using separate approaches. Cloning of the Na^+-dependent but Cl^--independent glutamate transporter EAAC1 (excitatory amino acid carrier 1) (Kanai and Hediger, 1992), was accomplished by the technique of expression cloning in *Xenopus* oocytes, using poly-A tail-isolated RNA obtained from mucosal tissue of rabbit small intestine. In addition, using high stringency northern blotting, PCR, and *in situ* hybridization, the authors revealed EAAC1 to be in both epithelial tissues as well as neuronal tissues, with EAAC1 transcripts in the brain localized to areas of known glutamatergic synapses. Substrate specificity of the EAAC1 protein was established by injecting cDNA-translated RNA into *Xenopus* oocytes and performing radiolabeled uptake assays. EAAC1 Na^+-dependent transport activity was

shown to be specific for $_{L}$-glutamate, $_{L}$-aspartate, and $_{D}$-aspartate, with less specificity for $_{D}$-glutamate.

A second group led by Kanner (Danbolt et al., 1992) first generated polyclonal antibodies against a highly purified preparation of the Na^+/K^+ coupled $_{L}$-glutamate transporter from rat brain. These antibodies were shown to recognize the $_{L}$-glutamate transporter in extracts of brain plasma membranes from rabbit, pig, cow, cat, and human. Electron microscopic analysis of immunocytochemical localization of the transporter in rat brain revealed the transporter to be located in glial cells rather than in neurons, with fine astrocytic processes in particular being strongly stained and glutamatergic nerve terminals non-immunoreactive (Danbolt et al., 1992). In a subsequent paper, the authors utilized these same antibodies to isolate a cDNA clone from rat brain, which they termed GLT-1 (Pines et al., 1992). Expression of the GLT-1 clone in HeLa cells revealed radiolabeled glutamate uptake was dependent on external Na^+ and internal K^+, and northern blot analysis demonstrated this transcript to be located only in neuronal tissue, consistent with their previous immunocytochemical findings (Danbolt et al., 1992) indicating that the protein was specific for glial cells.

A third study by Stoffel and colleagues (Storck et al., 1992) identified the glutamate transporter they termed GLAST ($_{L}$-glu/$_{L}$-asp transporter). In this study, during the isolation of the UDPgalactose:ceramide galactosyltransferase from rat brain, the authors copurified a hydrophobic glycoprotein with a molecular mass of 66 kDa. This protein was subjected to limited proteolysis, and the amino acid sequences of the resulting peptides were determined by Edman degradation

(Edman, 1949). A degenerate oligonucleotide probe corresponding to one of the peptide sequences was synthesized and used to screen a rat brain cDNA library. Subsequently, a 3kb clone was isolated and sequenced, and a sequence homology data search revealed sequence similarity of the clone to known bacterial glutamate transporters. This led the authors to examine the functionality of GLAST by expression in *Xenopus* oocytes, revealing the strict Na^+-dependence of radiolabeled $_L$-glutamate and $_L$-aspartate uptake, and northern blot and *in situ* hybridization analysis showed GLAST to be specific for neuronal tissue.

Subsequent to the cloning of EAAC1, GLT-1, and GLAST, Amara and colleagues in 1994 (Arriza et al., 1994) reported the cloning of three human excitatory amino acid transporters EAAT1, EAAT2, and EAAT3. To accomplish this, Amara's group utilized a degenerate oligonucleotide probe corresponding to the conserved sequence AA(I/V)FIAQ found in the previously cloned mammalian transporters to probe human motor cortex cDNA libraries. On the basis of nucleic acid and amino acid sequence homology, EAAT1, EAAT2, and EAAT3 corresponded to the glutamate transporters previously isolated from other species. EAAT1 was shown to have 96% amino acid sequence identity with rat GLAST1 (Storck et al., 1992). EAAT2 shared 95% identity with the sequence of rat GLT1 (Pines et al., 1992), and EAAT3 shared 92% identity with the rabbit sequence EAAC1 (Kanai and Hediger, 1992).

Finally, two additional glutamate transporters (EAAT4 and EAAT5) as well as two Na^+-dependent neutral amino acid transporters (ASCT1 and ASCT2) were also

identified based on sequence homology to the already sequenced glutamate transporters (Kanai and Hediger, 2004). For clarity, throughout the rest of this thesis I will use only the EAAT (1-5) nomenclature to define different transporter subtypes with EAAT1 corresponding to GLAST-1, EAAT2 corresponding to GLT1, and EAAT3 corresponding to EAAC-1.

2.3. Individual glutamate transporter isoforms: Expression and function

2.3.1. SLC1A1 (protein name; EAAT3)

The SLC1A1 gene locus encodes the glutamate transporter EAAT3. EAAT3 expression in brain is rather homogeneous, with particular expression in the hippocampus, basal ganglia, and olfactory bulb (Nieoullon et al., 2006). EAAT3 has also been shown to be significantly expressed in the kidney, intestine, heart, and placenta, but the role of EAAT3 in these peripheral organs is not clear at the present time (Danbolt, 2001).

In neurons, EAAT3 is localized to both the plasma membrane as well as the cytosolic compartment. Interestingly, EAAT3 appears to be mainly cytosolic (in contrast to glial transporters, see below), with only about 20% present at the plasma membrane (Conti et al., 1998; Kugler and Schmitt, 1999; Yang and Kilberg, 2002). As well as being cytosolic, EAAT3 is detected in neurons everywhere from axon terminals to somato-dendritic compartments (Coco et al., 1997; Guillet et al., 2005; He et al., 2000; Rothstein et al., 1994; Shashidharan et al., 1997). The diffuse cellular localization of EAAT3 therefore suggests a

function for EAAT3 other than simply the uptake of synaptically released glutamate.

Developmentally, EAAT3 is expressed first (as compared to EAAT1 and EAAT2), during early stages of fetal brain development (Furuta et al., 1997; Torp et al., 1994). Expression becomes stabilized or even slightly reduced in the adult (Sims and Robinson, 1999).

So what is the role of EAAT3, given its developmental and subcellular expression profiles? In the adult brain, for instance, the role of EAAT3 has to be considered in comparison to the glial transporters EAAT1 and EAAT2 (see below for more information on EAAT1 and EAAT2). In this light, actual transport activity of neuronal EAAT3 is likely much more important in areas of the brain such as the hippocampus and cerebral cortex, where the number of astrocytes surrounding nerve terminals is limited. Another role of EAAT3 may be to provide GABA-containing neurons with glutamate as an immediate precursor for GABA synthesis when EAAT3 is expressed in GABAergic neurons. In addition, because of the high affinity of EAAT3 for cysteine, yet another role for EAAT3 in the adult brain may be to contribute to the production of the major antioxidant agent, glutathione. In line with this idea, pharmacological inhibition of glutamate uptake (and thereby cysteine uptake) resulted in reduced neuronal glutathione synthesis in cultures of cortical neurons (Chen and Swanson, 2003; Himi et al., 2003). Because pharmacologically-induced block of glutathione biosynthesis can cause neurodegeneration (Jain et al., 1991; Schulz et al., 2000), alterations in neuronal cysteine uptake through EAAT3 could also contribute to neuronal death.

Developmentally, an interesting aspect of the early expression of EAAT3, as compared to EAAT1 and EAAT2, is the role of EAAT3 in the synthesis of GABA. During early developmental stages in both the hippocampus and cerebral cortex, rather than playing an inhibitory role, GABA instead plays an excitatory role. This is due to early expression of NKCC1, a Cl- transporter protein, which results in accumulation of Cl^- in neurons. Activation of GABA-A receptors therefore causes depolarization, due to net Cl^- efflux (Ben-Ari, 2002). In the hippocampus, for example, GABA-containing interneurons mature prior to excitatory glutamatergic pyramidal neurons and astrocytes, and therefore early activity dependent plasticity contributing to hippocampal neuronal network maturation is primarily due to the depolarizing action of GABA (Represa and Ben-Ari, 2005). During this time, the parallel expression of EAAT3 is thought to play a role in providing neurons with glutamate for the synthesis of GABA (Nieoullon et al., 2006).

Taken together, while the precise role of EAAT3 remains unclear, it is likely involved in the development and maturation of neuronal networks, and also to play a neuroprotective role, in addition to contributing to glutamate removal. Interestingly, in terms of a neuroprotective role, EAAT3 may be involved in the protection of dopaminergic neurons, known to be involved in the physiopathology of Parkinson's disease. These neurons are highly sensitive to oxidative stress, and preliminary data has shown that pharmacological inhibition of glutamate uptake preferentially induced the death of tyrosine hydroxylase-positive (dopaminergic) cells in culture, while the addition of N-acetylcysteine prevented dopaminergic cell death (Nieoullon et al., 2006). Overall, further experiments are

needed to fully understand the role of EAAT3 function in the developing and adult brain.

2.3.2. SLC1A2 (protein name; EAAT2)

The SLC1A2 gene encodes the glutamate transporter EAAT2. EAAT2 is the prominent glutamate transporter in the adult forebrain, with protein expression found primarily in astrocyte plasma membranes associated with excitatory synaptic contacts throughout the brain (Danbolt, 2001). Recent studies however have also shown EAAT2 protein in neurons in the mature hippocampus (Chen et al., 2004). The clear importance of EAAT2 was demonstrated by generation of homozygous EAAT2-deficient mice. While heterozygous mice showed no signs of defects compared to wild-type mice, homozygous EAAT2 mutants died prematurely, with a ~50% survival rate after six weeks. Premature death was found to be due to spontaneous epileptic seizures, similar in behavioral properties to NMDA-induced seizures (Rogawski et al., 1989). Electrophysiological analysis revealed that the peak concentration of synaptically-released glutamate was elevated, and remained elevated for longer periods, in mutant mice compared to wild-type mice. Finally, histological analysis confirmed selective neuronal degeneration in the hippocamal CA1 region of mutant mice. Together these results suggested a major role for EAAT2 in maintaining low levels of extracellular glutamate, and that in the absence of EAAT2, glutamate-induced excitotoxicity occurs.

The importance of EAAT2 has also been implicated in pathological conditions. Ischemic insult was shown to result in a decrease in EAAT2 mRNA levels (Torp et al., 1995). Similarly, traumatic brain injury was shown to result in a decrease in steady state levels of EAAT2 protein (Rao et al., 1998).

In addition, a substantial role for EAAT2 has been proposed in the selective loss of motor neurons observed in amyotrophic lateral sclerosis (ALS). In patients with ALS, less glutamate transport activity was found in the spinal cord, motor cortex, and somatosensory cortex as compared to patients with no evidence of neurological disease or a different form of neurologic disease (Rothstein et al., 1992). EAAT2 protein levels were specifically reduced in these same areas (Rothstein et al., 1995), but without a decrease in mRNA levels. This was suggested to be due to a more recent finding that aberrant splicing of the EAAT2 transcript can occur (Lin et al., 1998), and thus translation of the aberrantly spliced RNA is affected. However, loss of EAAT2 protein has also been suggested to possibly be due to the highly vulnerable nature of EAAT2 to oxidative stress (Pedersen et al., 1998; Trotti et al., 1999), which is known to occur in ALS via mutations in the gene for Cu/Zn superoxide dismutase (SOD1) (Brown, 1995; Robberecht et al., 1994; Rosen et al., 1994). In fact, the molecular target of the oxidative-vulnerability was shown to be located within the intracellular, carboxyl-terminal domain of EAAT2, which is rich in cysteines, tyrosines, tryptophans, and histidines. Replacement of this region with the carboxyl-terminal region of EAAT3, which is not enriched in residues susceptible to oxidation, completely inhibited oxidative sensitivity. Finally, a mutation

(N206S) has also been identified in the EAAT2 gene that is associated with sporadic ALS (Aoki et al., 1998), and this mutation results in reduced glutamate uptake activity and an increased reverse transport activity.

Overall, more information is needed to fully define the role of EAAT2 in normal and disease states, but clearly EAAT2 plays a large and important part in maintaining glutamate homeostasis in the adult CNS. In future experiments it will be important to determine whether the alterations in EAAT2 transporter expression actually are the root cause of disease or whether disease states subsequently affect expression and function of EAAT2.

2.3.3. SLC1A3 (protein name; EAAT1)

SLC1A3 encodes the glutamate transporter EAAT1. EAAT1 protein is expressed by astroglial cells throughout the CNS (Chaudhry et al., 1995; Lehre et al., 1995; Schmitt et al., 1997), and is the prominent glutamate transporter in the cerebellum (Lehre and Danbolt, 1998), inner ear (Furness and Lehre, 1997; Takumi et al., 1997), and retina (Rauen et al., 1998).

Consistent with EAAT1 being the prominent glutamate transporter in the above-mentioned regions, EAAT1-deficient mice were shown to have specific behavioral defects stemming from these regions. In terms of the cerebellum, EAAT1-deficient mice developed normally and could manage simple coordination tasks, however more challenging tasks such as staying on a quickly rotating rod were much more compromised compared to wild-type, consistent with a cerebellar defect (Watase et al., 1998). In addition, electrophysiological studies

revealed abnormal climbing fiber innervation of Purkinje cells in the adult, and EAAT1-deficient mice were shown to be more vulnerable to experimentally induced cerebellar injury (Watase et al., 1998).

In the retina, EAAT1 is expressed in Muller cells (Derouiche and Rauen, 1995; Rauen et al., 1996), in contrast to EAAT2, which is found in cones and bipolar cells (Rauen and Kanner, 1994; Rauen et al., 1996). In order to investigate the functional role of this difference in distribution, EAAT1 and EAAT2-deficient mice were analyzed (Harada et al., 1998) in terms of visual synaptic transmission as well as the effect of ischemia-induced retinal damage. The physiological function of EAAT1 and EAAT2 was analyzed for visual synaptic transmission integrity in vivo, by recording electroretinograms in mutant mice. EAAT1 was shown to be essential for proper neurotransmission of the light response from photoreceptors to bipolar cells, while EAAT2 was not required. In contrast, both EAAT1- and EAAT2-knockout mice were shown to be more sensitive to ischemia-induced retinal damage, but with the exacerbation of damage more prominent in EAAT1-knockout mice compared to EAAT2.

In terms of EAAT1 expression being dominant in the inner ear (Furness and Lehre, 1997; Takumi et al., 1997) it was hypothesized that noise-induced hearing loss may be caused, at least in part, by glutamate excitotoxicity (Hakuba et al., 2000). The reasoning behind this was that glutamate was proposed as the most likely candidate neurotransmitter for inner hair cell-auditory nerve synapes (Ottersen et al., 1998), and noise-induced dendrite damage is very similar to what is observed after cochlea exposure to glutamate receptor agonists (Puel,

1995; Puel et al., 1991). Using a microdialysis technique (Hakuba et al., 1997), the perilymph levels of cochlear glutamate in EAAT1 mutant mice were shown to be elevated basally, while also increasing significantly both during and after noise exposure, compared to WT mice. In addition, while noise exposure produced afferent nerve terminal swelling of inner hair cells in both WT and EAAT1-mutant mice, after two hours these changes returned to normal in WT mice, while swelling was still observed in mutant mice. Together these results confirmed the excitotoxic nature of noise-induced hearing loss.

2.3.4. SLC1A6 (protein name: EAAT4)

SLC1A6 encodes the glutamate transporter EAAT4. Cloning and functional analysis of this transporter revealed a prominent thermodynamically uncoupled chloride conductance activated by substrate (Fairman et al., 1995). EAAT4 is expressed prominently in cerebellar Purkinje cells (Dehnes et al., 1998; Massie et al., 2001; Yamada et al., 1996) where it is found at the highest level outside excitatory synapses on the dendritic spines (Dehnes et al., 1998; Tanaka et al., 1997b). Interestingly, the perisynaptic distribution of EAAT4 in Purkinje cells is very similar to the expression pattern of the metabotropic glutamate receptor 1 (mGluR1) (Baude et al., 1993; Dehnes et al., 1998; Tanaka et al., 1997a). This colocalization suggested that EAAT4 could limit the glutamate spillover in the periplasmic space, thereby regulating the activation of postsynaptic mGluR1. In line with this idea, pharmacological inhibition of neuronal glutamate transporters in Purkinje cells preferentially increases mGluR-EPSCs (excitatory post-synaptic

currents), and enhances long-term depression (LTD) (Brasnjo and Otis, 2004), and this effect was shown to be specific for EAAT4 using mice deficient for either EAAT4, EAAT3, or EAAT1 (Nikkuni et al., 2007). No significant differences in amplitude or rising kinetics of mGluR-EPSCs were observed in EAAT1 or EAAT3-deficient mice compared to WT mice, while EAAT4-deficient mice did show both larger amplitude and faster rising kinetics of the mGluR1-EPSCs. It was also shown that EAAT4-deletion did not affect the peak amplitude of AMPA receptor-meditated EPSCs or the early removal of glutamate after transmitter release (Nikkuni et al., 2007; Takayasu et al., 2005). Therefore, it was concluded that, among the glutamate transporters, EAAT4 specifically regulates the activities of mGluR1 by limiting the concentration of glutamate in the periplasmic space at parallel fiber synapses (Nikkuni et al., 2007). EAAT4 therefore seems to be necessary to protect mGluRs from exposure to excessive glutamate spillover and to keep mGluR activation in a proper range (Takayasu et al., 2009).

2.3.5. SLC1A7 (protein name: EAAT5)

The SLC1A7 gene encodes the glutamate transporter EAAT5. EAAT5 is expressed primarily in the retina, and is associated with large chloride conductances (Arriza et al., 1997). Prior to cloning of EAAT5, several studies noted large chloride currents elicited by glutamate in retinal cone (Eliasof and Werblin, 1993; Picaud et al., 1995a; Picaud et al., 1995b) and rod (Grant and Werblin, 1996) photoreceptors, and bipolar cells (Grant and Dowling, 1995). Subsequently, immunocytochemical studies of the rat retina revealed EAAT5 is

indeed associated with rod and cone photoreceptors and bipolar cells (Pow and Barnett, 2000; Pow et al., 2000). Current consensus of EAAT5 function in the retina is that the large chloride conductance associated with glutamate-binding likely serves as a regulator of cell excitability, and in particular as a feedback inhibitor (Picaud et al., 1995a; Wersinger et al., 2006) of neuronal signaling in the retina. In this light, it is interesting to note that the C-terminus of EAAT5 contains a protein-binding motif known to promote synaptic ion channel clustering (Sheng, 1996), and thus is indicative of the possibility that the channel-like properties of EAAT5 may be dominant in its role in retinal physiology as compared to its role as a neurotransmitter transporter (Arriza et al., 1997). Overall, further study is needed to fully understand the role of EAAT5 in retinal signal processing.

2.4 Mechanics of the glutamate transport cycle

Given the diverse roles and clear importance of glutamate transport, the focus of our current work is to improve understanding of the structural basis of glutamate transport. A brief overview of how transporters are thought to structurally accomplish uptake will therefore be presented here, followed by a more extensive review of the literature in the following section of this chapter (Section 3).

As previously mentioned, to accomplish uptake of glutamate against its concentration gradient, glutamate transporters couple uptake to inorganic ions. In this fashion, glutamate transporters utilize the free energy stored in pre-existing ion gradients to power the uphill transport of glutamate. Several

decades ago, all that was known about these transporters was that uptake was driven by the cotransport of sodium and the countertransport of potassium (Barbour et al., 1988; Kanner and Bendahan, 1982; Kanner and Sharon, 1978; Pines and Kanner, 1990) and that the movement of a pH-changing ion occurs during transport (Bouvier et al., 1992; Erecinska et al., 1983; Nelson et al., 1983). Further, uptake of glutamate recorded under voltage clamp revealed that uptake occurred with a net positive charge movement, and that this current also included a glutamate-activated, thermodynamically uncoupled, anion current (Billups et al., 1996; Eliasof and Jahr, 1996; Fairman et al., 1995; Larsson et al., 1996; Wadiche et al., 1995a) permeable to Cl^-, but also permeable to Br^-, I^-, NO_3^- and SCN^- (Eliasof and Jahr, 1996; Wadiche et al., 1995a). At this time, it was unclear exactly how many Na^+ ions were coupled to the uptake of glutamate, how many K^+ ions were coupled to the return-cycle of glutamate, and whether the pH-changing ion was a H^+ coupled to glutamate uptake or if an OH^- ion could potentially permeate through the Cl^- channel-like pathway. Additionally, there was no available information regarding the structural basis for ion-coupled glutamate uptake. Since this time, much work has been done to address all of these important questions.

To briefly summarize, it is now well established that in wild-type EAATs the uptake of glutamate is coupled to the cotransport of three Na^+ ions and one proton, and to the countertransport of one potassium ion (Levy et al., 1998; Zerangue and Kavanaugh, 1996). Therefore, each coupled transport cycle is associated with a net influx of 2 positive charges into the cell.

Conceptually, the transport cycle can be described according to an alternating access model (Jardetsky, 1966). In this model, the transporter first faces an outward (extracellular) conformation allowing for the binding of Na^+ ions, a proton, and a glutamate molecule. Subsequent to substrate and ion binding, the transporter undergoes a conformational change, exposing the glutamate-binding site to the cytoplasm. In the inward-facing state, the Na^+ ions, glutamate and a proton are released, at which point the binding of a K^+ ion to the transporter reorients the glutamate-binding site to the outward-facing conformation. Continual transitions between these two states, therefore, is what leads to the intracellular accumulation of glutamate.

Determining the order of these events as they relate to the transport cycle is therefore crucial to understanding how transporters structurally accomplish uptake. Currently, what is clear is that at least one Na^+ ion binds subsequent to the binding of glutamate (Kanai et al., 1995; Watzke et al., 2001). Therefore, at most two Na^+ ions bind prior to the binding of glutamate, one of which is clearly voltage dependent (Wadiche et al., 1995b), while the other might be voltage independent (Koch et al., 2007b). H^+ ions have been determined to bind prior to glutamate, and subsequent to at least one Na^+ ion (Larsson et al., 2004; Watzke et al., 2000). After the transporter has bound two Na^+ ions and a proton, the binding of glutamate leads to the activation of the uncoupled chloride conductance (Fairman et al., 1995) as well as the binding of a third Na^+ ion to the transporter (Kanai et al., 1995; Watzke et al., 2001). It is at this point, when the transporter is fully loaded with cotransported ions and substrate, that a

conformational change is proposed to occur which reorients the glutamate binding site to the cytoplasm. Following release of Na^+ ions, a proton, and glutamate, K^+ binds the empty transporter thus reorienting the substrate and ion binding sites to the extracellular-facing state (Zerangue and Kavanaugh, 1996). This binding sequence and associated conformational changes can be depicted by a simplified cyclical reaction diagram shown in Fig. 2. Kinetic modeling of data obtained from numerous electrophysiological experiments on mammalian EAATs supports this overall reaction scheme (Bergles et al., 2002; Larsson et al., 2004).

The studies on mammalian EAATs leading to this description of the reaction scheme in glutamate transporters were accomplished mainly by electrophysiological techniques. While considerable progress had been made using these techniques, the picture of the structural basis of glutamate transport was considerably enhanced upon the crystallization of a bacterial glutamate transporter homolog from *Pyrococcus horikoshii*, known as Glt_{Ph} (Yernool et al., 2004). The details of the crystal structure(s) will be presented in Section 3 of this chapter, but an overview will be first presented here.

Briefly, crystal structures revealed Glt_{Ph} to functionally assemble as a bowl-shaped trimeric protein, consisting of three individual monomeric subunits. Each subunit was shown to house a substrate-binding site and two Na^+ binding sites. As this is a bacterial protein it is still unclear as to whether substrate uptake requires only two Na^+ ions, or whether the third Na^+ ion was not resolvable in the crystal structures. This is a topic of debate and the coupling stoichiometry in

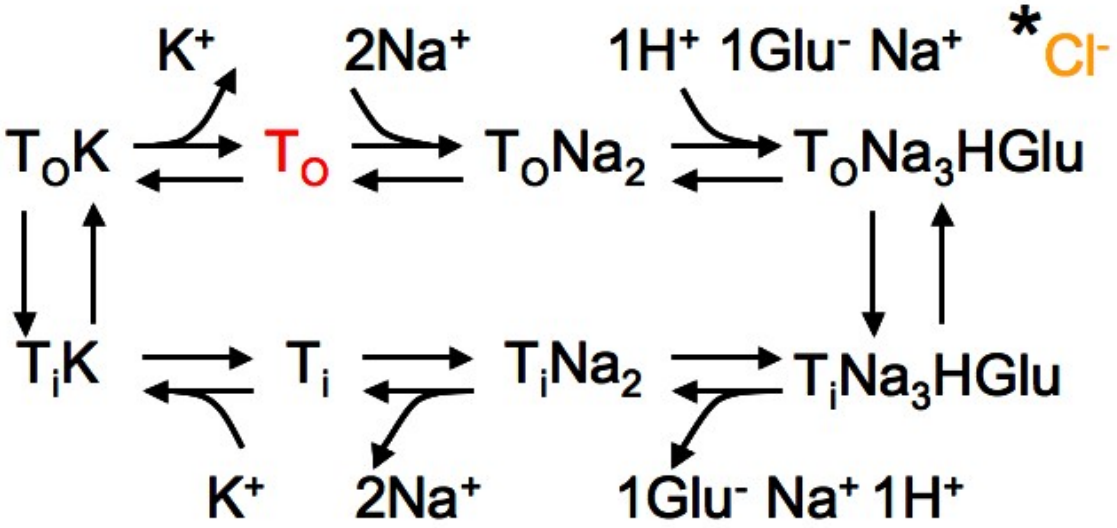

Figure 2. Schematic of glutamate transport cycle. The glutamate transport cycle can be depicted as follows: Two Na^+ ions first bind the empty transporter (T_0), followed by the binding of a proton, a glutamate molecule, and a third Na^+ ion. Substrate binding to the transporter activates an uncoupled chloride conductance (displayed with an asterisk). With substrate and ions bound, a conformational change occurs which reorients the substrate and ion-binding sites to the cytosol. Following the release of Na^+ ions, a proton, and a glutamate molecule, binding of a K^+ ion to the empty inward-facing transporter (T_i) occurs, reorienting the transporter to the outward-facing state.

Glt_{Ph} remains to be elucidated. In this light, a proton is also not coupled to substrate uptake in Glt_{Ph}, and finally, the bacterial transporter has also been shown to not require a K^+ ion for the reorientation step. Therefore the driving force for transporter reorientation is also an active area of research.

While the stoichiometry of substrate uptake in the bacterial transporter may not be equivalent to mammalian EAATs, the actual structure of Glt_{Ph} is in remarkable agreement with numerous mutagenesis studies on mammalian EAATs (Danbolt, 2001). Therefore, the crystal structures represent an excellent glimpse into the structural aspects of how glutamate transporters may function. Perhaps most intriguing from the initial crystal structures (Boudker et al., 2007; Yernool et al., 2004) was the presence in each monomer of two hairpin loop structures, one extracellular and one intracellular, between which sits the substrate-binding site. These two reentrant hairpin structures, deemed hairpin loop 1 (HP1) and hairpin loop 2 (HP2) were proposed to act like gates, consistent with the idea of alternate access to the substrate-binding site. In other words, the proposed extracellular gate appeared able to allow access to the substrate-binding site from the extracellular side of the membrane, while the proposed intracellular gate appeared to allow access to the substrate-binding site from the intracellular side of the membrane (see Fig. 4 for a schematic showing the reentrant loops).

These proposed gates are the subject of the work contained in this thesis. In particular, we have examined the role of the proposed extracellular gate (HP2), using the bacterial glutamate transporter homolog Glt_{Ph} as a model. We find that

HP2 does in fact appear to function as an extracellular gate, with conformational changes in the gate induced by not only the binding of substrate, but also by the binding of Na^+ to the substrate and ion-free state of the transporter. These conformational changes we have observed in the proposed extracellular gate are significant in that they have provided insight into the dynamic structural changes accompanying substrate uptake.

The next section of this thesis will therefore expand on the topic briefly mentioned here, in order to provide an in-depth introduction to the studies and experiments that have provided the basis of our understanding of the structural properties of glutamate transporters. Following this in-depth introduction, the next chapter of this thesis will present the work we have done to gain new insight into the conformational changes that occur in the proposed extracellular gate and how these conformational changes are structurally related to the overall transport cycle.

3. Structural properties of glutamate transporters

3.1. Mutagenesis and electrophysiological studies in mammalian EAATs

3.1.1. Ion-coupling stoichiometry

The coupling stoichiometry was first analyzed in detail using EAAT3 expressed in *Xenopus* oocytes (Zerangue and Kavanaugh, 1996). In this study, a fluorescent pH-sensitive dye was monitored during uptake of glutamate recorded under voltage clamp, in the presence of either an inwardly or outwardly directed proton gradient. In line with previous findings (Billups and Attwell, 1996), transport

current was decreased by raising extracellular pH, and even with an inwardly directed gradient for OH^- ions an intracellular acidification was detected by the pH-senstive dye. This result strongly supported a model in which the flux of a pH-changing ion was thermodynamically coupled to glutamate uptake.

To determine the stoichiometry of the thermodynamic coupling of Na^+, pH-changing ion, and K^+ gradients to glutamate, the effects of these gradients on the transport current reversal potential was next examined. To properly measure reversal potentials, the authors made use of the fact that extracellular K^+ was known to cause reverse transport in salamander retinal glial cells in the absence of external glutamate (Szatkowski et al., 1990). Extracellularly applied K^+ similarly resulted in reverse-transport in EAAT3 (in Cl^--depleted oocytes to eliminate Cl^- conductance), allowing for accurate measurement of EAAT3 reversal potentials. Key to these experiments was the subtraction with the inhibitor DHK that reveals the reversal potentials of the subtracted currents. Shifts in reversal potentials were then examined by varying extracellular concentrations of Na^+, H^+, K^+, and glutamate in order to determine their individual flux coupling coefficients. Briefly, increasing concentrations of glutamate, Na^+, and H^+ all resulted in positive shifts in reversal potential, whereas increasing concentrations of K^+ resulted in a negative shift in reversal potential. Importantly, the shifts caused by altering the glutamate and K^+ concentrations were in opposite direction to those expected for uncoupled flux of these species. Plotting reversal potentials versus ion/substrate concentrations revealed slopes for H^+ and glutamate ~ equal to 1, and K^+ ~ equal to -1, whereas the slope of Na^+ was ~

3. Additionally, Hill equations obtained by plotting the concentration dependence of forward and reverse transport currents revealed Hill coefficients of ~ 1 for glutamate, H^+, and K^+, whereas the concentration dependence of Na^+ on forward transport revealed a hill coefficient of ~2.25.

The zero flux equation (Fig. 3) was then used to predict the external glutamate concentration at equilibrium as a function of membrane potential. A model involving cotransport of one glutamate, three sodium ions, and a proton, and the countertransport of one K^+ ion were in good agreement with the measured reversal potentials. Predictions for flux coupling utilizing two rather than three sodium ions was shown to be inconsistent with experimentally derived data.

3.1.2. Glutamate transporter topology

Individual monomeric subunits

Prior to crystal structures, the mammalian glutamate transporter topology was a highly debated topic. The first models suggested topologies consisting of six (Storck et al., 1992), eight (Pines et al., 1992), or ten (Kanai and Hediger, 1992) transmembrane domains. Hydropathy plots clearly depicted the first six transmembrane domains (Kanai et al., 1993), and trypsinization studies in conjunction with the use of sequence-directed antibodies to parts of EAAT2 demonstrated the internal location of the amino and carboxyl termini and externally located large glycosylated loop between TMs 3-4 (Grunewald and Kanner, 1995). The C-terminal region topology however was quite ambiguous. To obtain information on the C-terminal topology, engineered cysteine

$$\Psi = (RT/F(n_{Na} + n_H - n_k - n_{Glu}))\ln(([Na_0]/[Na_i])^{n_{Na}}$$

$$\times ([Glu_0]/[Glu_i])^{n_{Glu}}([H_0]/[H_i])^{n_H}([K_i]/[K_0])^{n_K})$$

Figure 3. Zero flux equation. This equation was used (Zerangue and Kavanaugh, 1996) to predict the external concentration of glutamate at equilibrium as a function of membrane potential. A model in which three Na^+ ions and one proton are cotransported with glutamate, with countertransport of one K^+, matched experimentally derived data. In addition, using this equation a flux coupling model with three Na^+ ions per cycle resulted in the ability of glutamate transporters to reduce extracellular glutamate concentrations to ~2nM, in close agreement with recent findings predicting extracellular glutamate concentrations in the ~25nM range (Herman and Jahr, 2007).

accessibility in EAAT2 to biotinylation was utilized to predict external as well as internally localized residues in the C-terminal region (Grunewald et al., 1998). This study resulted in a model in which the region between TMs 6 and 7 consisted of a large intracellular loop, and the region after TM7 consisted of a reentrant loop followed by a linker region. Further refinement of this model was achieved by cysteine-scanning mutagenesis and accessibility measurements of the predicted internal loop region for the bacterial glutamate transporter homolog GltT (Slotboom et al., 1999) and EAAT2 (Grunewald and Kanner, 2000). Both of these studies revealed the loop between TMs 6-7 to be intracellular, but with a region forming a reentrant pore-loop structure (Fig. 4) of which a portion was externally accessible to sulfhydryl reagent. Importantly, the external accessibility of these residues could be prevented by the application of substrate, suggesting the binding of substrate resulted in some sort of conformational change that restricted access to the externally exposed, intracellular reentrant loop. Based on these studies it was predicted that the C-terminal region of glutamate transporters consist of two reentrant loops, termed loop I and loop II (Fig. 4) (Grunewald and Kanner, 2000). Subsequently, cysteine mutants engineered into both reentrant loop I and II were shown to form disulfide-bonds as well as coordinate a Cd^{2+} binding site, providing the first evidence that these loops were in fact close in space (Fig. 4) (Brocke et al., 2002).

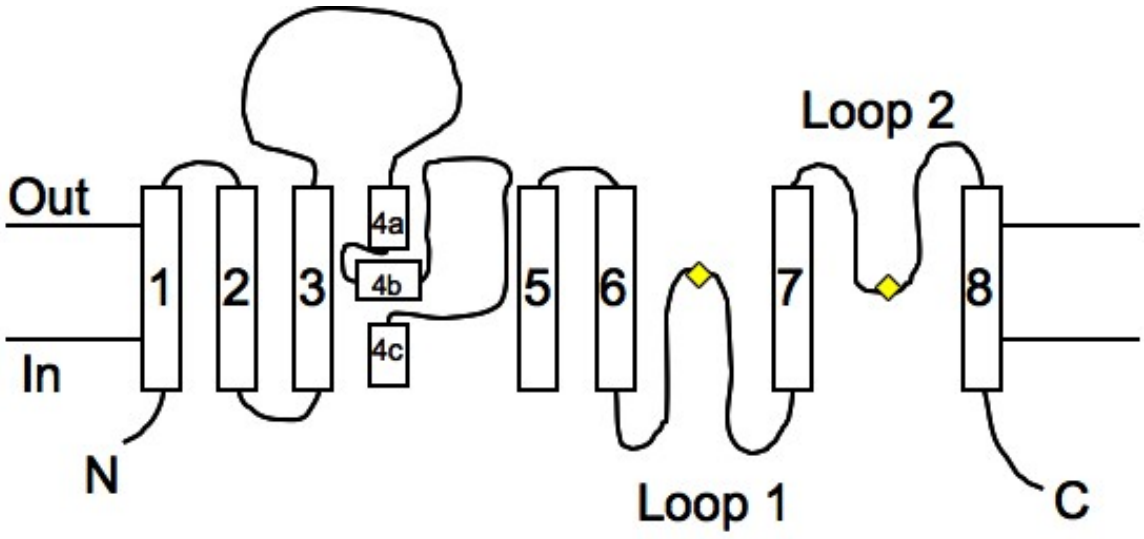

Figure 4. Glutamate transporter topology. Individual glutamate transporter monomers consist of eight primarily α-helical transmembrane domains (labeled 1-8), and two helical hairpin loops (loop 1 and loop 2) (Danbolt, 2001). The spatial proximity between the two reentrant loops was revealed by demonstrating that engineered cysteine residues into the tips of each loop (yellow diamonds) could participate in the formation of a disulfide bond and coordination of a Cd^{2+} binding site (Brocke et al., 2002).

In addition, significant protection against disulfide bond formation and the formation of a Cd^{2+} binding site was observed in the presence of the nontransportable blocker DHK. This was indicative of the possibility that the distance between these two reentrant loops could change and suggested a role for the two reentrant loops in comprising the gating mechanism of glutamate transporters. As mentioned above, these two reentrant loops would come to be known as hairpin loop 1 (HP1) and 2 (HP2), HP1 comprising the intracellular reentrant loop, and HP2 comprising the extracellular reentrant loop.

Functional oligomeric protein assembly

While initial studies focused mainly on the secondary structure and to a lesser extent on the tertiary structure of individual monomeric subunits, the quaternary structure remained unknown. Freeze-fracture electron microscopy initially reported that the functional unit assembled in a pentameric structure, consisting of five individual subunits (Eskandari et al., 2000). However, this proposed pentameric nature of EAATs was subsequently shown to be incorrect by a FRET study on eukaryotic transporters (Koch and Larsson, 2005), as well as crystallography studies on bacterial transporters (Boudker et al., 2007; Reyes et al., 2009; Yernool et al., 2004;), as will be seen in more detail below. That the authors arrived at a pentameric structure in their freeze-fracture study is most likely due to the fact that the study was conducted on eukaryotic transporters, which have a large stretch of amino acids (4B-4C loop) located mainly on the perimeter of the protein complex (Koch and Larsson, 2005). The bacterial

glutamate transporter subsequently utilized for crystallography (see below) (Yernool et al., 2004), lacks this 4B-4C loop. (Koch and Larsson, 2005; Yernool et al., 2004), and it is now accepted that glutamate transporter proteins functionally assemble as trimers, and that the individual monomers function independently (Grewer et al., 2005; Koch et al., 2007a; Koch and Larsson, 2005). That the individual monomers function independently was arrived at through the elegant use of a cysteine mutation (S334C) that, when labeled with a fluorophore, abolished glutamate-activated currents (Koch and Larsson, 2005). Very important was the fact that labeling this particular residue resulted in high FRET efficiency, indicating that multiple subunits could be labeled in a trimeric protein at one time. Thus the authors were therefore able to make use of an assay known as Fluorescence Labeling Inactivation Correlation, or FLIC. Briefly, if the transporter subunits function completely independently, then labeling S334C with a fluorophore is predicted to *reduce* glutamate-activated current, and *increase* fluorescence, at a ratio of 1:1. However, if individual subunits function cooperatively, then labeling one subunit should affect glutamate-activated current in other subunits, and thus the reduction in glutamate-activated current caused by fluorescent labeling will be greater than the increase in fluorescence measured over time. Indeed, the increase in fluorescence correlated 1:1 with the decrease in glutamate-activated currents, revealing the functional independence of the glutamate-activated conductance between individual subunits. Using the same methodology, it was subsequently shown that monomeric subunits functioned independently, and not cooperatively, in gating the anion conductance

(Koch et al., 2007a). Taken together, these studies have nicely demonstrated the functional independence of individual subunits and trimeric assembly (Koch and Larsson, 2005; Yernool et al., 2004) of glutamate transporters.

3.1.3. Structural basis for substrate and ion specificity

Substrate binding site

Sequence alignment revealed an arginine residue located in TM8 that was conserved in all dicarboxylic acid transporters, but not in the neutral amino acid transporters (Arriza et al., 1993; Kekuda et al., 1996; Shafqat et al., 1993; Utsunomiya-Tate et al., 1996). Mutation of this residue to neutral or negative amino acid residues abolished transport of $_{L}$-glutamate and $_{D}$- and $_{L}$-aspartate but did not affect transport of neutral amino acids (Fig. 5) (Bendahan et al., 2000). Competition experiments revealed that this defect occurred at the binding step. It was therefore proposed that this arginine interacts with the gamma-carboxyl group of $_{L}$-glutamate, in line with previous evidence that arginine plays a role in glutamate-binding in a crystallized ligand binding domain of the glutamate receptor GluR2 (Armstrong et al., 1998). Another interesting aspect of this study was the fact that in the R447C mutant, uptake of cysteine was shown to be electroneutral. To further examine this finding, current-voltage relationships were examined under conditions known to induce reverse transport, specifically the elevation of external K^+ (Szatkowski et al., 1990). These experiments revealed a probable defect in K^+-binding as well (measured by the inability of external K^+ to

activate the anion conductance) suggesting that this single arginine sequentially controls both substrate-binding as well as interaction with K^+.

Potassium binding

Defects specifically in the K^+-binding step were found for a conserved glutamate residue in TM7 (Fig. 5) (Kavanaugh et al., 1997). Mutation of this residue to an aspartate resulted in transporters which could not carry out net flux of substrate, and therefore could not carry out the whole transport cycle, but which could exchange substrates from one side of the membrane to the other. Interestingly, substrate-dependent anion conductance as well as sodium affinity was unimpaired in this mutant. The only affect was seen when external K^+ was utilized to induce exchange in the absence of Na^+, suggesting this residue as a potential liganding group for K^+. Consistently, it was subsequently shown that the neighboring tyrosine residue was also involved in K^+-coupling, using similar methodology (Zhang et al., 1998). A notable difference in this study however was that depending on the nature of the side chain of the substituted amino acid residue at this site, sodium affinity could also be affected. This pointed towards the potential that a sodium-selective site was located close to the potassium site, such that they partially overlap. Finally, note also that this glutamate residue is implicated in the proton-binding site (see below and Fig. 5 for details) (Grewer et al., 2003).

Sodium binding

In wild-type EAATs, uptake of one glutamate is coupled to uptake of three sodium ions (Levy et al., 1998; Zerangue and Kavanaugh, 1996). Because at least one sodium is predicted to bind subsequent to glutamate binding (Kanai et al., 1995; Watzke et al., 2001), this means that at most two sodium ions bind prior to glutamate. It has been shown that at least one of these sodium ions binds in a voltage-dependent manner (Auger and Attwell, 2000; Bergles et al., 2002; Billups et al., 1996; Larsson et al., 2004; Otis and Jahr, 1998; Wadiche et al., 1995b), while the other sodium ion(s) binding events prior to substrate-binding might be voltage independent (Koch et al., 2007b).

Numerous studies have examined the potential locations and residues involved in sodium binding. In EAAT2, mutation of a serine residue to glycine at the tip of reentrant loop 2 (Fig. 5) was shown to result in the ability of lithium to drive net influx of substrate, the efficiency of which was determined by the nature of the amino acid side chain located three residues away (Zhang and Kanner, 1999). In EAAT3 a glycine normally resides at the equivalent residue as the serine in EAAT2, resulting in the natural property of lithium-driven transport in EAAT3. Strikingly, mutation of this glycine to serine results in transporters in which currents are only observed in sodium, and not in lithium-containing media (Borre and Kanner, 2001). It was subsequently shown that, in EAAT3, lithium also supports transport, and binds to the same sites as Na^+, but does so with a 5-10 fold lower affinity (Larsson et al., 2004).

In TM7 there is a highly conserved stretch of five amino acids known as the NMDGT motif. While most conservative mutations of this region render

transporters non-functional (Seal et al., 2000), in EAAT3 a serine to threonine mutation remains functional enough to observe that this mutation abolished the ability of lithium to drive uptake (Fig. 5). In this same region, mutation of the aspartate residue to asparagine dramatically impaired sodium binding to the transporter, measured by the ability of sodium to activate the anion conductance (Fig. 5) (Tao et al., 2006). This aspartate residue was subsequently shown to also be able to bind thallium (Tao et al., 2008).

In TM8, a conserved glutamate residue located upstream from the substrate-binding residue arginine (Fig. 5) (Bendahan et al., 2000) was recently shown to result in a large decrease in the apparent affinity and rate of Na^+-binding to the glutamate-bound transporter, when mutated to asparagine (Tao and Grewer, 2007). Interestingly, the Na^+-binding affinity and rates were essentially unaffected in the absence of glutamate. It was therefore proposed in this paper that the rate and affinity of Na^+-binding is intricately linked to the bound substrate and the amino acid side chain at this position. This mutation was proposed to alter the interaction of glutamate with the transporter, thus impairing Na^+-coordination. Along these same lines, interaction of substrate with the binding site was shown to be dependent on the nature of the cation coupled to binding and transport (Menaker et al., 2006). In this study, lithium was shown to drastically increase the K_m for $_L$-glutamate and $_D$-aspartate, but did not have a major effect on the K_m for $_L$-aspartate. In addition, the K_i of the competitive, non-transportable blocker of EAATs known as $_{DL}$-threo-b-Benzyloxyaspartic acid ($_{DL}$-TBOA), was similarly unaffected. Thus, it was proposed that the effect of

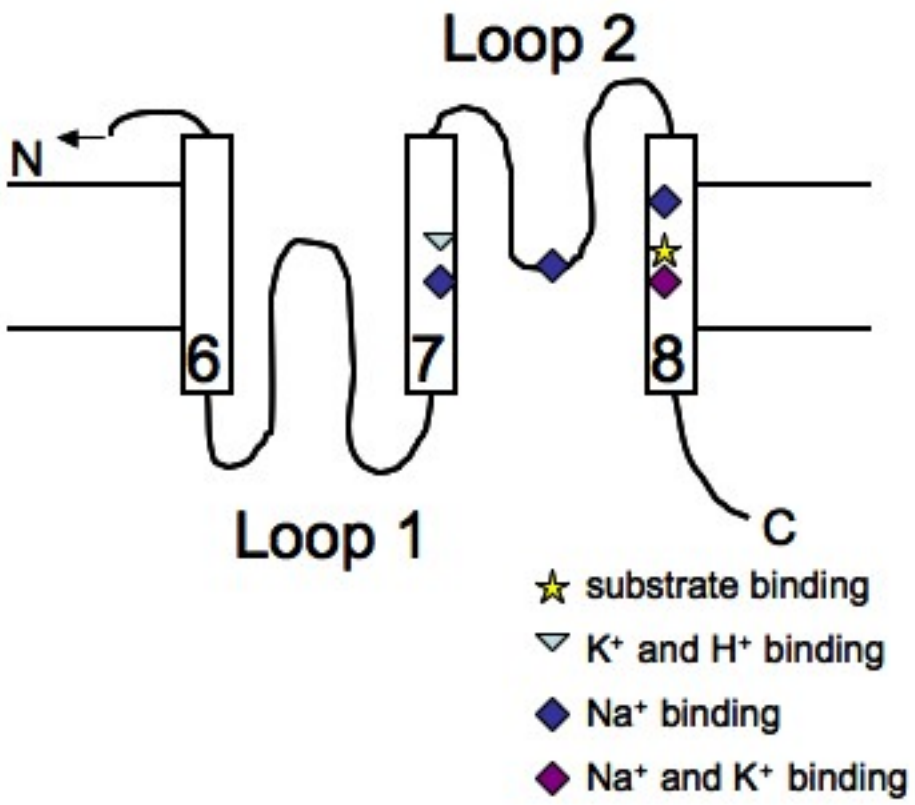

ate binding sites. A
conferring specificity to
dahan et al., 2000).
entrant loop 2 and TM7
diamonds) (Borre and
Tao and Grewer, 2007;
return step (downward
98) and proton-binding
y the C-terminus (TM

the coupling ion in determining substrate specificity is manifested at a step subsequent to substrate binding, and that the extra carboxyl group on the dicarboxylic acid substrates could potentially contribute to a sodium binding site. Another aspartate residue in TM8 downstream of the substrate-binding arginine residue is also implicated in Na^+-binding (Fig. 5). Interestingly, mutation of this residue to cysteine or serine resulted in the inability of lithium to replace sodium, however sodium-binding itself was unimpaired (Teichman et al., 2009). When mutated to an asparagine, the ability of lithium to support transport was restored, but a specific defect in potassium-binding was observed. Thus, this aspartate residue was proposed as participating in both the sodium-binding transport step of the transport cycle, as well as the return step, and therefore comprising an overlapping sodium and potassium-binding site (Fig. 5).

Proton-binding

Discovery of thermodynamic coupling of protons to glutamate transport raised the question of whether the proton is transported during the uptake hemicycle or whether the proton is transported during the K^+-binding return step. Kinetic experiments utilizing rapid glutamate concentration jumps induced by laser-pulse photolysis of caged glutamate supported proton uptake coincident with the uptake of glutamate (Watzke et al., 2000). This study demonstrated that EAAT3 is protonated prior to glutamate binding and translocation, and that the dissociation of substrate and ions on the intracellular side is due to a change in pK of the proton-binding residue.

Further confirmation that the proton binds before glutamate was subsequently shown using voltage clamp fluorometry (VCF) on the mammalian transporter EAAT3 (Larsson et al., 2004). Voltage clamp fluorometry experiments make use of the fact that a fluorophore is sensitive to local enviroment. Therefore, conformational changes can be manifested as a change in fluorescence when a fluorophore is covalently attached to a particular protein location. Voltage-dependent fluorescence changes were shown to be dependent on extracellular pH concentration. Fluorecence-voltage curves shifted depending on the extracellular proton concentration, with higher pH concentrations shifting the fluorescence-voltage curves left, and lower pH concentrations shifting the curves to the right. Importantly, these experiments were done in the absence of potassium and glutamate, thus indicating proton binding prior to glutamate. If the proton bound predominantly after glutamate, shifts in the fluorescence-voltage curves would not be expected in the absence of glutamate.

While the coupling of a proton to transport is thus well established, the precise molecular nature of the proton-binding site is unclear. A recent study has provided evidence that potentially a glutamate residue located in TM7 may coordinate proton binding (Fig. 5) (Grewer et al., 2003). Interestingly, this residue is the same residue previously implicated in potassium binding (Kavanaugh et al., 1997), located just downstream from the highly conserved NMDGT motif. Because this residue is acidic, implicated in potassium binding, and close to the substrate-binding site (Bendahan et al., 2000), it was more closely examined as a potential liganding residue for protons. Indeed, mutation

of this glutamate residue to a non-ionizable glutamine residue resulted in a pH-independent transporter that does not interact with protons (Grewer et al., 2003). Because homoexchange was unimpaired in this mutant, it was assumed that the mutant glutamine side chain is always protonated, and therefore proton release on either the intra- or extracellular side of the membrane cannot occur. This explains the pH-independent nature of this mutant, as well as why the potassium return step is impaired. The glutamine side chain, being unable to be deprotonated, cannot complete the transport cycle. In light of these results, a model was proposed in which the native glutamate residue needs to be protonated to permit glutamate binding. Following translocation, the glutamate residue becomes deprotonated, and therefore negatively charged in order to bind potassium and reorient the transporter to the extracellularly-facing state.

3.1.4. Anion Conductance

Degenerate oligonucleotides complementary to two regions of amino-acid sequence similarity between EAATs1-3 were utilized to identify additional members of the EAAT family expressed in the cerebellum. This strategy led to the identification of EAAT4 (Fairman et al., 1995). In the process of characterizing this newly discovered EAAT family member, it was observed that the reversal potential of the currents elicited by $_{L}$-aspartate was very close to previously reported values of E_{Cl} in *Xenopus* oocytes (Barish, 1983). In addition, the $_{L}$-aspartate-induced reversal potentials were found to shift by ~60 mV per 10-fold change in the external chloride concentration, in accordance with the Nernst

equation for a chloride-selective conductance. Removal of external chloride abolished the $_L$-aspartate-induced outward currents previously observed at depolarized potentials, but did not significantly alter the uptake of radiolabeled $_L$-aspartate in oocytes clamped at -60 mV. In fact, experimental manipulation of the chloride reversal potential revealed $_L$-aspartate transport to occur regardless of the direction of chloride flux. These chloride currents were found to be $_L$-aspartate-induced, and not due to endogenous *Xenopus* oocyte chloride currents. These results taken together strongly supported a model in which EAATs harbor a thermodynamically uncoupled chloride flux.

Interestingly, it was found that the reversal potentials of the currents differed between substrates. For instance, the reversal potential for $_L$-aspartate-induced current was -22 mV, while for $_L$-glutamate-induced current it was -3.5 mV. The substrate-dependent reversal potentials are therefore a combination of chloride conductance and substrate transport current, with differences in reversal potential due to differences in the contribution of each component. For instance, the EAAT4 $_L$-glutamate-induced current is composed of a larger transport component and a lesser chloride component as compared to $_L$-aspartate-induced currents. Together this data suggests that amino-acid transport does not directly correlate with chloride flux, implying an intricate mechanism of substrate-dependent chloride-channel activation in EAAT4.

Expanding on these findings, the voltage dependence of EAAT1-3 currents were subsequently examined (Wadiche et al., 1995a). EAAT1 was found to reverse at ~9 mv and EAAT3 at ~38 mV, while EAAT2 did not reverse at potentials up to

+60 mV. Again, the reversal potential of EAAT1 and EAAT3 currents was shifted ~50 mV per ten-fold change in external chloride concentration. Depletion of oocyte intracellular chloride by dialysis revealed that a significant amount of the inward substrate-induced current was due to chloride efflux. In addition, the permeation of anions other than Cl^- was examined in EAAT1 by recording currents activated by $_D$-aspartate at physiological concentrations of $Cl^-_{(in)}$, revealing a general selectivity sequence of $NO_3^- > I^- > Br^- > Cl^- > F^-$. This selectivity sequence was identical to that of a neuronal chloride channel (Franciolini and Nonner, 1987; Franciolini and Nonner, 1994) in which the conductance properties were presumed to result from anion-cation interactions in the channel pore. Given these results, it was suggested that activation of a chloride conductance during transport could provide a mechanism to offset the inherent depolarization associated with transport as well as providing neurons with a way to dampen cell excitability. In addition, due to the thermodynamic independence of the chloride and substrate fluxes, it was hypothesized that some sort of gating mechanism must exist in which to switch back and forth between Na^+-coupled transport and chloride permeation.

Subsequent mutagenesis and electrophysiological studies provided important clues toward the molecular basis for uncoupled anion conductance in glutamate transporters. Particularly interesting was a finding that lithium ions could substitute for sodium and support coupled uptake, however lithium selectively disrupted the uncoupled anion conductance (Borre and Kanner, 2001). The fact that activation of the anion conductance could be disrupted without disrupting

coupled uptake suggested that the molecular mechanism of substrate translocation was distinct from the anion conductance. Further evidence from several groups reinforced this idea. In EAAT3 a residue was found on HP2 that, when mutated to cysteine and modified with the sulfhydryl-specific methanethio-sulfonate reagent MTSET, abolished coupled uptake without affecting the chloride conductance (Fig. 6) (Borre et al., 2002). In this study, treatment of MTSET-modified I421C with dithiothreitol (DTT) was shown to restore the voltage dependent $_{D}$-aspartate-induced currents. Two other groups published similar reports in EAAT1 around the same time. Sulfhydryl modification of V449C (Fig. 6) (Seal et al., 2001) and V452C (Fig. 6) (Ryan and Vandenberg, 2002) both were shown using electrophysiology and uptake assays to specifically disrupt the coupled flux of transporter while leaving the anion conductance intact. The fact that these three publications described the same effect of cysteine modifications in very close regions of transporters from different species implied that this region of the transporters corresponding to HP2 is extremely important for the translocation process. Because binding of substrate and activation of anion conductance remained intact in these sulfhydryl-modified mutants it was suggested that this region was not crucial for conformational changes that activate the anion conductance.

Despite these advances, the question as to the molecular nature of the anion conductance remained to be elucidated. To examine this question more closely, Ryan and Vandenberg (Ryan et al., 2004) noted that the second transmembrane domain in the amino-terminal half of EAATs contains positive charges on both

ends as well as a number of polar residues that are highly conserved between transporter subtypes. These properties are consistent with ion permeation pathways of ion channels (Dutzler et al., 2002; Xu and Akabas, 1996), and in particular, chloride channels (Smith et al., 1999). Based on these observations, a number of conservative mutations were made within TM2. Interestingly, for a number of TM2 mutants it was shown that changes in current-voltage relationships of the mutants were due to changes in gating/permeation properties of the chloride channel, with little to no effect on coupled substrate transport (Fig. 6). In addition, mutation of TM2 residues to cysteines and subsequent modification by MTSES, MTSET and Hg^{2+} revealed that a large portion of TM2 was accessible to the external aqueous environment, consistent with this domain lining a water-filled pore. Together these results suggested that TM2 plays an important role in the anion conducting properties of glutamate transporters.

3.1.5. Conformational changes

The precise molecular mechanism whereby glutamate transporters harness the energy stored in pre-existing ion gradients to drive uptake is currently unknown. A prevailing model for this process is termed the alternating access model (Jardetzky, 1966), in which a substrate binding site is bordered by two gates, one extracellular and one intracellular, thereby allowing for alternating access of the substrate to the extracellular and intracellular solutions.

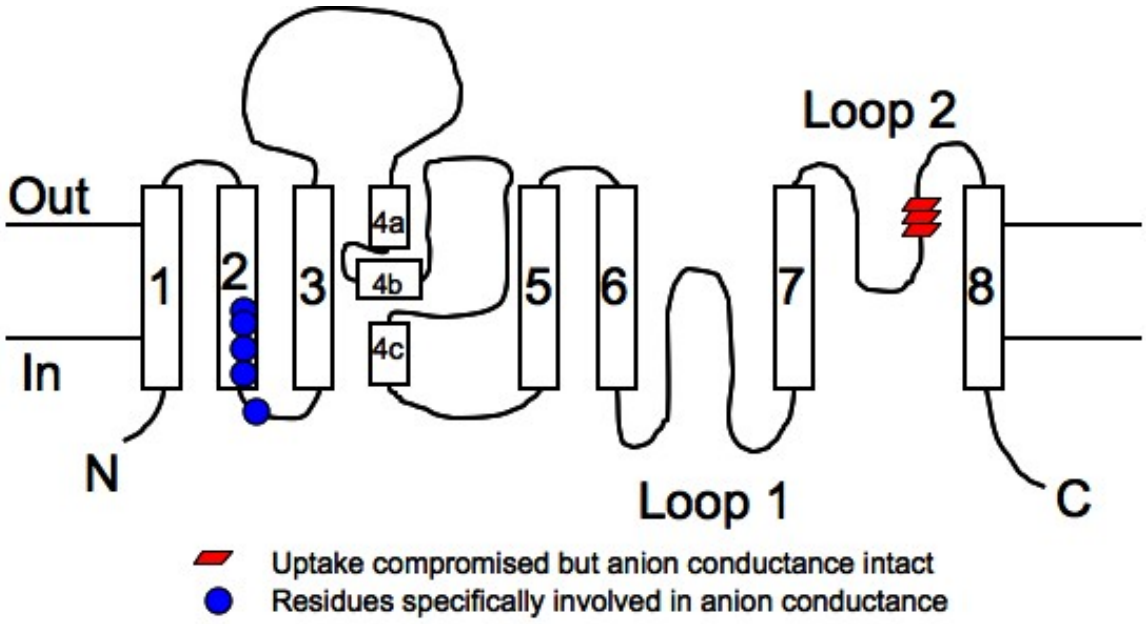

Figure 6. Structural basis of the uncoupled anion conductance. Sulfhydryl modification of engineered cysteine residues on HP2 (red squares) (Borre et al., 2002; Ryan and Vandenberg, 2002; Seal et al., 2001) specifically disrupts coupled glutamate uptake while leaving the anion conductance intact. Conversely, conservative mutations engineered into TM2 revealed that changes in current-voltage relationships of the mutants were due to changes in gating/permeation properties of the chloride channel, with little to no effect on coupled substrate transport (Ryan et al., 2004).

Numerous studies have examined conformational changes in mammalian EAATs (see Fig. 7 for details). Briefly, 1) trypsin-sensitive sites in EAAT2 were shown to be differentially accessible to cleavage depending on whether the transporter was substrate, co-substrate, or inhibitor-bound, suggestive of conformational changes (Grunewald and Kanner, 1995). 2) A conserved tyrosine residue in EAAT2 located downstream from the NMDGT motif and previously implicated in sodium and potassium-binding was shown to be more accessible to methanethiosulfonate derivatives when mutated to cysteine in the presence of the nontransportable glutamate analogue dihydrokainate (DHK), but less accessible in the presence of substrate (Zarbiv et al., 1998). Interestingly, in this study it was also shown that the presence of substrate did not protect this residue from accessibility to the membrane permeant molecule N-ethylmaleimide, suggesting that this tyrosine residue is alternatey accessible to both sides of the membrane. 3) In EAAT1, mutation of an alanine residue, located just upstream from the NMDGT motif in TM7, to cysteine was shown to cross-link with residues mutated to cysteines located on both HP1 as well as HP2 (Leighton et al., 2006). Interestingly, this only occurred in the absence of glutamate and $_{DL}$-TBOA, with the presence of glutamate and $_{DL}$-TBOA preventing cross-linking. Also, sodium binding facilitated cross-linking of the residues in HP1 and TM7, but not HP2 and TM7. These results provided evidence that the alanine in TM7 is close in space to both HP1 and HP2, and that conformational changes between these three domains occur during different steps of the transport cycle (Leighton et al., 2006). 4) Further evidence that HP2 undergoes

conformational change has been determined by a combination of accessibility (Grunewald et al., 2002; Leighton et al., 2002; Seal and Amara, 1998; Zhang and Kanner, 1999), fluorescence (Larsson et al., 2004), and cross-linking (Qu and Kanner, 2008; Ryan et al., 2004) studies. 5) Similarly, other accessibility (Grunewald and Kanner, 2000; Shlaifer and Kanner, 2007) and cross-linking (Shlaifer and Kanner, 2007) studies have implicated conformational changes in HP1. 6) The tips of HP1 and HP2 were shown (Brocke et al., 2002) to come within close enough proximity to one another to form a disulfide bond, the extent of which was modulated by the nontransportable blocker dihydrokainate (DHK). Finally, 7) the temperature dependence of glutamate transport in EAAT3 at steady state and pre-steady state were used to obtain thermodynamic parameters for glutamate- and sodium-binding, transport, and the potassium return-step (Mim et al., 2007). This study predicted that at least two conformational changes are associated with glutamate translocation, while at least one conformational change occurs during the potassium-dependent relocation step.

Taken together all of the above-mentioned studies (Fig. 7) have provided ample evidence for conformational changes associated with the C-terminal domain in mammalian glutamate transporters, in particular the reentrant HP loops. Consistently, a recent FRET study on EAAT3 (Koch and Larsson, 2005), has also shown that uptake is accomplished by small molecular motions situated near the substrate-binding sites. Notably however, in EAAT3, voltage clamp fluorometry experiments conducted on the TM4B-4C extracellular loop, located

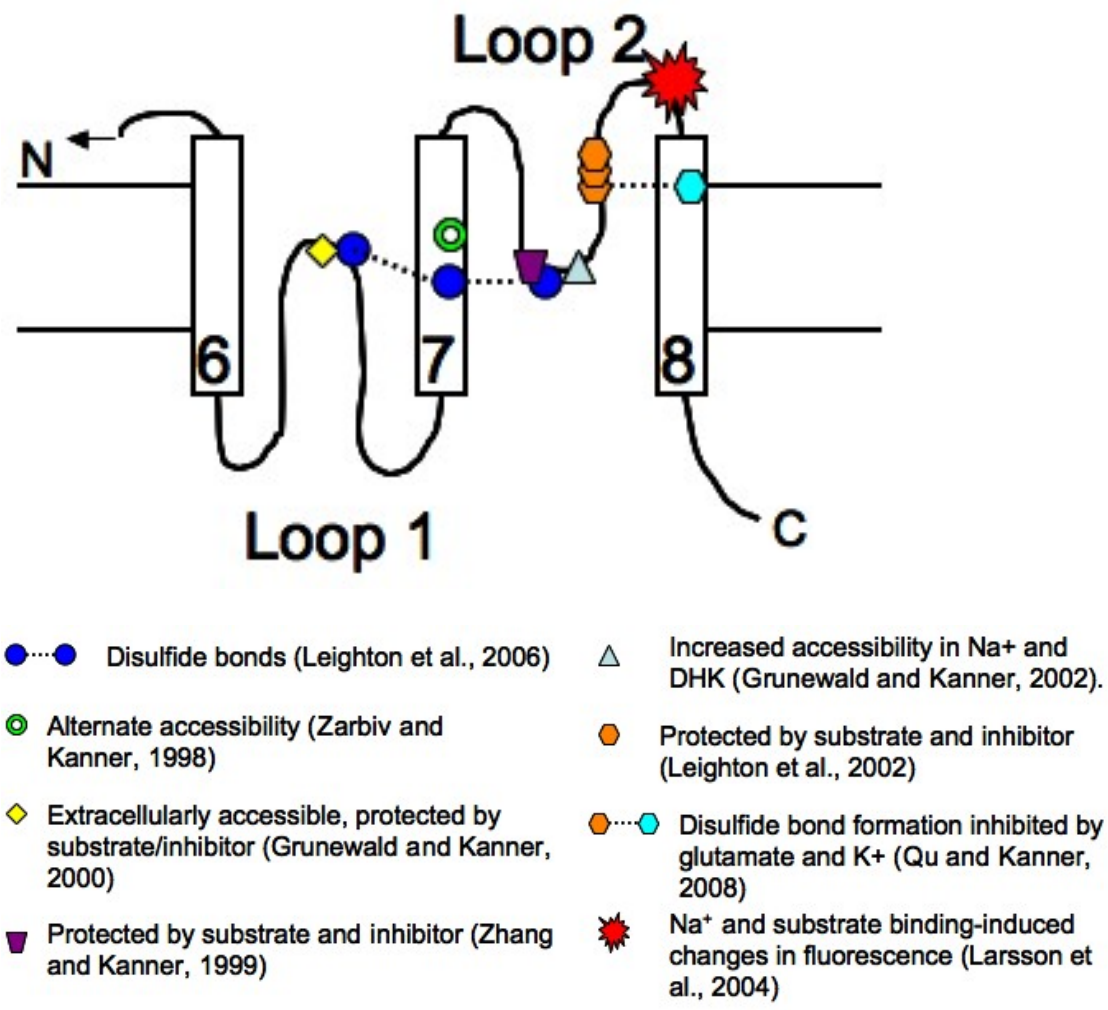

Figure 7. Localization of residues involved in conformational change. An abundance of electrophysiological studies have been performed in order to examine the conformational changes associated with glutamate transport. Summarized in this figure are some of the more important studies, revealing the importance of the highly conserved C-terminal region in participating in structural changes involved in the transport cycle.

far from the substrate binding site, revealed that residues in this area report on sodium and glutamate binding-induced conformational changes (Koch et al., 2007b). Thus, the conformational changes accompanying uptake appear to extend through large portions of the transporter structure. Future experiments are expected to refine and clarify the precise series of conformational changes that occur during the process of transport. Particularly interesting are recent crystal structures of a glutamate transporter homolog, revealing structural aspects of the transporter in multiple conformational states (described in detail below).

3.2. Bacterial transporter Glt_{Ph}: crystal structures and function

3.2.1. Crystallization of Glt_{Ph} in substrate-bound state

A major advance in the understanding of the molecular architecture of glutamate transporters was the publication of a crystal structure of a glutamate transporter homologue from *Pyrococcus horikoshii*, Glt_{Ph} (Yernool et al., 2004). Glt_{Ph} shares ~36% amino acid identity with eukaryotic EAATs, and even greater conservation in functionally important regions (Boudker et al., 2007). Crystals revealed that Glt_{Ph} assembles as a bowl-shaped trimer (Fig. 8a), with the aqueous basin facing the extracellular side of the membrane and with the more pointed base facing the cytoplasm (Fig. 8b). The aqueous basin is quite large, ~50 Å in diameter and ~30 Å in depth, and its surface is hydrophilic, allowing for easy access of aqueous solution to reach the midpoint of the membrane bilayer.

Consistent with previous accessibility studies (Grunewald and Kanner, 1995; Grunewald et al., 1998; Grunewald and Kanner, 2000), each monomer consists of 8 transmembrane domains (TMs1-8), and two reentrant helical hairpin loops (HP1 and HP2) (see Fig. 4). Transmembrane domains 1-6 form an N-terminal cylinder-shaped motif (Fig. 9a), which participates in all intersubunit contacts in the trimer. The highly conserved C-terminal half (TM7, HP1-2, and TM8) implicated in substrate/ion binding (Kanner, 2006), is essentially inserted into the middle of each N-terminal cylinder, thus forming a functional unit contained inside an N-terminal cylinder (Fig. 9b-c).

The C-terminal portion of each monomer reveals how the highly conserved aspects of the transport machinery are oriented (Fig. 9b). Helical hairpin 1 is a helix-turn-helix structure inserted into the middle of an N-terminal cylinder from the cytoplasmic side. The tip of HP1 is partially exposed to the extracellular solution, in agreement with previous cysteine accessibility studies (Grunewald and Kanner, 2000; Seal et al., 2000; Slotboom et al., 1999). HP1 connects to TM7, a transmembrane domain passing through the center of the N-terminal cylinder and which then becomes HP2. Interestingly, HP2 is also composed of a helix-turn helix motif, but its positioning in terms of the membrane is different than HP1. HP2 is nearly parallel to the membrane with a large portion of its extracellular surface solvent exposed, while HP1 is essentially perpendicular to the membrane. HP2 connects to TM8, an amphipathic alpha-helical segment that, similarly to TM7, also extends directly through the middle of the N-terminal

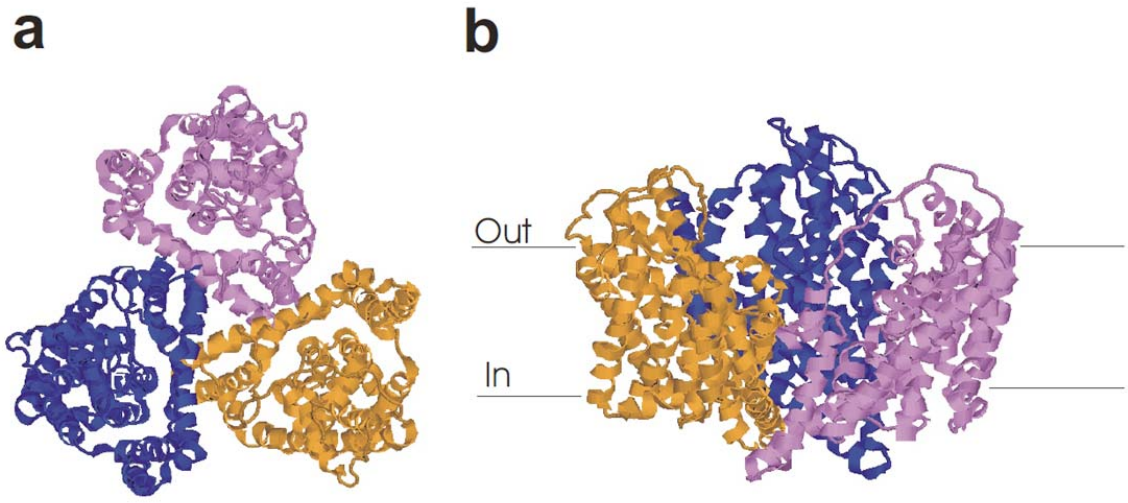

Figure 8. **Glt_{Ph} assembles as a trimer.** (a) view of Glt_{Ph} from the extracellular side. Each individual monomer is represented as a different color. (b) side-view of Glt_{Ph} inserted into the membrane. Each individual monomer is colored as in (a).

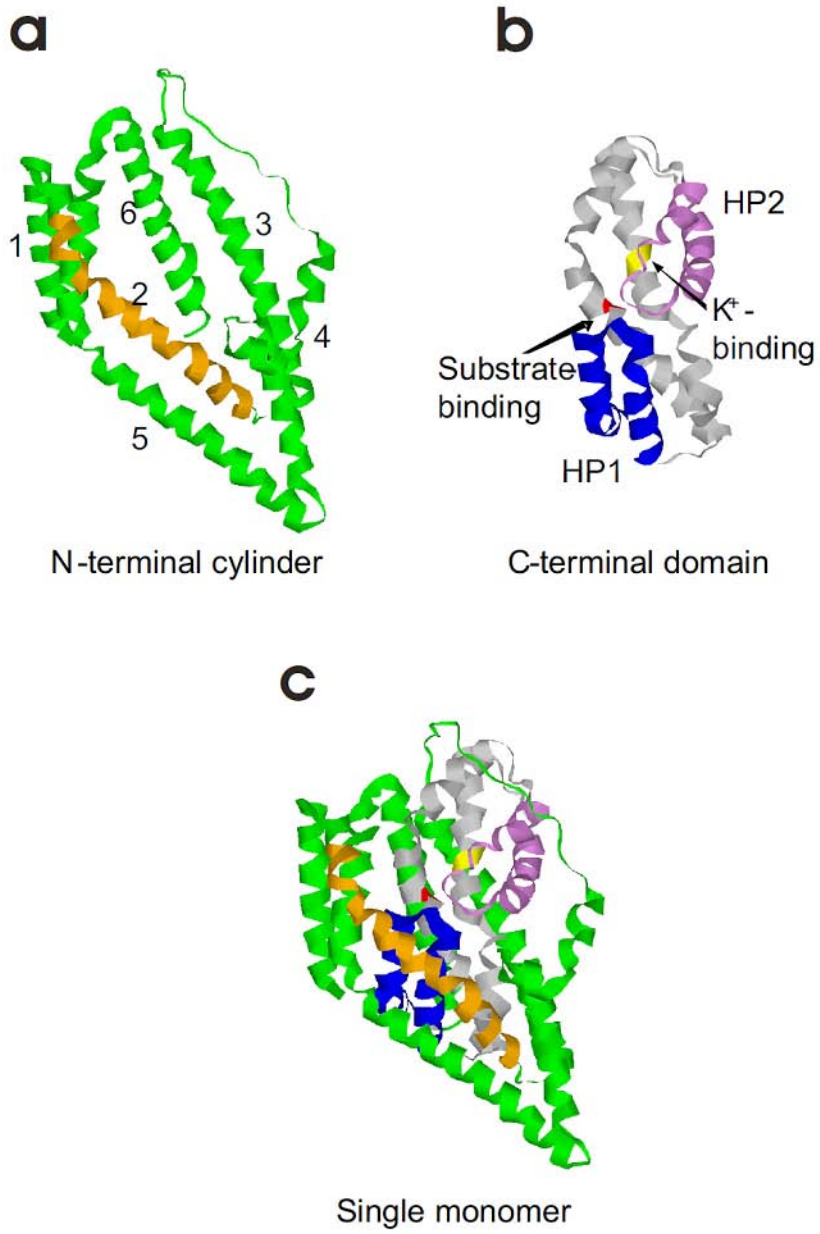

Figure 9. Structural fold of a Glt_{Ph} monomer. (a) fold of the first six transmembrane domains, revealing the cylinder-like shape in which (b) the C-terminal region is inserted into (c). In (a) and (c) TM2 is colored orange to highlight the region thought to be involved in chloride conductance. In (b) HP1 is

colored blue and HP2 is colored purple. The conserved arginine residue in TM8 involved in substrate-binding (Bendahan et al., 2000) is shown in red. In TM7 the location of the residue that in mammalian transporters is involved in potassium-binding (Kavanaugh et al., 1997) is shown in yellow. Situated in the area of the proposed substrate-binding site was a non-protein electron density, hypothesized to be bound substrate (Yernool et al., 2004).

cylinder and which is implicated in contributing to the formation of a water-filled substrate transport pathway (Slotboom et al., 2001).

In the center of the C-terminal region of the Glt_{Ph} structure, a non-protein electron density approximately the size of a glutamate molecule was observed (Fig. 9b). The resolution of this structure (~3.5 Å) did not allow Yernool and colleagues (Yernool et al., 2004) to conclusively determine that this density corresponded to bound substrate. However, the location in which this non-protein electron density was discovered, in addition to the fact that glutamate was included in all steps of the purification and crystallization process, suggested that this density corresponded to the substrate-binding site. That this non-protein electron density was in fact bound substrate was highly probable due to its proximity to conserved amino acids known to be crucial for functional activity; for example, its proximity to 1) A397, a residue previously implicated in conferring specificity to substrates with beta- and gamma-carboxy groups (Bendahan et al., 2000), 2) the highly conserved NMDGT motif, critical for glutamate transport in mammalian EAATs (Seal et al., 2000), and 3) residues important for sodium- and potassium-binding (Borre and Kanner, 2001; Kavanaugh et al., 1997; Seal et al., 2000; Tao et al., 2006; Tao and Grewer, 2007; Tao et al., 2008; Zhang and Kanner, 1999).

Based on the positions of HP1 and HP2 relative to this proposed substrate-binding site, the authors suggested that transport occurs through an alternating access model (Fig. 10a) in which HP2 comprises the extracellular gate and HP1 comprises the intracellular gate. The conformational state captured by this crystal structure with substrate and ions bound was deemed an occluded state

(Fig. 10b), with both the extracellular and intracellular gates closed. To define this state as occluded, a 1.4 Å radius computational probe was utilized to reveal that neither substrate nor ions were accessible to the probe (Gouaux, 2008). In addition, given the proposed position of substrate, no pathway large enough to allow for passage of the substrate into the cytoplasmic solution was apparent. It was therefore concluded that the binding of ions and substrate resulted in a closing of HP2, yielding an occluded state with both gates closed. Further conformational change of HP1 was speculated to be required for intracellular substrate and ion release.

Expanding on this initial structure, three years later another set of crystal structures were published which provided further evidence for the location of the substrate-binding site and the idea that HP2 functions as the extracellular gate. In this paper, a combination of radiolabeled uptake, fluorescence, and isothermal titration calorimetry (ITC) studies were utilized to reveal that Glt_{Ph} is preferentially a Na^+-dependent aspartate transporter, rather than a glutamate transporter (Boudker et al., 2007). Crystals obtained in the presence of $_L$-cysteine sulphinic acid were used to define the position of aspartate in the substrate-binding site, due to the anomalous scatterer (sulphur) of $_L$-cysteine sulphinic acid. Assuming that the β-carboxylate group of aspartate occupied the same position of the sulphinic acid of $_L$-CS enabled the fitting of aspartate into its electron density. This set of crystal structures again revealed Glt_{Ph} to adopt an occluded state in the presence of ions and substrate.

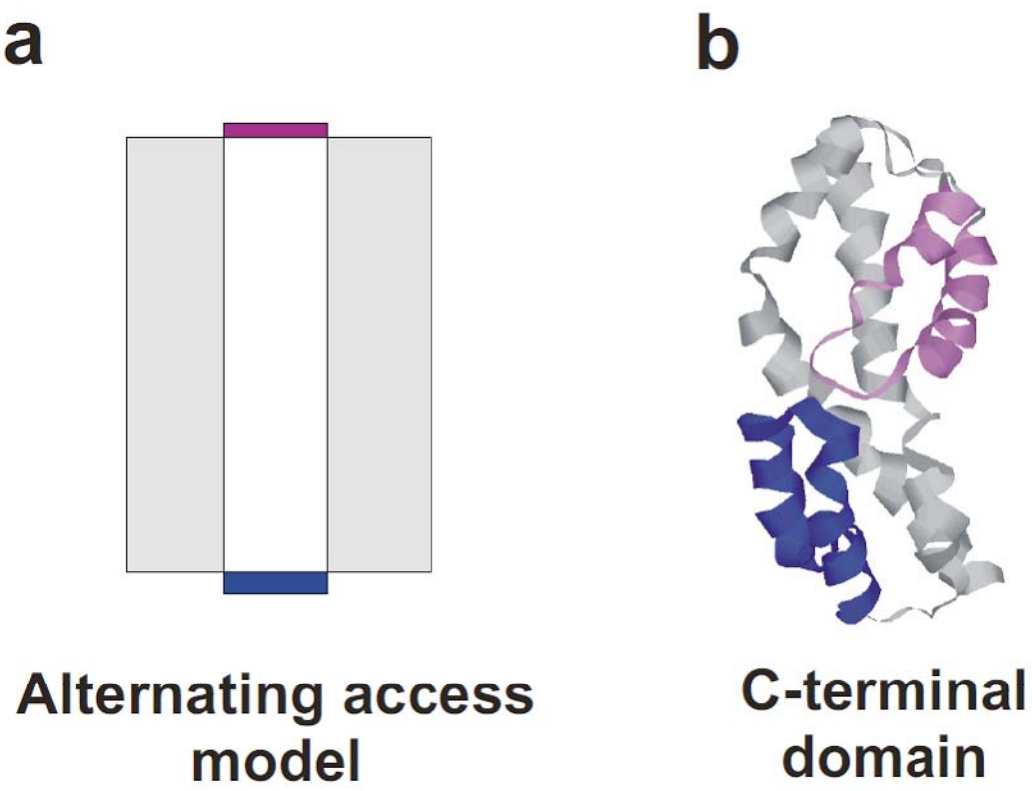

Figure 10. Alternating access model and the occluded state. (a) schematic of a transporter with both gates closed (occluded state). According to the alternating access model (Jardetzky, 1966), opening of the extracellular gate (purple) is followed by substrate-binding and conformational change. This results in closing of the extracellular gate and opening of the intracellular gate (blue), allowing for substrate access to the cytoplasm. (b) occluded state of the crystal structure of the C-terminal domain of Glt_{Ph} with HP2 (purple) comprising the extracellular gate and HP1 (blue) comprising the intracellular gate. Subsequent movement of HP1 was speculated to be required for substrate translocation (Yernool et al., 2004).

3.2.2. Crystallization of Glt_{Ph} in the inhibitor-bound state

Information on the role of HP2 in comprising the extracellular gate was obtained by crystallizing Glt_{Ph} in the presence of the non-transportable blocker TBOA, after first verifying the effectiveness of TBOA as an inhibitor in radioactive uptake assays on Glt_{Ph} (Boudker et al., 2007). In the TBOA-bound crystals, HP2 adopted what appeared to be an 'open' conformation (Fig. 11b-c), with the tip of HP2 displaced about 10 Å compared to substrate bound crystals (Fig. 11a). Using 3-bromo-TBOA in order to model TBOA into the observed electron density, it was found that the benzyl group of TBOA props open the tip of HP2, thereby preventing HP2 closure. Therefore, not only did these crystals provide strong evidence for HP2 comprising the extracellular gate, but also shed light on the potential mechanism of competitive inhibition by TBOA (Shimamoto et al., 1998).

3.2.3. Glt_{Ph} Na^+-binding sites

Aspartate-binding, as measured by fluorescence and ITC experiments, resulted in binding curves with Hill coefficients near ~1 (Boudker et al., 2007). This was in contrast to sodium titrations in the presence of aspartate, for which binding curves fitted by the Hill equation revealed Hill coefficients around 2 (Boudker et al., 2007). In addition, a linear fit with a slope of about 2 was obtained from log plots of Na^+ concentration versus aspartate Kd (Boudker et al., 2007). Together these experiments indicated that the binding of a single aspartate was coupled to

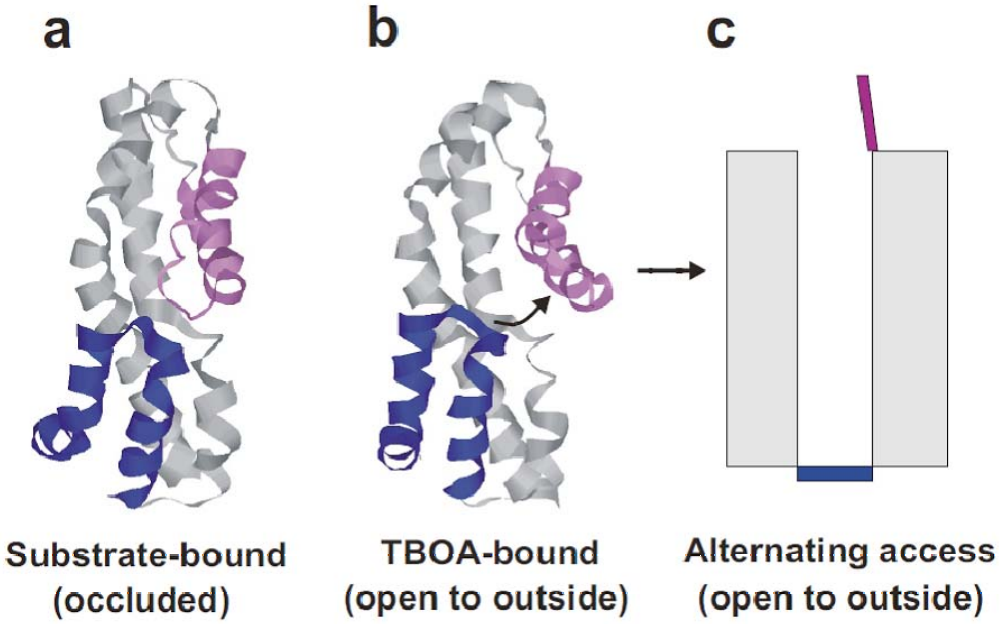

Figure 11. HP2 position in substrate- and inhibitor-bound state. The C-terminal domain is shown in the substrate-bound (occluded) state (a) with both HP1 (blue) and HP2 (violet) in a closed conformation, or the TBOA-bound state (b) in which steric restrictions prevent HP2 (violet) from closing. (c) Schematic of the alternating access model with the extracellular gate (violet) open to the outside.

the binding of at least two sodium ions. In contrast to the binding of aspartate, the binding of TBOA was found to be coupled to about 1 sodium ion (Boudker et al., 2007).

Crystal structures in thallium(I) (Tl^+), confirmed the results from this binding analysis (Boudker et al., 2007). Two sites per subunit were observed to bind Tl^+, designated site 1 and site 2 (Fig. 12a-b), with only Na^+ (but not Li^+ or K^+) disrupting the thallium anomalous density peaks. In contrast, crystal structures obtained in the presence of TBOA revealed only one Tl^+ peak localized to site 1. In these structures, steric restrictions of HP2 caused by the bulky benzyl group of TBOA were observed to disrupt the ability of Tl^+, and Na^+ to bind to site 2 (Fig. 12c). Taken together, these results suggest a mechanism whereby HP2 comprises the extracellular gate, and that closing of the gate is prevented by TBOA due to the steric restrictions of HP2 resulting in disruption of Na^+ binding to site 2.

3.2.4. Evidence for a Cl^- channel in Glt_{Ph}

An important and unresolved aspect, among others, is the chloride conductance associated with glutamate uptake in mammalian EAATs. Elucidation of crystal structures of the bacterial aspartate/glutamate transporter homolog Glt_{Ph} lends the possibility to gain structural insight into the mechanism of chloride flux in this EAAT homolog, provided that a chloride conductance is also observed in Glt_{Ph}. To demonstrate a chloride conductance in Glt_{Ph}, Mindell and colleagues first

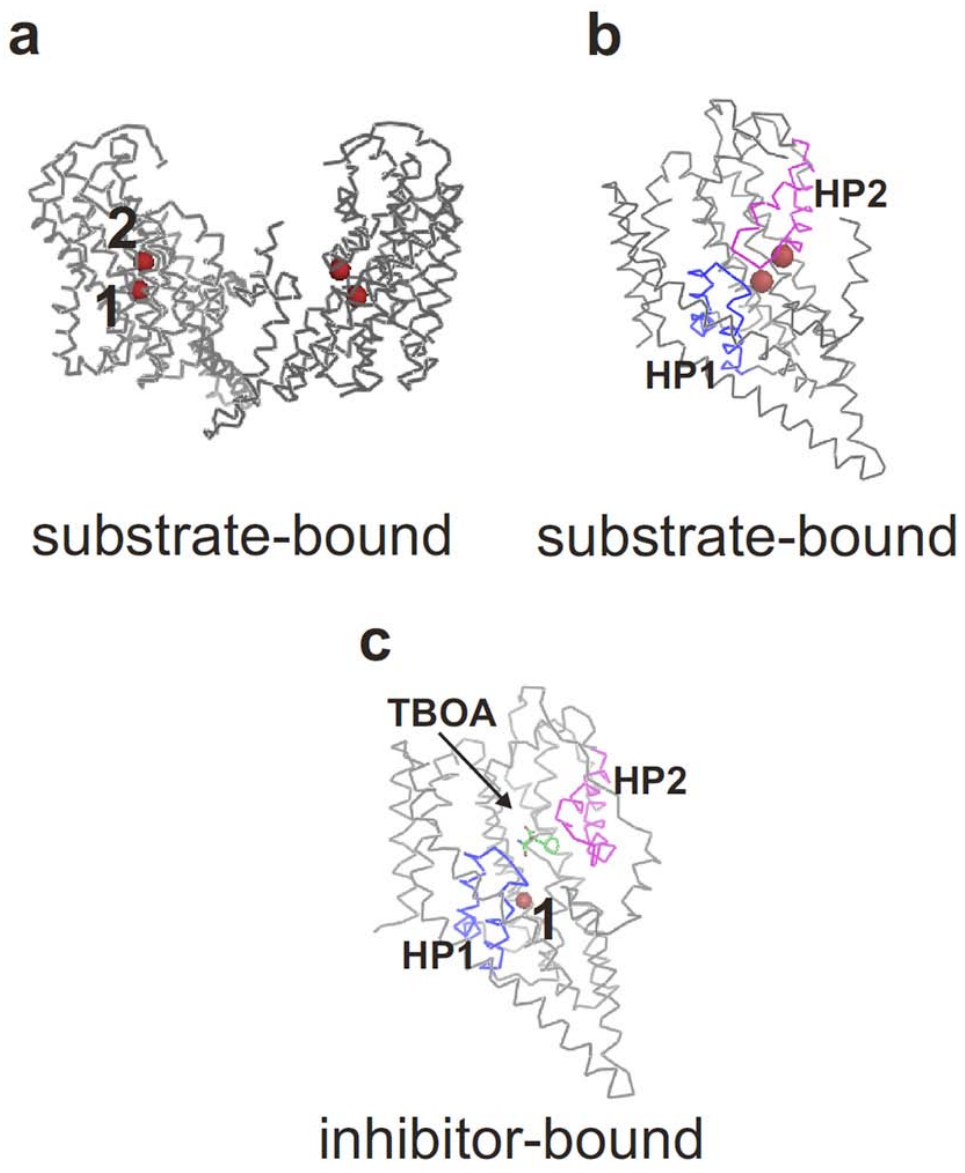

Figure 12. Glt_{Ph} Na^+ binding sites. (a) two subunits with two ion-binding sites (red) labeled 1 and 2. Data was obtained from substrate-bound Glt_{Ph} soaked in Tl^+. (b) close-up view of a single monomer, with the positions of HP1 (blue) and HP2 (violet) shown. As in (a), two Tl^+ sites (red) are observed. (c) Only one (1) Tl^+ binding site is observed when Glt_{Ph} is bound by TBOA. Site 2 is disrupted by the steric restrictions of HP2 (violet) due to bound TBOA (green molecule).

established the electrogenicity of Glt_{Ph} aspartate transport using Glt_{Ph} reconstituted into liposomes (Ryan and Mindell, 2007). Briefly, if aspartate uptake in Glt_{Ph} is electrogenic, then this charge movement should quickly generate an electrical potential across the membrane and inhibit further transport. Indeed, the use of K^+ ionophore valinomycin was shown to dissipate the aspartate-uptake induced electrical potential, increasing the initial rate of transport compared to uptake in the absence of valinomycin. In conducting these experiments however, it was noted that a quite substantial amount of transport was observed even in the absence of valinomycin. The amount of uptake exceeded what would be expected based on simple calculation of the amount of charge movement required to further inhibit transport, and therefore a chloride conductance was hypothesized. Indeed, the removal of extracellular chloride was shown to decrease the initial rate of transport significantly in the absence of valinomycin, suggesting Glt_{Ph} has a chloride conductance. This conductance was deemed uncoupled because even in the absence of chloride, aspartate uptake was still observed, demonstrating that chloride is not stoichiometrically coupled to aspartate uptake. This uncoupled chloride conductance was subsequently shown to have a selectivity sequence similar to the EAATs (Billups et al., 1996; Wadiche et al., 1995a; Wadiche and Kavanaugh, 1998), with NO_3^- and I^- supporting greater initial rates of transport than Cl^- or Br^- due to the increased permeability of these ions and greater dissipation of membrane potential.

Because a chloride conductance was observed in Glt_{Ph}, it was of interest to know whether the structural features of Glt_{Ph} that promote chloride conductance are similar to those found in EAATs. A mutation in EAAT1 (S103V) was previously shown to alter chloride conductance without affecting glutamate uptake (Ryan et al., 2004). The homologous mutation in Glt_{Ph} (S65V) also revealed an alteration in chloride conductance, resulting in initial transport rates that were similar whether or not extracellular chloride was present (Fig. 13). This result indicates that in the Glt_{Ph}-S65V mutant extracellular chloride was incapable of dissipating the transport-generated membrane potential. Similarly to the EAAT1-S103V mutant, no measurable effect was seen on Na^+-dependent aspartate transport. Taken together these experiments provide the rationale for the use of Glt_{Ph} as a model to better understand the structural basis of chloride permeation in EAATs.

3.2.5. Crystallization of Glt_{Ph} in the inward-facing state

During the process of writing this thesis, a new crystal structure proposed to capture the inward-facing state of Glt_{Ph} was published (Reyes et al., 2009). To accomplish this, the authors made use of a previous study conducted in EAAT1 (Ryan et al., 2004), in which a spontaneous disulfide bond was reported to be formed between two residues which in previous crystal structures were located quite far (~25 Å) apart (Fig. 14). For these residues (364 and 55 in Glt_{Ph}, located on HP2 and TM2 respectively) to come into close enough proximity to form a disulfide bond, clearly a substantial conformational change was required, leading the authors to suppose that this conformational change could represent the

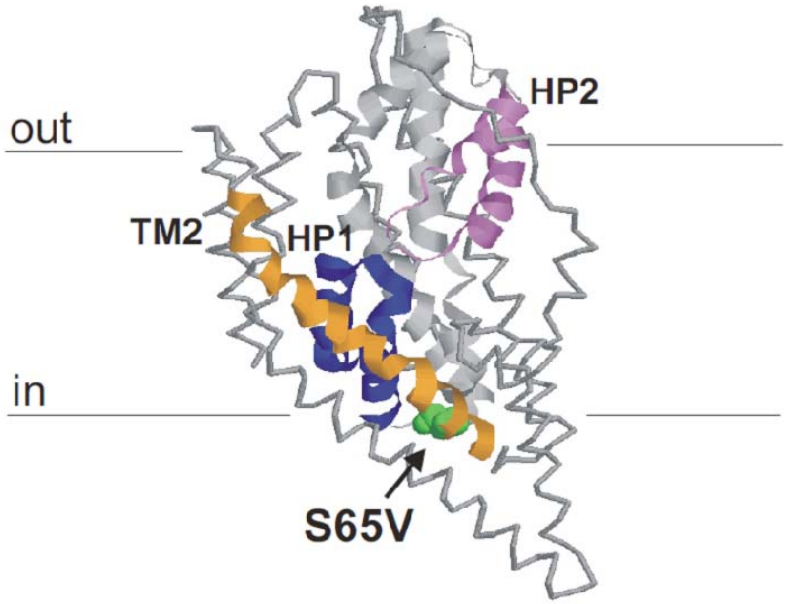

Figure 13. Altered anion conductance in Glt_{Ph}-S65V. In EAAT1, it was previously reported that the S103V mutation strongly affected anion conductance without measurable effects on glutamate transport (Ryan et al., 2004). The equivalent residue in GltPh (S65, green), when mutated to valine, showed a similar effect, thus implicating TM2 (orange) in participating in the anion conductance. HP1 (blue), HP2 (violet).

inward-facing state of the transporter. The authors therefore generated Glt_{Ph}(K55C/A364C) double mutants, and SDS-PAGE analysis revealed a higher electrophoretic mobility band corresponding to intra-molecularly linked Glt_{Ph} monomers, subsequent to exposure of these mutant proteins to copper 1,10-phenanthroline (CuPhen). These results were obtained in both detergent-solubilized protein, as well as in unpurified protein within *E. coli* crude membranes. In addition, crosslinking occurred both the presence and absence of Na^+ and $_L$-asp. This cross-linking reaction was not complete (evidenced by the presence of two SDS-PAGE bands) in the presence of CuPhen, and therefore was not quite good enough for crystallographic analysis. This lead the authors to test the use of Hg^{2+}, which in both the presence and absence of Na^+ and $_L$-asp, and in both detergent and crude membranes, yielded an essentially complete crosslinking within seconds, sufficient for crystallography.

In the Glt_{Ph}(55C/364C-$_{Hg}$) crystal structures (Reyes et al., 2009), the measured distance between β-carbon's on residues 55C and 364C is only 5-6 Å, whereas as mentioned above, the β-carbon distance between these residues in the aspartate-bound structure (Yernool et al., 2004; Boudker et al., 2007) is 25 Å. The Glt_{Ph}(55C/364C-$_{Hg}$) crystal structure thus clearly indicates the occurrence of a large conformational change which brings these residues into close proximity. Examination of the Glt_{Ph}(55C/364C-$_{Hg}$) crystal structure reveals that two structural features are readily apparent, and these represent major advances in the understanding of how glutamate transporters function.

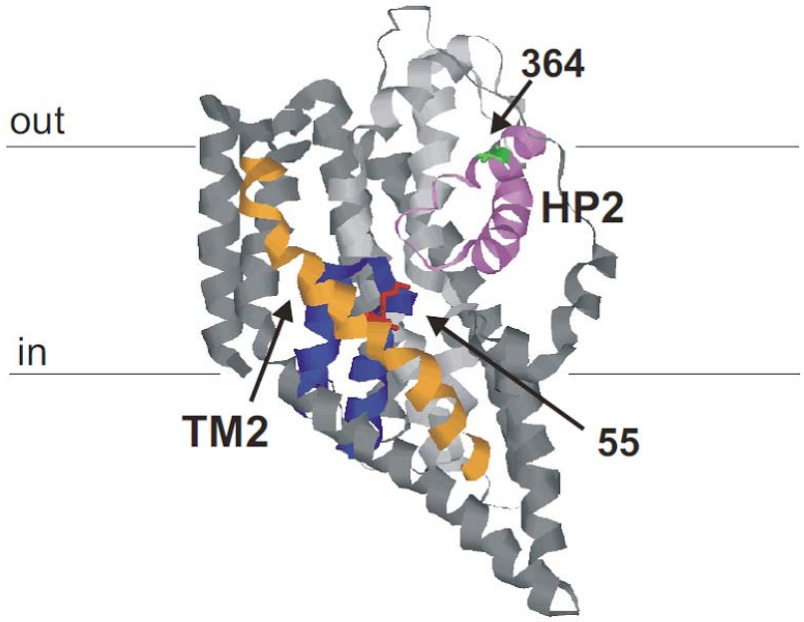

Figure 14. Proximity of residues implicated in disulfide bond formation. A single Glt_{Ph} monomer in the occluded state (Yernool et al., 2004) is shown, with residues 364 (green) and 55 (red) located ~25 Å apart. These equivalent residues in EAAT1 were previously (Ryan et al., 2004) shown to form disulfide bonds when mutated to cysteines, implicating a substantial conformational change. TM2 (orange), HP1 (blue), HP2 (violet).

The first is that there is a large displacement of the substrate binding site in the substrate-bound Glt_{Ph}(55C/364C-$_{Hg}$) crystal structure, as compared to the substrate-bound WT Glt_{Ph} crystal structure (Fig. 15a,b). In the Glt_{Ph}(55C/364C-$_{Hg}$) structure, the substrate-binding site is located approximately 5 Å from the intracellular solution, while in the WT structure (Yernool et al., 2004), the substrate-binding site is located approximately 5 Å from the extracellular solution. This displacement is shown (Reyes et al., 2009) to be largely due to movement of TM domains 3, 6, 7 and 8, and HP1 and HP2, which move essentially as a group, and thus are referred to as the "transport domain". On the other hand, TM domains 1, 2, 4 and 5 undergo very little movement, as can be observed by comparing crystal structures of these domains under different conditions (Fig. 16 a,b,c) (ie., outward-facing substrate-bound (Yernool et al., 2004), outward-facing inhibitor bound (Boudker et al., 2007), and inward-facing substrate bound (Reyes et al., 2009). Thus, these transmembrane domains (1, 2, 4, 5) are referred to as the "trimerization domain". It was hypothesized therefore that the trimerization domain is stabilized in the membrane, and counterbalances the movements of the transport domain. Due to the location of the substrate binding site and position of HP1 and HP2 in the Glt_{Ph}(55C/364C-$_{Hg}$) crystal structures (Fig. 15b), it was proposed that this structure represents the inward-facing, occluded state, and that HP1 must therefore undergo further conformational change to allow for intracellular ions and substrate dissociation, similar to extracellular movements of HP2 (Fig. 17) (Boudker et al., 2007; Huang and Tajkhorshid, 2008; Shrivastava et al., 2008).

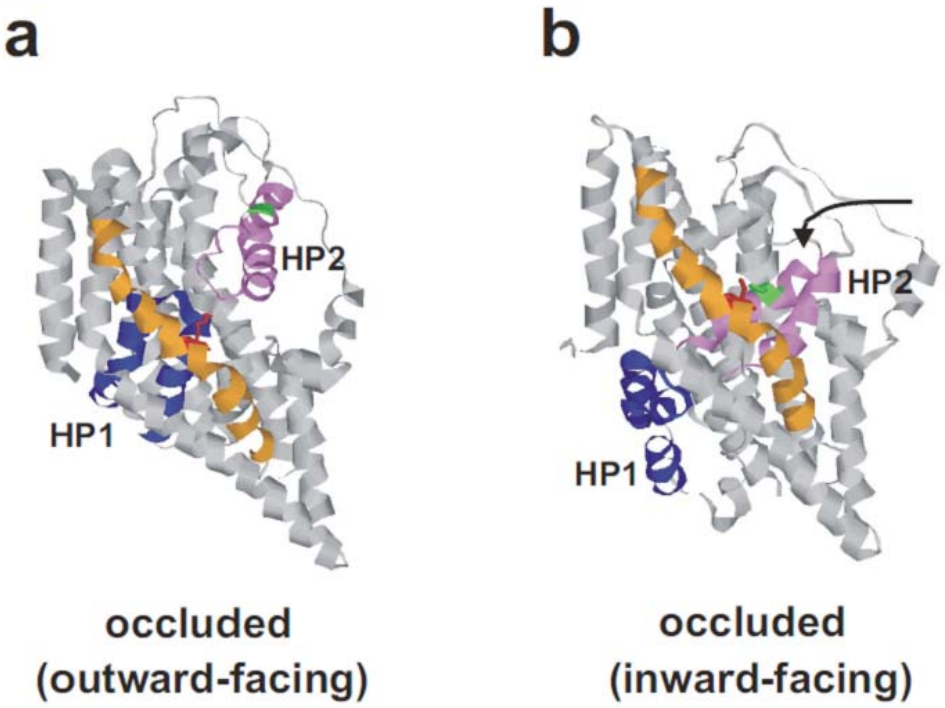

Figure 15. The inward-facing state and "transport domain". In the (a) occluded, outward-facing state, residues 364 (green) and 55 (red) are far apart, HP2 (violet) is nearly parallel to the membrane, and HP1 (blue) reaches up from the cytoplasm. Crosslinking (b) residues 364C and 55C renders the transporter in the occluded, inward-facing state, with HP2 moving into the middle of the protein (arrow), occupying space previously occupied by HP1. A single monomer with TM2 colored orange is shown for clarity.

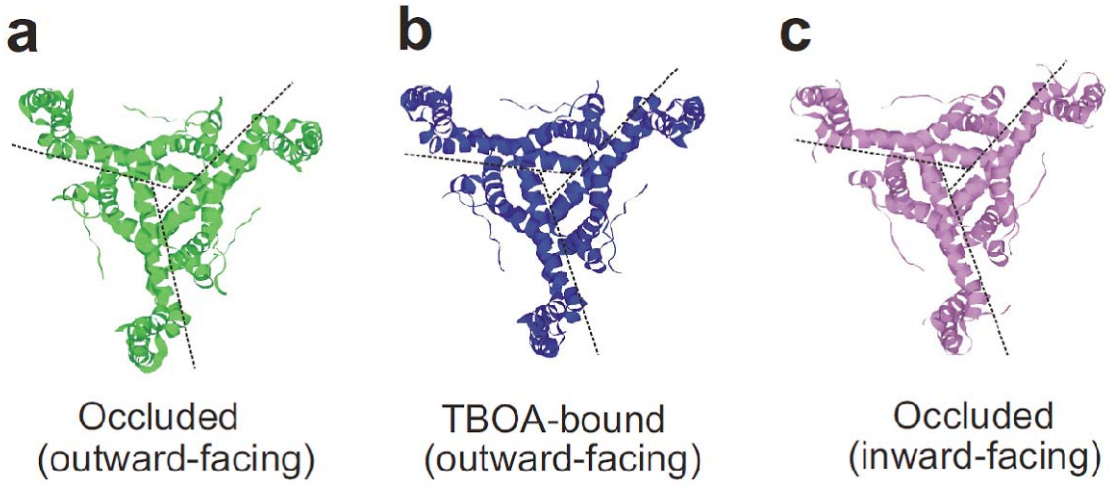

Figure 16. Trimerization domain. Extracellular view of the trimerization domain (TMs 1, 2, 4, 5) in the (a) occluded, outward-facing state, or substrate-bound (Yernool et al., 2004), (b) TBOA-bound, outward-facing state (Boudker et al., 2007), and (c) the Glt_{Ph}(364C/55C-$_{Hg}$) inward-facing, occluded state (Reyes et al., 2009).

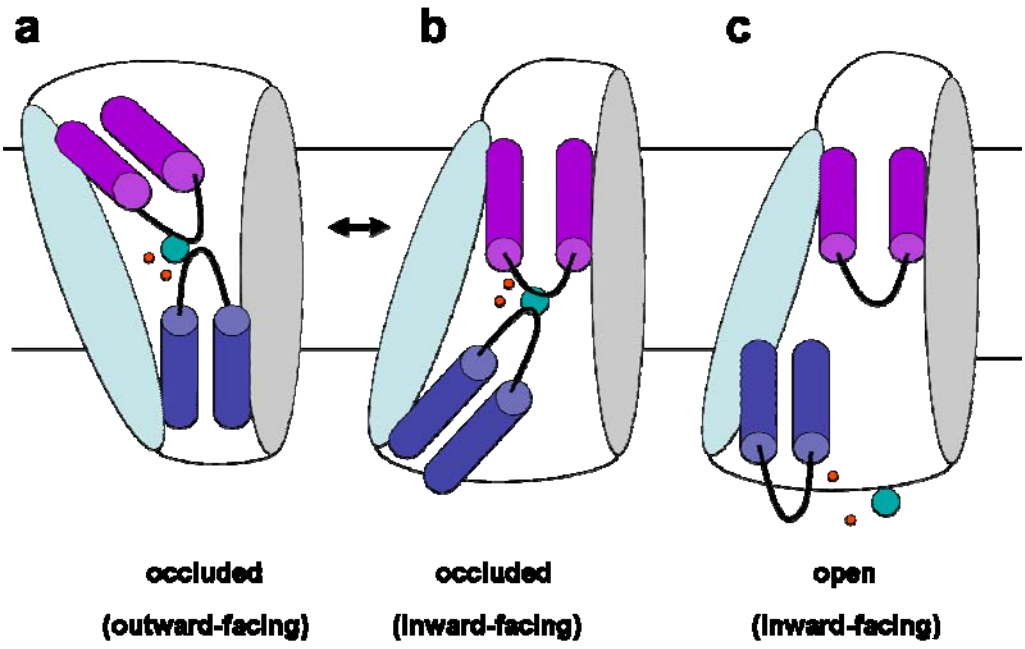

Figure 17. Transport model. (a) Subsequent to substrate and ions binding, HP2 (violet) closes, representing the outward-facing, occluded state. Conformational change consisting primarily of the transport domain (light blue, violet, and dark blue) renders the transporter in (b) the inward-facing, occluded state. (c) subsequent conformational change of HP1 (dark blue) is proposed to allow intracellular ions and substrate dissociation. Shown is a single monomer. Sodium ions are red, substrate is turquoise, and the trimerization domain is grey.

Interestingly, at nearly the same time as the Glt_{Ph}(55C/364C-$_{Hg}$) crystal structure came out, a modeling study was published also suggesting a conformation for the inward-facing state of Glt_{Ph} (Crisman et al., 2009). Modeling was based on the observation that there are two inverted repeats per Glt_{Ph} transporter monomer, and thus swapping of the extracellular conformations for the intracellular conformations could yield an inward-facing state of Glt_{Ph}. Strikingly, the models are in very close agreement with the crystallography results of Glt_{Ph}(55C/364C-$_{Hg}$) and suggest further that inverted-topology repeats are crucial aspects of transporter structure, consistent with previous analysis (Forrest et al., 2008).

3.3. Summary and conceptual overview of transport cycle

Taking into account all of the previous discussion of the vast number of studies undertaken to elucidate the structural basis of glutamate transport, a brief summary will be presented here, followed by a conceptual view of how the glutamate transporter structurally accomplishes uptake.

Major movements inferred from structural studies

The C-terminal domain of individual transporter subunits houses the substrate and ion binding sites, and is nestled in the center of an N-terminal cylinder. This N-terminal cylinder, with the exception of TM3, undergoes very little movement and appears to act as a stability platform in the membrane for the more dynamic C-terminal region (and TM3). Conformational changes in this C-terminal domain

likely underlie the main structural rearrangements required for substrate uptake. Specifically, these conformational changes appear to encompass 1) movement of HP2 that allows for the extracellular binding, and the subsequent enclosing, of ions and substrate within the C-terminal core. 2) A conformational change induced upon the binding of substrate to the transporter that is somehow transduced into a movement of TM2, thus gating the anion conductance. 3) A rather large, concerted movement of the entire C-terminal domain (and TM3) vertically through the membrane in order to place the substrate and ion binding sites closer to the cytosol. Importantly, it appears as if this concerted movement occurs with both HP2 and HP1 in a "closed" conformation. 4) A "proposed" movement of HP1 subsequent to the concerted movement of the C-terminal domain that exposes the substrate and ion binding sites to the cytosol. This movement promotes the release of cotransported ions and substrate, thus creating the binding site for the potassium ion. 5) Binding of K^+ promotes a final conformational change that reorients the transporter to the extracellular-facing state, where it can repeat the cycle to accumulate intracellular glutamate. Of course, because the bacterial glutamate transporter does not require K^+ for the reorientation step, a H^+ ion for forward transport, and may only require two cotransported Na^+ ions (as opposed to three for mammalian transporters), there are certainly going to be differences in the mechanistic details of transport between bacterial and mammalian transporters. Nonetheless, the majority of data on structural movements in mammalian transporters is consistent with the

view provided from crystal structures of bacterial transporters, and thus the overall structural movements are likely to be shared.

With the assumption that the majority of structural movements involved in coupled transport are 1) gate movements and 2) a concerted movement of the C-terminal domain, next will be presented an unreferenced, conceptual overview of the mechanistic details of how glutamate transporters accomplish uptake, based on the vast amount of papers presented in this thesis section. Included in this discussion will be the principles underlying "coupled" transport.

Conceptual overview of the glutamate transport cycle

In the brain, neurons have a resting potential around -65 mV, set mainly by the K^+ leak conductance, and are bathed in a solution of high extracellular Na^+. Studies on glutamate transporters have shown that at least one Na^+ ion binds prior to glutamate, in a voltage-dependent fashion (Wadiche et al., 1995b). A transporter in the outward-facing state therefore, in the absence of ions and substrate (or apo-state), would likely very rapidly bind Na^+ due to the high extracellular concentration of Na^+ and the driving force for Na^+ to bind the transporter due to the membrane potential. Where does this Na^+ ion bind? Due to the voltage-dependent nature of the binding of this Na^+ ion, it likely binds deep within the protein, below the substrate-binding site, coordinated by a negatively charged aspartate residue(s) on TM7 or TM8 and backbone carbonyl oxygens (Boudker et al., 2007; Wadiche et al., 1995b). The next step in the transport cycle I would predict is the binding of the second Na^+ ion. Because Na^+-binding to the

transporter has been shown to induce conformational changes in HP2 (Larsson et al., 2004), I would suggest that the binding of these first and second Na^+ ions result in a conformational change in HP2, which positions residues to be in the optimal positions for glutamate-binding.

In my view, the next step is the binding of a proton to the transporter. The residue implicated in proton-binding is a glutamate residue on TM7 (Grewer et al., 2003), and the binding site for the H^+ is presumed to be the γ-carboxylate. The pKa of the γ-carboxylate of glutamate in aqueous solution is around 4.2, thus in order for protonation to occur, this pKa must be highly altered in the context of the protein environment. Consistent with this view, it has been shown in glutamate transporters that the pKa of the ionizable residue is ~8 in the absence of substrate (Watzke et al., 2000). It is possible that the binding of the first two Na^+ ions causes a slight conformational change that subtly alters the environment of this glutamate residue, thus changing the pKa of the γ-carboxylate and allowing for H^+ binding. Interestingly, it was also shown that this pKa shifts to ~6.5 when the substrate binding site is exposed to the cytoplasm, which would release the proton (more on this below) (Watzke et al., 2000).

The binding of the first two Na^+ ions and a proton therefore in effect serves to "create" the binding site for glutamate. This idea is backed up by the fact that glutamate cannot bind the transporter in the absence of Na^+ (Larsson et al., 2004). Also important for glutamate binding to this site is the conserved arginine residue on TM8 that has been shown to likely interact with the gamma carboxyl group of glutamate (Bendahan et al., 2000; Boudker et al., 2007). Finally, the

binding of glutamate creates a binding site for the third and final sodium ion (Kanai et al., 1995; Menaker et al., 2006; Watzke et al., 2001), with the Na^+ ion most likely interacting with the α-carboxyl group of the bound glutamate. With substrates and ions bound, the extracellular gate closes, and the whole C-terminal region undergoes a movement that brings the substrate and ion binding sites closer to the cytoplasm (Reyes et al., 2009). At this point, the new environment causes substrates and ions to become destabilized, starting with the first Na^+ ion, which was voltage dependent. As mentioned above, the pKa of the proton-bound glutamate changes in this intracellular environment to ~6.5, which results in the proton not being stably bound to the transporter any longer (Watzke et al., 2000), which in turn also disrupts the affinity of the bound glutamate. Somehow this destabilization of bound ions and substrates leads to a movement of HP1, which allows for the release of ions and substrate to the cytoplasm, though exactly how this occurs is yet to be elucidated. At this point in the transport cycle, with HP1 open to the intracellular side, the binding of a potassium ion occurs. Interestingly, the same glutamate residue implicated in proton binding is also implicated in the potassium return step (Grewer et al., 2003; Kavanaugh et al., 1997). Most likely, the acidic glutamate residue is not responsible for *binding* of K+ to the transporter (Grewer et al., 2003), but instead the negative charge on the glutamate residue controls the *rate* of K+-dependent conformational change. It appears that the negative charge is one of the two negative charges necessary for counterbalancing the positive charge of the potassium ion to facilitate its movement across the membrane barrier.

This mechanistic scheme nicely reveals the principles of coupled transport. By coupling glutamate uptake to the cotransport of three Na^+ ions and a proton, and to the counter transport of a K^+ ion, neurons make use of preexisting free energy stored in ion gradients to drive glutamate uptake against its concentration gradient, from the extracellular space to the intracellular space. In theory, this is a simple idea to understand; to move a charge across an electrical field requires a certain amount of work. The same applies to moving a molecule against a concentration gradient. So in neurons the amount of energy required (ΔG) to move a charge against its concentration and electrical gradient will simply be the sum of these electrical and chemical energies. Clearly, the ΔG for glutamate to move against both an electrical and chemical gradient would be insurmountable unless the amount of energy required to take up glutamate into the cell is compensated for by an outside input of energy. Na^+ and K^+ ions moving down their concentration and electrical gradients provide this energy by offsetting the ΔG for glutamate uptake, and making the overall process of glutamate uptake favorable (overall negative ΔG).

While this is a simple concept to grasp, the ability of biological proteins to accomplish this task is remarkable, and involves both coupled *binding* as well as the coupled *transport* step. For instance, as was just seen in the brief discussion of the mechanistic scheme of glutamate transport, glutamate cannot bind prior to at least one sodium ion and a proton, and the third sodium ion cannot bind prior to the glutamate molecule binding. Therefore, the binding order of ions and substrate are inextricably coupled to one another (easily observed by the simple

fact that changing the extracellular concentration of sodium ions changes the binding affinity for glutamate (Boudker et al., 2007)). Only after all substrate and ions have cooperatively bound is the overall ΔG negative enough to drive glutamate uptake against its concentration gradient into the cell. Because all of the ions that take part in coupled binding are also transported, this is termed a "coupled" transport process. The molecular determinants of this process are the subject of this thesis.

Conclusion

This discussion has presented a brief overview of the binding order of ions and substrate in the mammalian glutamate transport cycle, and has provided an explanation as to the basics of "coupled transport". As mentioned above, the bacterial transport cycle will be different, as substrate uptake is not coupled to cotransport of protons, or to counter transport of potassium ions. However, it is highly likely that many mechanistic structural aspects of transport are conserved between the mammalian and bacterial transporters, thus validating the use of Glt_{Ph} as a model to study conformational changes associated with substrate uptake. In the conclusion of this thesis I will present a model of how we think the bacterial glutamate transport cycle works, in comparison to the mammalian transport cycle presented here.

II. Chapter 2

Materials and Methods

1. Overview

The objective of our research is ultimately to reveal the precise molecular mechanism(s) whereby glutamate uptake is accomplished by glutamate transporters. As mentioned in Chapter 1, numerous electrophysiological studies have provided a wealth of information regarding the substrate and ion-binding sites in mammalian glutamate transporters, and have shed light on the conformational changes accompanying the glutamate transport cycle. While all of these studies are invaluable in our understanding of glutamate transporter function, we wanted to develop an alternative approach for several reasons. First, only so much information can be obtained from single-cysteine mutagenesis accessibility studies. Certainly, secondary structure, and regions of proteins in which accessibility of a particular residue changes upon substrate/ion-binding, can be examined by this methodology. However, the use of this approach does little to provide information on whether the accessibility of a particular residue changes due to movement of the protein domain associated with that residue, or rather, whether other protein domains are moving, relative to the amino acid residue of interest. Therefore, experimental approaches that provide information on how protein domains change relative to each other during, for instance, glutamate uptake, are more informative for deciphering

conformational changes. In this light, the formation of disulfide bonds between two introduced cysteine residues, as well as FRET studies with the ability to determine the distance between two covalently labeled cysteine residues, enable protein-domain proximity determination, and how substrate/ion-binding, etc., can result in proximity changes.

While powerful techniques, these approaches too have limitations. Although the formation of a disulfide bond indicates two cysteine residues in close proximity, a change in the ability of those residues to form disulfide bonds, for instance in response to substrate- or inhibitor-binding, is more difficult to interpret. Substrate- or inhibitor-binding may simply block access of an oxidizing agent to the cysteines of interest, or may subtly change bond angles between cysteine side-chains without altering the distance and without measurable conformational change between cysteine residues.

Similarly, FRET is useful for measuring relatively long distances and large conformational changes, but is less useful for measuring small distances and small conformational changes. The reason for this is because for donor and acceptor fluorophores separated by about 0-30 Å, the efficiency of energy transfer is near 100% (Stryer and Haugland, 1967). In this range it is therefore not possible to discern precise distances between fluorophores, which also negates the ability to determine conformational changes occurring in this distance range. In the ~30-80 Å range however, the efficiency of energy transfer decreases by the 6^{th} power of the distance separating the donor and acceptor fluorophore, enabling estimation of the relative distance between pairs of donor

and acceptor fluorophores (Selvin, 1995; Stryer and Haugland, 1967). In this range it is therefore also possible to measure conformational changes that involve distance changes between donor and acceptor fluorophores.

Our lab previously conducted a FRET study on the mammalian transporter EAAT3, but it did not reveal much information regarding conformational changes associated with glutamate transport (Koch and Larsson, 2005). Because crystal structures of the bacterial glutamate transporter homolog Glt_{Ph} (Boudker et al., 2007; Yernool et al., 2004) were obtained with purified protein however, this pointed toward the possibility of utilizing a different approach, namely double site-directed spin-labeling electron paramagnetic resonance (DSDSL-EPR) spectroscopy, to measure distances and conformational changes in Glt_{Ph}. Importantly, this approach could allow for the accurate determination of distance changes in the range of 8-25 Å, rather than the 30-80 Å for FRET. Also, this technique could be performed in the native environment of a lipid bilayer, thus allowing for the possibility of expanding on information provided by crystal structures by obtaining measurements on conformational states for which no crystal structures exist.

Work thus described in this thesis consists of the development of the technique of DSDSL-EPR spectroscopy using purified Glt_{Ph} protein reconstituted into liposomes, and the subsequent use of this technique to describe the small conformational changes associated with the binding of ions, substrate, and inhibitor to Glt_{Ph}.

2. Introduction to electron paramagnetic resonance spectroscopy

2.1. Overview

Electron paramagnetic resonance (EPR) spectroscopy, combined with site-directed spin labeling (SDSL) is a powerful method for investigating protein structure and dynamics. The technique involves introducing a cysteine residue(s) at a protein site(s) of interest, and covalently labeling with a sulfhydryl-specific spin label containing a stable free radical, which serves as the EPR detectable probe (Fig. 1). Because many biological samples do not normally contain unpaired electrons, the technique is highly sensitive and specific, enabling a broad range of protein structural features to be investigated. Briefly, SDSL-EPR can provide information about 1) the mobility of the spin label, in turn providing information about the structural location of the label (Columbus and Hubbell, 2002), 2) accessibility of spin-labeled residues to very small probes such as Ni^{2+} and O_2 (Malmberg and Falke, 2005; Oh et al., 2000), and 3) the distance between two spin labels through the use of double site-directed spin labeling (DSDSL) (Steinhoff, 2004).

As mentioned above, the work in this thesis is comprised primarily of the use of DSDSL-EPR to measure distances between protein domains (Fig. 2) in the bacterial glutamate transporter homolog Glt_{Ph}, and how those distances change in response to ion-, substrate-, and inhibitor-binding. In that sense, our work makes use of the technique of EPR, and is not therefore a body of work on the

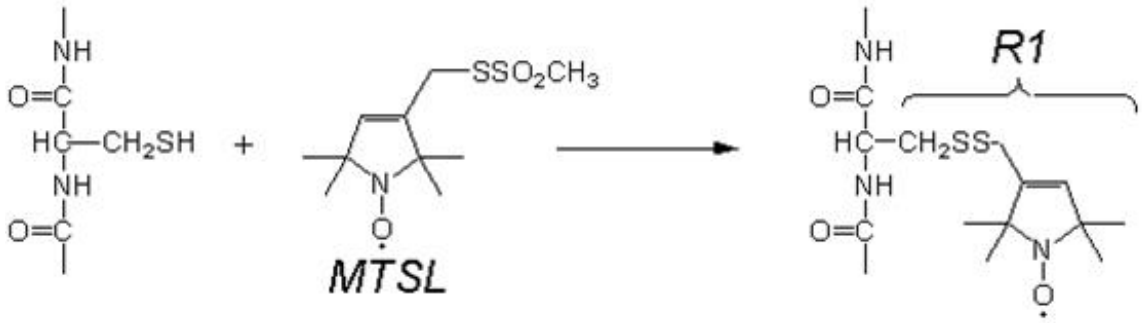

Figure 1. Site-directed spin labeling (SDSL). The basic strategy of SDSL involves substituting a cysteine residue for a native residue of interest, followed by modification of the reactive SH group with a selective spin-label reagent. The most commonly employed reagent is a methanethio-sulfonate (MTS) derivative that generates a disulfide-linked nitroxide side chain, designated R1. It is the free electron that serves as the EPR detectable probe (Klug and Feix, 2008).

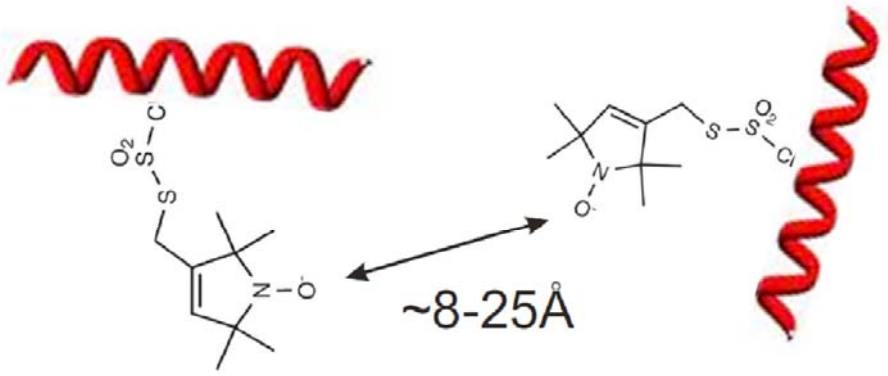

Figure 2. Double site-directed spin-labeling. In our current work described in this thesis, we make use of the fact that in the range of 8-25 Å, distance measurements can be made between two paramagnetic spin labels, due to dipolar interactions between them. The range of 8-25 Å is suitable for measuring the small conformational changes proposed to be associated with glutamate transport (Boudker et al., 2007; Koch and Larsson, 2005).

science of EPR itself. However, to fully understand our work and its implications, a general understanding of the theory behind EPR is important and will be briefly discussed. Following this introduction to EPR spectroscopy, we will present our experimental methodology. In subsequent chapters the results from our studies using DSDSL-EPR will then be presented along with a discussion and significance of our findings.

2.2. Brief Theory

2.2.1. Origin of an EPR signal

Spectroscopy is the measurement and interpretation of energy differences between atomic or molecular states. It is possible to measure these energy differences (ΔE) because of a relationship between ΔE and absorption of electromagnetic radiation. Electromagnetic radiation will be absorbed if the difference in energy between a lower energy state and a higher energy state (ΔE) is exactly equal to $h*\nu$, where h is Planck's constant and ν is the frequency of radiation. Thus, in conventional spectroscopy, simply sweeping through frequencies of electromagnetic radiation and observing frequencies which result in absorption provides information on energy differences between two states.

Energy differences studied in electron paramagnetic resonance (EPR) spectroscopy are due to the difference between lower and higher energy states of unpaired, free electrons in the presence of a magnetic field. This energy difference is present because electrons are charged, spinning particles, and thus have associated magnetic moments. In the presence of a magnetic field,

electrons align their magnetic moments in either a parallel or antiparallel orientation; those aligned parallel representing a lower energy state and those aligned antiparallel representing a higher energy state (Fig. 3a). In the absence of a magnetic field, electrons have no preference for either spin state, and thus no energy difference is measurable.

This energy separation (ΔE) induced by an external magnetic field between higher and lower electron energy electron spin states varies directly in proportion to the strength of the applied magnetic field. The energy difference between a lower energy and a higher energy electron spin state is represented by the equation $\Delta E = g\beta H$, where β is the Bohr magneton (value of the intrinsic magnetic moment associated with the spin of a free electron), g is a proportionality constant, and H is the strength of the magnetic field. From this equation it is apparent that the difference in energy between electron spin states is linearly dependent on the externally applied magnetic field (Fig. 3b).

The electromagnetic radiation in EPR spectroscopy induce transitions between the lower and higher energy electron spin states so that the electron spin changes its orientation relative to the magnetic field (parallel to antiparallel). For this to occur, conditions in a sample must be such that the frequency, ν, of the incoming electromagnetic radiation is such that the photon energy, E (equal to $h\nu$) is equal to the energy difference ΔE between parallel and antiparallel spin states resulting from the external magnetic field strength. Under these conditions, absorption of the electromagnetic radiation by the electron will occur, resulting in transitions between the two electron spin states (Fig. 3c-d).

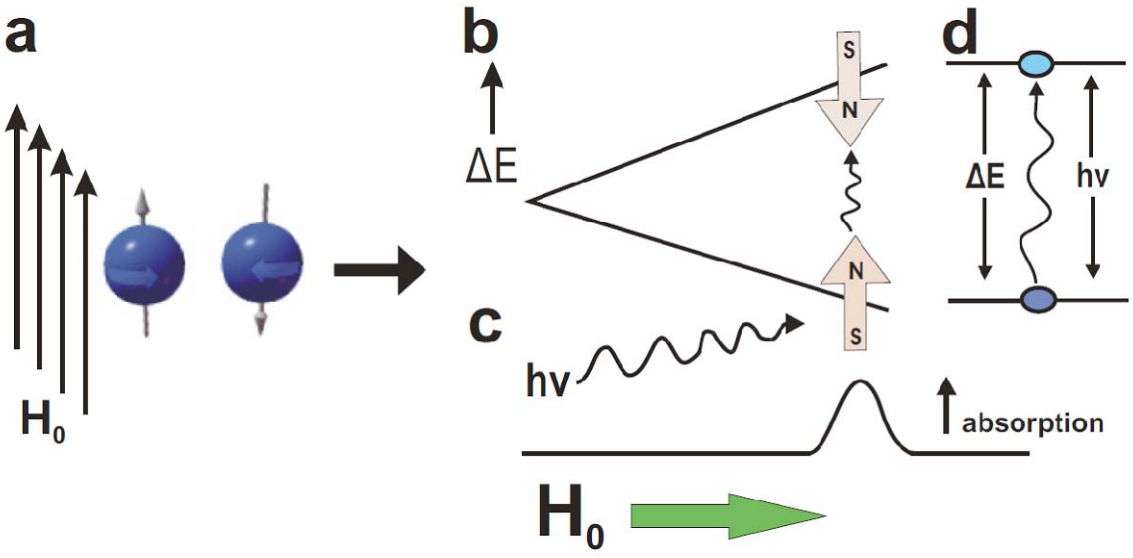

Figure 3. Origin of an EPR signal. (a) electrons have a magnetic moment due to the fact they are charged, spinning particles. Thus, they align parallel or antiparallel in the presence of an external magnetic field. The energy difference between these two states (b) diverges linearly as the magnetic field is increased. In the presence of a constant source of electromagnetic radiation in the form of a microwave (c), the electron will absorb radiation when the energy difference between two electron spin states exactly matches the energy (hv) supplied by the microwave (d).

Thus, there are two means of acquiring EPR spectra. 1) One could apply a constant magnetic field and sweep the electromagnetic radiation frequency, or 2) one could keep the electromagnetic radiation frequency constant, and sweep the magnetic field. In the latter case, electron absorption of the electromagnetic radiation will occur when the magnetic field tunes the spin states such that their energy difference exactly matches the incoming electromagnetic radiation energy. This is in fact the preferred method of obtaining EPR spectra. The reasoning for this is simply due to limitations in microwave electronics, as radiation in the gigahertz (microwave) range is required for electron spin transitions. A resonance cavity is necessary to create standing waves of the microwaves used to induce the electron spin transitions. If the magnetic field were held constant and the microwave frequency were swept, then the resonance cavity would have to be retuned as the microwave frequency changes. In contrast, if the microwave frequency were held constant and the magnetic field were swept, then the resonance cavity only has to be tuned to one microwave frequency. Sweeping the magnetic field and thus holding the microwave radiation frequency constant therefore offers superior experimental performance and precision.

2.2.2. Hyperfine interaction and MTSL spin-label lineshape

Unpaired electrons are very sensitive to local surroundings. Often nuclei of atoms also have magnetic moments, which thereby produce a local magnetic field at the electron. This interaction is known as the hyperfine interaction. The significance of this hyperfine interaction is that it “splits” the EPR signal from a

single electron into a number of signals, depending on the nuclear spin number(s) of a nearby nucleus, or nuclei.

The basis of EPR signal splitting is as follows. As an example, consider a nucleus with a spin number I = ½. A nucleus with a spin number ½ can exist in two states. This nucleus acts as a local magnet, producing a local magnetic field at the electron. Because the nucleus can exist in two states, the magnetic field produced at the electron will either add to, or subtract from, the externally applied magnetic field from the EPR magnet. The nuclear magnetic field which adds to the externally applied magnetic field will result in less externally applied magnetic field required to induce electron resonant absorption of the microwave. In contrast, the opposite will happen for nuclear magnetic fields that subtract from the externally applied magnetic field. In this case, more external magnetic field is needed to induce resonant absorption of the microwave. The result of the interaction of a nucleus with a spin number ½ with a free electron is therefore the splitting of the EPR signal into two absorption peaks. As the spin number (I) of the nuclei near the free electron gets larger, the number of absorption conditions increases accordingly (2I+1).

This discussion is important for understanding the origin of EPR lineshapes in SDSL-EPR studies. In our work, we have utilized the sulfhydryl-specific spin lable MTSL, also known as a nitroxide spin label (Fig. 4a). This spin label contains an unpaired electron localized primarily in the p_z orbital of the ^{14}N atom (Klug and Feix, 2008), and in biological systems the free electron only interacts with this ^{14}N atom. ^{14}N atoms have spin number I = 1, and therefore can exist in

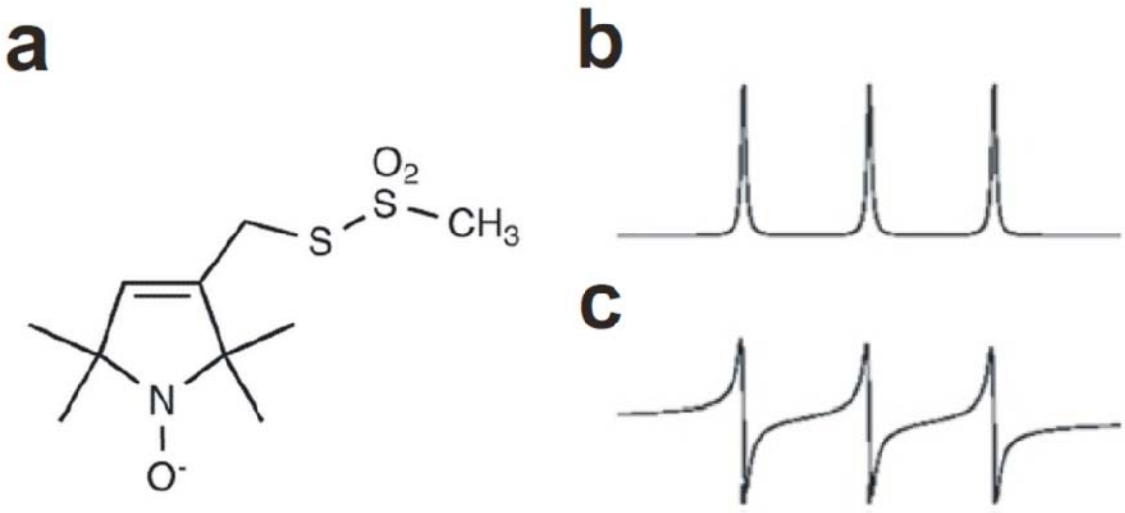

Figure 4. MTSL spin label and hyperfine interaction. (a) for the nitroxide spin label MTSL, the unpaired electron interacts primarily with the nitrogen nucleus (I=1), thus splitting the EPR absorbance spectra into (2I+1) three separate lines (b) corresponding to three different states of the ^{14}N nucleus. (c) To improve signal to noise, magnetic field modulation is applied and signals which do not have the same encoding are filtered out, resulting in an EPR spectra which is a first-derivative of the original absorption spectrum (Klug and Feix, 2008).

three (2I+1) separate nuclear spin states. These three nuclear spin states contribute in three different ways (-1, 0, +1) to the energy of the electron spin states and generates three separate absorption conditions. Thus, these three separate conditions are reflected in the EPR lineshapes recorded in our studies (Fig. 4b). Because the amount of energy absorbed by a sample is quite small, phase sensitive detection is used to enhance the sensitivity of EPR spectrometers. Due to the use of this methodology to detect absorbance of microwave radiation by a sample, the recorded EPR spectra, rather than a simple absorbance peak, is instead displayed as a first derivative of the actual absorbance peak (Fig. 4c) (Klug and Feix, 2008).

2.2.3. Mobility affects lineshapes

One of the most informative types of information that can be obtained from EPR spectra is simply the degree of spin-label motion. The mobility of the spin label affects the EPR spectral lineshape. The main reason for this is that the hyperfine interaction has two different components: an isotropic component, or orientation independent component, and an anisotropic component, or orientation dependent component. To examine this idea more closely, consider the structure of an MTSL nitroxide spin label. The unpaired electron is largely located in the 2p Π orbital that lies along the z-axis. Since the free electron is localized in this orbital, there is a strong directionally dependent (anisotropic) hyperfine interaction (or a-factor anisotropy) along the z-axis, referred to as a_z. In addition, there is a weaker anisotropic hyperfine interaction along the x and y

axis (a_x and a_y). In oriented crystals these parameters can be experimentally determined, by examining the amount of hyperfine splitting when the external magnetic field is successively pointed along each of the three principle axes of a particular molecule. With the magnetic field directed along the z axis the hyperfine splitting is maximum. Therefore, if a spin label in solution is not tumbling rapidly enough to average out anisotropic components in the time required to obtain spectral information, resonance occurs over a wide range of applied field, as different net fields are experienced by the molecule in each of its various orientations. The result is a considerable broadening (and thus decrease in amplitude) of the EPR lineshape (Fig. 5b). On the other hand, the directionally independent (isotropic) hyperfine splitting constant, known as a0, is the value of the coupling constant for the same radical in solution but where rapid tumbling averages the anisotropic contribution to zero, to give $a0 = (1/3)(a_x + a_y + a_z)$. In this case, the result is an orientation-averaged, orientation-independent (isotropic) EPR spectra influenced locally only by the nuclear spin (3 possible states in the case of ^{14}N), and therefore consisting of three equally spaced sharp lines of equal height (Fig. 5a).

In addition to anisotropic hyperfine interaction, or a-factor anisotropy, there is an additional anisotropic component known as g-factor anisotropy, which determines the point about which the spectrum is centered. As mentioned above, the energy difference between a lower energy and a higher energy electron spin state is represented by the equation $\Delta E = h\nu = g\beta H$, where β is the Bohr magneton (value of the intrinsic magnetic moment associated with the spin

of a free electron), g is a proportionality constant, and H is the strength of the magnetic field. Rewriting this equation in the form $g=h\nu/g\beta H$ highlights the fact that g, known as the spectroscopic splitting constant, is important in determining the magnetic field (H) that corresponds to resonance at a fixed frequency. This value of g will vary with the orientation of a molecule with respect to the external magnetic field due to anisotropic components that influence the magnetic field required for resonance. Again, these anisotropic components are expressed as g_x, g_y, and g_z. These correspond to the g factors that are obtained when a magnetic field is oriented along x, y and z-axes of an oriented crystal. If a spin label does not tumble sufficiently rapid to average out these anisotropic effects, the value of g, and thus the field for resonance will be slightly affected. On the other hand, if a nitroxide spin label in solution tumbles sufficiently rapid to average out any anisotropic components, the averaged g factor is given by $g0 = (1/3)(g_x + g_y + g_z)$.

So what is the end-result of these orientation-dependent local magnetic fields? Attaching the nitroxide spin-label to a large protein results in a considerable slowing of the overall motion of the nitroxide label. In this case, tumbling of the large protein is not rapid enough to average out anisotropic (directionally dependent) components in the time required to obtain spectral information. As a result, resonance occurs over a wide range of applied field, thus broadening (and decreasing in amplitude) the EPR lineshape (Fig.5b).

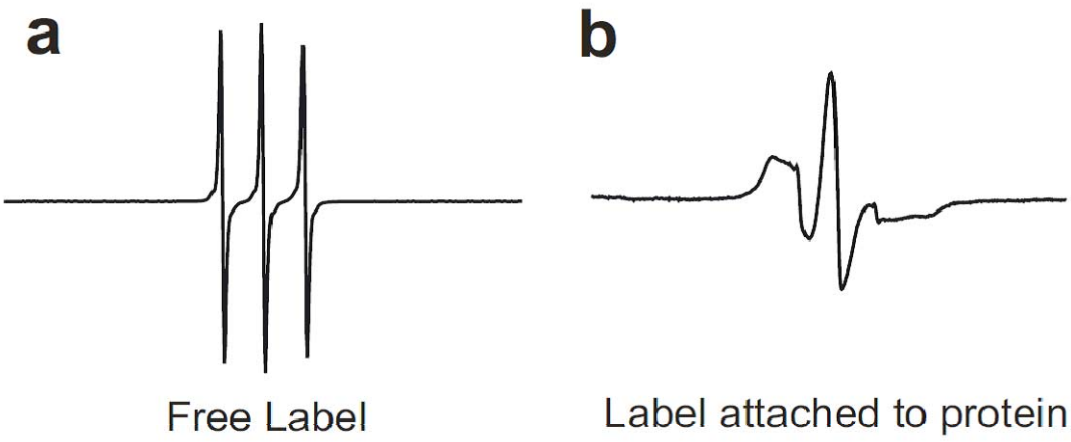

Figure 5. Motional effects of spin label side chain on EPR spectra. (a) For a freely tumbling MTSL spin label in a non-viscous solution, directional (anisotropic) components of the electron's position in relation to the nucleus and external magnetic field are averaged out, resulting in three separate lines of approximately equal height (a), corresponding to the electrons interaction with the three states of the nitrogen nucleus. Attaching MTSL to a large protein (b) results in considerable motional restriction on the EPR timescale and thus directionally-dependent (anisotropic) components contribute to substantial line-broadening and corresponding decrease in peak heights.

While attaching a spin-label to a large protein results in spectral broadening, much more information is encoded in the mobility of the spin-label side chain itself. In fact, in most SDSL applications, it is the motion of the spin label side chain that is of primary interest, as it is this facet of motion that is sensitive to tertiary contacts and protein structure in the local environment of the spin label (Fig. 6a). This aspect of SDSL EPR has been explored thoroughly using T4 lysozyme, in which correlation between side chain mobility and protein structure was examined in detail (McHaourab et al., 1996; McHaourab et al., 1999). Briefly, spin labels on protein surfaces or in loops show a high degree of mobility, reflected in the EPR lineshape by sharper lines, and less overall spectral broadening. Comparatively, spin label interaction with neighboring side chains due to placement in the protein interior or subunit interfaces is represented spectrally by much broader lines due to the lack of side chain motion (less averaging out of orientation-dependent spectral features). This broadening of EPR lineshapes can be analyzed by simply measuring the inverse line width of the central resonance line (ΔH_0^{-1}) (Fig. 6b). Plotting of this parameter as a function of residue number can reveal secondary structure, as periodicity of spin label mobility refers to the sequence of surface, contact, or buried sites (Mehboob et al., 2005; McHaourab et al., 1996; Pfeiffer et al., 1999). In addition, side-chain mobility as reflected in EPR spectral lineshape can also serve as a sensitive monitor of conformational changes, as changes in the relative amounts of motional components indicate a change of protein conformation (Fig. 6b) (Inanami et al., 2005; Perozo et al., 2002; Rink et al., 1997). In our current work,

attaching spin labels to the large (~135 kDa) trimeric protein Glt_{Ph} results in considerable slowing of the rotational tumbling rate of the complex, and thus our signals are quite broad as compared to free-tumbling spin labels. Motional components of our EPR spectra are therefore associated with nitroxide spin-label motion, and in our case changes in the motional components due to binding of ions, substrate, or inhibitor are indicative of conformational changes. These changes in the motional components serve as an internal control in our experiments, because changes in motional components indicate that ion, substrate, and inhibitor are in fact binding to the protein and inducing conformational changes. The extent and directionality of these conformational changes are then determined by measuring the ion, substrate, or inhibitor-induced distance changes between spins, discussed below.

2.2.4. Spin-Spin Distance

SDSL with two spin labels can be utilized to determine distances between two sites in a protein. There are typically two types of experiments that can be performed. The first, known as continuous wave (CW) EPR is capable of extracting distances in the 8-25 Å range. In CW-EPR, distances are determined by analyzing the extent of line-broadening due to dipolar interactions between spins. The second, known as double-electron electron resonance (DEER), is capable of determining distances in the 20-70 Å range. Utilizing DEER, a spin echo is produced that is modulated at the frequency of the dipolar interaction, and distances are determined by examining the oscillations in the spin-echo

amplitude (Fanucci and Cafiso, 2006). In our studies we utilize CW-EPR spectroscopy, the theory of which will be presented below.

In the range of ~8-25 Å, magnetic dipolar interactions between spins result in distance-dependent line broadening and a corresponding decrease in signal amplitude. This distant-dependent line broadening is simply the result of each free electron exerting its magnetic field on the other, thus further affecting the strength of external magnetic field required to induce resonant absorption of microwave radiation (in addition to the splitting of EPR spectral lineshape caused by the nuclear magnetic interaction). Theory for the determination of the distance between two spins is well-developed for two extreme cases: 1) the slow motional limit (Hustedt and Beth, 1999; Hustedt et al., 1997; Rabenstein and Shin, 1995), or rigid lattice condition, typically achieved by freezing the sample, and 2) the fast motional limit, in which rapid rotational diffusion of the protein averages dipolar interactions (molecular weight less than 15 kDa) (McHaourab et al., 1997).

In our current study, we insert two spin labels into a single monomer, in order to make distance measurements between spins. Each monomer is ~45 kDa, which is higher than the 15 kDa cutoff for the fast motional limit. Also, as mentioned above, is the fact that our proteins are functionally assembled as a trimer, thereby making the protein complex ~135 kDa. In addition, we insert these large protein complexes into artificial cells called liposomes, which are 400 nM in diameter. Thus, the molecular rotational tumbling in our systems is extremely

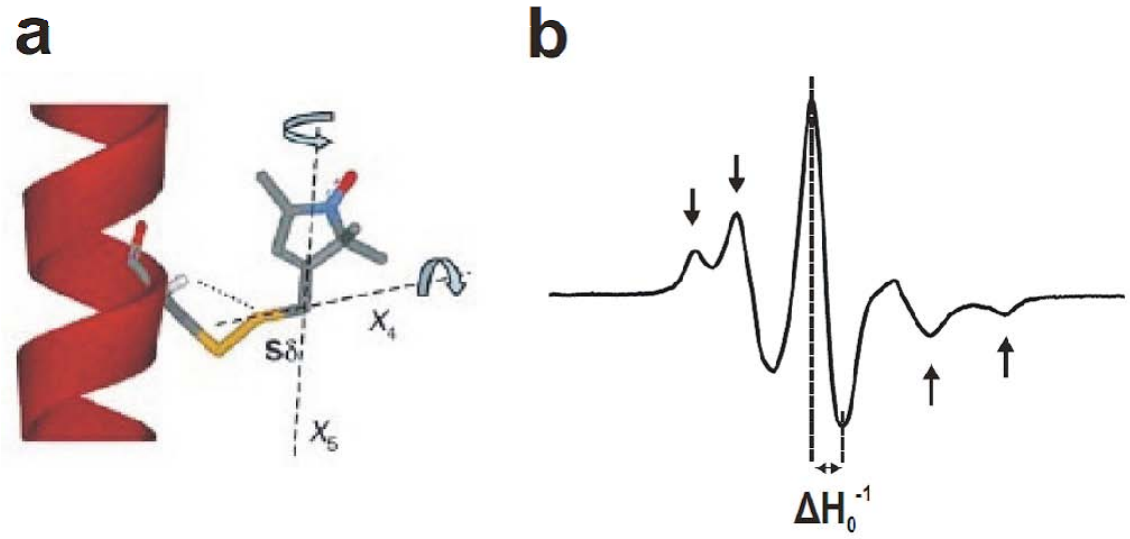

Figure 6. Effect of side-chain mobility on EPR lineshape. (a) at α-helical sites, motion of the MTSL side chain is limited to rotations around the two bonds closest to the nitroxide ring (X_4 and X_5) by an interaction of the Sδ of the disulfide bond with the backbone Cα hydrogen. The degree of relative spin label motion can be quantified by measuring the inverse central line width (ΔH_0^{-1}) (b). The EPR spectrum in (b) is complicated, consisting of multiple spin label components (arrows). Changes in the relative amounts of each of these components, in response to ligand-binding for example, can be used as a sensitive measure of conformational change.

slow, and approaches the rigid lattice condition, even though our samples are not frozen. The main difference between our samples and frozen samples, is the fact that our nitroxide spin label can still undergo side chain rotation at physiological temperature, which means that the rigid lattice condition does not rigorously apply.

Fortunately much work has been done on systems such as these, where the motion of the interspin vector is sufficiently slow so as not to completely average the major dipolar anisotropy, but where each individual nitroxide has motion relative to the protein at physiologically relevant temperature. In 2001, Altenbach and colleagues (Altenbach et al., 2001) evaluated the use of rigid lattice theory to estimate distances at physiological temperatures under conditions in which the molecular rotational tumbling was slow, but where individual nitroxide side chains had rapid internal motions. In this study it was concluded that the rigid lattice theory could be utilized to estimate interspin distances and distributions at physiological temperatures, but that precise distances were difficult to obtain due to the rapid nitroxide side chain motion. They therefore suggested that to gain sufficient information to make structure determinations in spin systems such as these, multiple distance determinations should be utilized, allowing for distance distribution patterns to be recognized. This approach was successfully utilized to monitor conformational changes in rhodopsin (Farrens et al., 1996), and this is precisely what we have attempted to do in our current work. We utilize a system where molecular tumbling is very slow such that the interspin vector is stationary on the EPR timescale while nitroxide mobility still occurs (Fig. 7), and make use

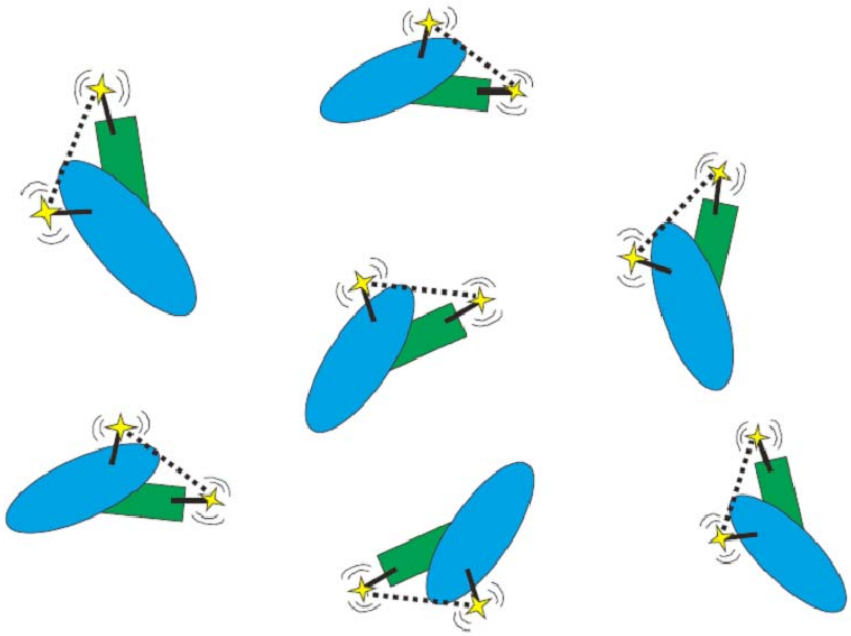

Figure 7. Interspin vector is stationary on EPR timescale. Shown in this figure are two protein domains (green and blue), with spin-labels (stars) attached to each. Proteins are positioned in random orientations due to molecular tumbling, but this tumbling is slow on the EPR timescale. For all different orientations of the protein, the interspin vector (dotted line) does not change much, even though there is the possibility for rapid motion of the individual spin-label sidechains.

of a number of different distance measurements to reveal patterns that can be structurally interpreted.

So how exactly do we make our distance measurements? As just mentioned, there is the possibility of using the rigid lattice theory (Fourier deconvolution methodology) to make distance estimates between two spins separated by 8-25 Å based on the extent of EPR line broadening (Altenbach et al., 2001; Rabenstein and Shin, 1995). However, there is also a simpler way to interpret the distance between interacting spins, which we make use of in our current work. This methodology is based on the simple fact that line broadening is accompanied by a concomitant decrease in signal amplitude. Therefore, the extent of decrease in central peak height observed for an "interacting" spectra normalized to the same spin concentration as a "non-interacting" spectra is indicative of the degree of interaction between two spins (Klug and Feix, 2008) (Fig. 8). For our purposes, this is sufficient to show a directional conformational change, and through the use of multiple measurements such as these we are able to interpret an overall movement of one protein domain relative to others, depending on whether ions, substrate, or inhibitor are bound to the protein. A brief description of precisely how we utilize this methodology to make our distance measurements will be provided below, along with a number of studies making use of the same technique.

There are two types of interactions between spins that can occur; exchange interactions and dipole-dipole interactions. For distances less than 8 Å, exchange interactions, which are electrostatic and operate directly between two

atoms through a single bond (or indirectly through multiple bonds), make precise distance determinations theoretically difficult. For distances greater than 8 Å, dipolar interactions, which are purely magnetic in nature and operate "through space", dominate and are well defined theoretically for the rigid lattice condition. According to this theory, magnetic interactions decrease by the 3rd power of the distance separating spins, and thus interactions between spins separated by >~25 Å are negligible (using CW-EPR). For these combined reasons, distance measurements in EPR are limited to the 8-25 Å range. For our studies, we have chosen to utilize central peak height measurements in order to determine the extent of spin-spin coupling. To make measurements in this fashion, interacting spectra need to be compared to non-interacting spectra. Non-interacting spectra are obtained in our current work by reacting a double mutant with a mixture of 33% paramagnetic spin label and 67% diamagnetic analogue (Fig. 8a). This protocol results in EPR spectra in which the majority of double mutants will only have one paramagnetic spin label, and thus no dipole-dipole interaction is possible. The central peak heights of interacting spectra (100% paramagnetic spin label) can then be compared to the central peak heights of non-interacting spectra, normalized to the same number of spins (Fig. 8b). For distances $\geq$ 20-25 Å, central peak heights for normalized spectra are not different from each other, while central peak heights decrease as distances between spins come closer to one another, as compared to central peak heights in non-interacting spectra (Fig. 8b).

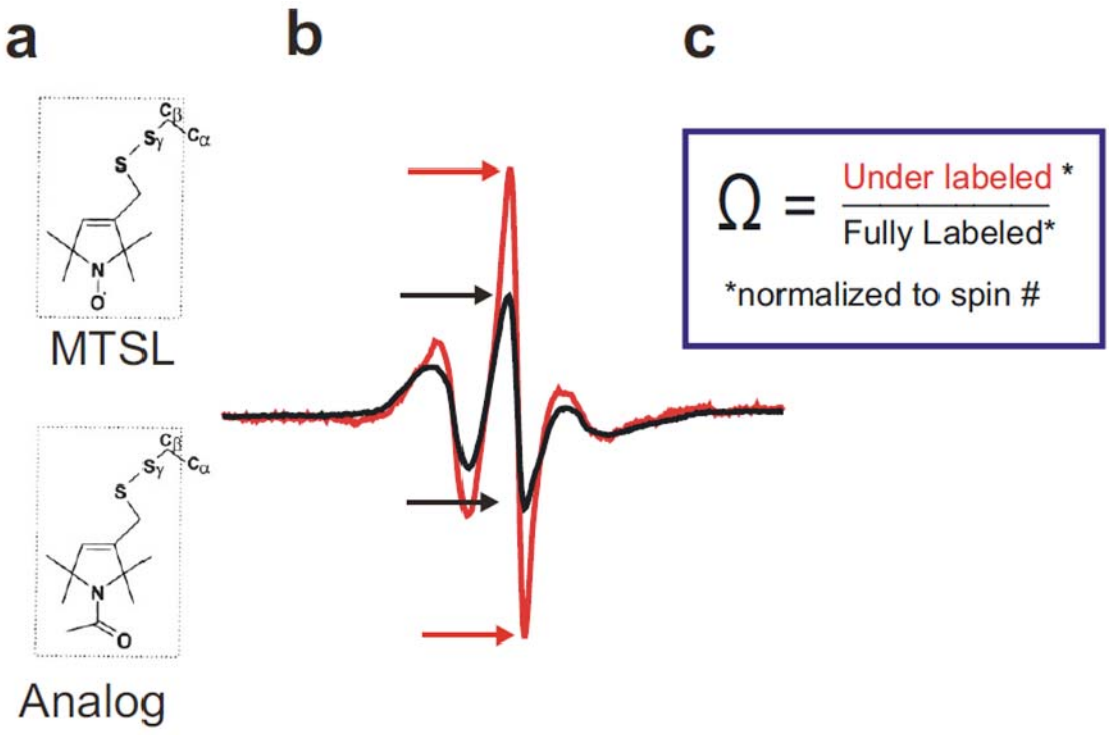

Figure 8. Distance estimates using DSDSL-EPR. (a) Interacting and non-interacting spin-labeled proteins are generated by either 1) labeling with 100% paramagnetic MTSL, or 2) 33% paramagnetic MTSL and 67% diamagnetic analog. Spectra for each condition are then normalized to the same number of spin, and central peak heights are measured (b), in order to obtain an Omega Interaction Parameter (c), indicative of the magnitude of interaction between spins (Perozo et al., 1998).

This use of central peak heights of interacting and non-interacting spins to estimate the magnitude of spin-spin interactions is operationally defined as the omega interaction parameter (Fig. 8c) (Perozo et al., 1998). This parameter has been successfully used to examine conformational changes associated with the gating mechanism of the Streptomyces lividans K^+ channel (SKC1) (Perozo et al., 1998), the open (Perozo et al., 2002) and closed (Perozo et al., 2001) states of the mechanosensitive channel MscL from *E. coli*, and conformational changes in the maltose binding protein from *E. coli* (Austermuhle et al., 2004), to name a few. In many cases, this omega interaction parameter is sufficient to demonstrate directional conformational changes, which is also true in our current work. For higher resolution structural analysis, more quantitative methodology can be utilized but again the resolution of these methods is determined primarily by the distribution of distances between spin labels that arises due to the inherent flexibility of the nitroxide side chain. Future experiments utilizing unnatural amino acids with a more defined location of the free radical, as well as chemically synthesized spin labels without rotational mobility, will contribute to better ability to precisely quantify distances between spins. For our purposes, qualitative measurement of spin-spin interaction is sufficient to gain insight into conformational changes in the bacterial glutamate transporter homolog Glt_{Ph}.

2.3. Experimental Methodology

2.3.1. Site-directed mutagenesis

Site-directed mutagenesis was performed on Glt_{Ph} using the QuikChange Kit (Stratagene, La Jolla, CA). The one endogenous cysteine at position 321 was replaced by an alanine. The double cysteine mutations used for spin labeling were made in this cysteine-less C321A background.

2.3.2. Expression and purification of Glt_{Ph}

Glt_{Ph} (WT, cysteine-less, and all double cysteine mutants) was expressed as His_7 fusion proteins, using the pBCH/G4-7CATS vector and *Escherichia coli* DH5α or TOP10 cells. Proteins were purified essentially as described (Yernool et al., 2004), with the following modifications. Membranes were solubilized with n-dodecyl-β-D-maltopyranoside (Anatrace, Maumee, OH) ($C_{12}M$; final concentration 40 mM) at 4°C for 2 hours with gentle agitation. After solubilization the mixture was diluted to a total volume of ~30 ml ($C_{12}M$ concentration of 10-15 mM) in buffer #10 (20 mM HEPES, pH 7.6, 0.2 M NaCl, and 5 mM glutamate) and centrifuged at 150,000g for 1 hour. 3 ml of Ni-NTA superflow (Qiagen, Valencia, CA) was then added to the supernatant and the mixture was incubated at 4°C overnight. The following day, the Ni-NTA superflow was washed once with buffer #10 followed by protein purification on a BioLogic LP system (BioRad, Hercules, CA). Buffer #10 containing 40 mM imidizole was used to wash the column to remove non-specific protein-binding and then pure Glt_{Ph} was eluted with buffer #10 containing 200 mM imidizole (Sigma, St. Lousi, MO). Protein was either concentrated at this step using an Amicon Ultra concentrator (Fisher Scientific, Pittsburg, PA) (100 kDa cutoff) and stored at -80°C until future use or

immediately spin-labeled as described below. Purification yields were consistently 1-2mgs of Glt_{Ph} per 1L culture.

2.3.3. Spin labeling protocol and isolation of trimeric transporter state

Purified proteins were treated with 500 uM TCEP (Thermo Scientific, Rockford, IL) for 30 minutes at room temperature to reduce oxidized cysteines before being concentrated by an Amicon Ultra concentrator (100 kDa cutoff). Immediately following TCEP treatment, proteins were spin-labeled with a 20:1 ratio of spin-label: protein (mol/mol). Two separate labeling reactions were utilized in order to generate both maximally spin-labeled protein (100% MTSL) (Toronto Research Chemicals, North York, ON, Canada) as well as underlabeled protein (33% paramagnetic spin label MTSL, 67% diamagnetic N-acetylated spin label analog (Toronto Research Chemicals, North York, ON, Canada). Labeling was allowed to proceed for thirty minutes at room temperature before incubating overnight at 4°C. The following day, excess label was removed by FPLC (Superdex 200 10/300 GL, GE Healthcare, Chalfont St. Giles, United Kingdom), which simultaneously allowed the isolation of trimeric transporters and verified overall protein stability. The extent of labeling was determined by whole mass electrospray mass spectrometry (OHSU Proteomics Shared Resource, Portland, OR).

2.3.4. Glt_{Ph} proteoliposome preparation

Pure protein was reconstituted into liposomes as previously described (Ryan and Mindell, 2007), with slight modifications. Briefly, a 3:1 ratio of *Escherichia coli* polar lipids and 1-palmitoyl-2-oleoyl-*sn*-glycero-3-phosphocholine (POPC) (Avanti Polar Lipids, Alabaster, AL) was resuspended in either A) buffer (15 mM HEPES, pH 7.4, 100 mM NaCl, 1 mM mM $MgCl_2$ and 2 mM KCl) containing 1 mM $_{DL}$-TBOA (Tocris, Ellisville, MO) or 0.5 mM $_{L}$-aspartate (Sigma, St. Louis, MO) or B) buffer containing either 100mM Na+ or 100mM K+ in the absence of any substrates. For protein reconstitution we typically used 4 mg of lipid for each condition and 250-500µg protein. Proteoliposomes were either A) concentrated by centrifugation at 135,000g for 2 hours at 4°C and resuspended in ~ 8 µl buffer containing either substrate or inhibitor, B) subjected to several rounds of centrifugation and resuspension in Na^+-free buffer after gramicidin-A incorporation (25ug/ml) into liposomes to remove Na^+, or C) resuspended in buffer containing 100mM K^+ (for uptake assays). Spin-labeled proteoliposomes were always used immediately for the EPR studies. To confirm reproducibility of our EPR spectra acquired for each condition was not feasible in the time-frame of the project. However, each double mutant in the presence of aspartate was replicated two times, and the EPR spectral lineshape and omega interaction parameters were essentially the same for each double mutant pair in our experiments. Therefore, this procedure provided confidence in our approach, and the replication of all conditions for each double mutant was deemed unnecessary.

2.3.5. EPR Spectroscopy

Continuous wave EPR spectra were obtained at room temperature on a Bruker E500 X-band EPR spectrometer equipped with a superX microwave bridge and an ER4123D dielectric resonator (Bruker Biospin, Fremont, CA). Approximately 4 µL of proteoliposome suspension at ~100 µM were loaded into gas permeable methylpentane polymer (TPX) capillaries (Bruker Biospin, Fremont, CA), which hold aqueous samples but allow for rapid exchange of gasses inside the capillary. Using these capillaries, samples were deoxygenated by continuous flushing of the cavity with N_2. The microwave frequency was 9.78 GHz, the modulation frequency 100 kHz, the modulation amplitude 2 G, and the microwave power 2 mW. Each spectrum corresponds to the accumulation of 10 scans.

2.3.6. Data Analysis: Double integration procedure for analyzing EPR signals.

EPR spectra were imported into the computer program GRAM AI (Version 7.0, Thermo Galactic) as two column ASCII files using the converter ASCII_XY. The output file type was designated .spc. These .spc files were then directly opened in GRAM AI (Version 7.0), which displays the EPR lineshape. The double integration procedure was next conducted by first cropping the EPR trace to only include the spectral lineshape. This was done by examining where the spectral lineshape started and ended, or in other words, where the lineshape deviated from, and returned to, baseline. Importantly for this cropping, a region was

chosen in which both sides of the spectral lineshape show nice straight baselines. We next manually selected two points at the extremities of the cropped region where the baseline was straight, and ran the two-point baseline application to perfectly level the lineshape. Next we utilized the mathematical integration application twice, which computed the total area encompassed by the spectral lineshape. Three separate integration procedures as just described were performed for each lineshape in order to determine the reproducibility of the double integration procedure for each spectra.

2.3.7. Glt_{Ph} Transport Assay

Frozen proteoliposomes were removed from -80°C and thawed on ice. For radioactive transport assays, proteoliposomes were previously loaded with internal buffer (15 mM HEPES, pH 7.4, 100 mM KCl, 0.8 mM $MgCl_2$). The uptake reaction was initiated by diluting proteoliposomes into external buffer containing 100 mM NaCl, 2 mM KCl, 1 mM $MgCl_2$, 5 mM HEPES, pH 7.4, and 400 nM L-^{14}C-aspartate. Uptake was performed at 25°C for 6 minutes. Background was defined as the counts observed when the proteoliposomes were diluted into the buffer with which they were loaded.

2.3.8. Scintillation Proximity Assay (SPA)

Cu2+ chelate YSi scintillation SPA beads (GE Healthcare) were utilized essentially as previously described (Quick and Javitch, 2007), and according to manufacturers instructions.

2.3.9. Molecular Biology for the human EAAT3 isoform

Site-directed mutagenesis, in vitro synthesis of RNA, and RNA injection into Xenopus laevis oocytes were performed as described previously (Larsson et al., 2004). Briefly, stage IV-V oocytes were defolliculated via collagenase treatment, followed by injection with 50 ng of RNA and incubation at 8°C in sodium Ringer's solution (in mM: 98.5 NaCl, 5 HEPES, 1.8 CaCl2, and 1 MgCl2; pH 7.5). Oocytes were moved to 15°C 12-15 h before experiments began. Experiments were performed 3-5 days after injection.

2.3.10. Voltage Clamp Fluorometry

VCF experiments were performed as described previously (Larsson et al., 2004). Oocytes were labeled for 60 min with 10 μM Alexa-546 maleimide (Molecular Probes) in sodium Ringer's solution. Fluorescence changes were recorded under voltage clamp using an upright microscope (Leica) with a x20 quartz objective and a photo-diode (pin-020A, UDT Sensors, Inc., CA). The objective was focused on the animal pole, and fluorescence was monitored through a rhodamine filter cube: exciter, HQ545/x30; dichroic, Q570LP; and emitter, HQ620/60m. Fluorescence signals were low-pass filtered at 200-500 Hz and digitized at 1 kHz. Fluorescence traces were monitored with Clampex 8.2 (Axon Instruments, Inc.) The oocytes were voltage clamped using a Two-Electrode Voltage Clamp (Gene Clamp, Axon Instruments).

2.3.11. DeepView modeling protocol

We devised a simple *in silico* approach to obtain an estimate of the range of potential distances between spin labels for each pair of cysteines. It is known that molecular rotations of the spin label side chain R1 are limited by a weak interaction that occurs between Sδ and Cα proton, making the molecular volume and conformations of R1 (MTSL side chain) similar to tryptophan side chains (Czogalla et al., 2007). Therefore, we mutated the Glt_{Ph} pairs of residues in DeepView (http://spdbv.vital-it.ch/) to tryptophans, and using stringent constraints for side-chain conformations, measured the range of potential distances between the outer tips of the tryptophan side chains.

Our precise protocol is as follows. PDB files of Glt_{Ph} obtained in either TBOA or aspartate were visualized in Deepview. Upon opening PDB files, the Control Panel was opened and all of the residues were hidden from view by clicking on the “show” button. Individual pairs of residues that we utilized in our experiments were next selected, allowing for the visualization of only those two particular residues. These individual residues were next mutated to tryptophan residues. To accomplish this, first the MUTATE button was selected using the Swiss-PDBViewer toolbar. Next, one of the residues we had chosen was selected simply by clicking on it with the mouse. This brings up a pulldown menu, allowing for the residue to be changed to a tryptophan residue. Upon choosing the tryptophan residue, a message appears in red just below the top row of icons on the Swiss-PDBViewer toolbar. This message indicates rotamer number (R), score (S), and probability (P). Automatically, a rotamer will be selected that has

the lowest energy (fewest collisions and most favorable hydrogen bonds, if any). There may be several rotamer positions with equally low energy. Negative values of S indicate highly favorable rotamers, while increasingly positive values of S are unfavorable. Starting with the lowest energy rotamer, the mutation to tryptophan was confirmed by again clicking on the mutate button and accepting the residue change. Following the same procedure, the second residue was also mutated to tryptophan, and the lowest energy rotamer, automatically chosen, was accepted.

At this point, the range of potential distances between the outermost ring of tryptophan was measured. To accomplish this, we measured 6-8 distances between the outermost four carbons from one tryptophan ring to the outermost four carbons on the other tryptophan ring using the distance-measuring function in the Swiss-PDBViewer toolbar (shown as a button with the heading “1.5 Å” in the toolbar). In making our measurements, we aimed to find the range of possible distances between 1) the shortest possible distance between any two of the outermost carbons located on separate tryptophan residues, as well as 2) the farthest distance between any two of the outermost carbons located on separate tryptophan residues. In making 6-8 measurements we obtained the range of potential distances between residues. This thus provided us an average distance between the outermost rings of the two tryptophan residues for a given rotamer pair.

We next proceeded to obtain the same measurements for different rotamer pairs, utilizing the same protocol. While technically DeepView only shows realistic

rotamers when using the MUTATE function, only rotamer pairs that each had a score (S) of 10 or below were deemed acceptable. In this fashion, we obtained approximate distances between tryptophan residues, for a number of rotamer pairs for each of our double mutants. Because the molecular volume and conformations of the R1 side chain of MTSL are very similar to that of tryptophan side chains, this analysis provided an estimate of the range of distances possible between spin labels in our experiments. For instance, for a given double mutant, two rotamers may be found to be close in space, but two other rotamers may be further away. This would provide a larger range of potential distances than two rotamer pairs that did not differ much in the overall conformations. Importantly, in the text of this thesis, when a certain residue is stated to come "within" a certain distance of another residue, this refers to the rotamer pair that comes into closest contact (out of a number of potential rotamer pairs), and in addition refers to the closest measurement *for* this rotamer pair that we measured out of the 6-8 total distance measurements.

Upon making all of our Deepview measurements and obtaining a theoretical range of potential distances between each pair of double mutants, we next attempted to "constrain" rotamer conformations to a "best-fit". Utilizing residue 355 as an example, what this means is that because residue 355 was used for all residue pairs except for 353-130, we wanted to see if we could "lock" 355 in one particular conformation such that all of the omega interaction parameters for double mutant pairs having 355 as one of the residues made sense, in the context of the crystal structures. Our protocol is as follows. First a rotamer for

355 was locked in place. In TBOA only two rotamer conformations were deemed acceptable by our stringent use of the DeepView program, but in aspartate 7 rotamer conformations were deemed acceptable. Using the TBOA data as an example, we first locked 355 in one of the conformations. We next measured the range of distances between 355 and the other residues (130, 129, 279, and 51). Importantly, the other residues (130, 129, 279, and 51) were not fixed, but the *range* of distances measured for different rotamers was utilized to determine distances from 355. For instance, in the text we refer to the fact that interaction between 355-130 was limited to 11-16 Å. This means that with 355 fixed, the range of distances between 355 and 130 was 11-16 Å, taking into account all rotamer conformations for 130. In this fashion, we measured the range of distances between 355 and the other residues (129, 130, 279, 51). We next did this for 355 in the second conformation. Of the two data sets, the one that corresponded most similarly to our omega interaction parameter data was discussed in the text. In aspartate, seven 355 rotamers were deemed acceptable by Deepview. Therefore, following the same protocol, residue 355 was fixed in seven different conformations, and in each conformation the range of distances between other residues (130, 129, 279, 51) was measured. Again, the other residues (130, 129, 279, and 51) were not fixed, but the *range* of distances measured for different rotamers was utilized to determine distances from 355. The data set that correlated most closely to our omega interaction parameter data set was discussed in the text. This is what we refer to as a “best fit”, and simply provides a qualitative correlation between our omega interaction

parameter data with the crystal structures. In other words, it shows that the omega interaction parameter data we obtained is theoretically possible. Because 353 was only paired with residue 130, we present in the supplemental text simply the range of all possible combinations of distances between 353 and 130 (the range of distances between the closest and farthest rotamer conformations).

III. Chapter 3

Results

Opposite movements of the external gate in glutamate transporters upon binding different ligands measured by EPR

Paul Focke[1], Pierre Moenne-Loccoz[2], Hans Koch[3], and H. Peter Larsson[3]

[1]Neuroscience Graduate Program, Oregon Health & Science University, 505 NW 185th Avenue, Beaverton OR 97006,
fockep@ohsu.edu

[2]Department of Science and Engineering, School of Medicine, Oregon Health & Science University, 20,000 NW Walker Road, Beaverton, OR 97006-8921,
ploccoz@ebs.ogi.edu

[3]Department of Physiology and Biophysics, University of Miami Miller School of Medicine, 1600 NW 10th Avenue, RMSB 5123, Miami, FL 33136,
PLarsson@med.miami.edu

Currently this paper is in the process of being resubmitted.

Paul Focke performed the experimental work and analysis on the bacterial glutamate transporter homolog Glt_{Ph}. Dr. Hans Koch performed the experimental work and analysis on the mammalian glutamate transporter EAAT3. Dr. Hans Peter Larsson provided support for the project, and analytical insight into both experiments performed on Glt_{Ph} as well as EAAT3. Dr. Pierre Moenne-Loccoz contributed invaluable expertise on the topic of electron paramagnetic resonance spectroscopy as applied to our experiments.

1. Overview

Hairpin two (HP2) has been proposed as the extracellular gate of glutamate transporters. To test this hypothesis, we use double site-directed spin-labeling electron paramagnetic resonance spectroscopy on the bacterial transporter Glt_{Ph} to examine conformational changes in HP2. Surprisingly, the two co-ligands Na^+ and aspartate apparently induce opposite movements of HP2. We find that Na^+ binding to the apo state of the transporter opens the extracellular gate, while the subsequent binding of aspartate closes the gate. In addition, using voltage clamp fluorometry on the mammalian excitatory amino acid transporter EAAT3, we confirm that the opposite conformational changes of HP2 induced by Na^+ and amino acid substrates also occur in mammalian amino acid transporters. Our findings are consistent with HP2 comprising the extracellular gate of glutamate transporters, and that Na^+ binding opens and stabilizes the extracellular gate thereby allowing for amino acid substrate binding.

2. Introduction

Mammalian excitatory amino acid transporters (EAATs) are essential for terminating synaptic excitation and for maintaining extracellular glutamate concentrations below neurotoxic levels (Kanner et al., 2001). EAATs couple neurotransmitter uptake to the co- and counter-transport of sodium and potassium ions (Zerangue and Kavanaugh, 1996). How this is structurally accomplished by EAATs is not known. Recently, structures of Glt_{Ph}, a bacterial

aspartate transporter and EAAT homolog, suggested that hairpin two (HP2) functions as the extracellular gate (Boudker et al., 2007; Yernool et al., 2004). Differences in two crystal structures, obtained in the presence of the transportable substrate $_{L}$-aspartate or the non-transportable inhibitor $_{DL}$-TBOA, were localized to the tip of HP2. We here wanted to directly measure the movements of HP2 for a transporter in a number of different states in a membrane environment.

Formation of disulfide bonds between cysteines inserted in HP2 and surrounding domains have been shown to be modulated by substrates and inhibitors. However, these studies could not unequivocally show that HP2 moves upon substrate binding (Brocke et al., 2002; Leighton et al., 2006; Qu and Kanner, 2008). Substrate binding may restrict access to these cysteines, cause movement of other parts of the protein, or alter bond angles between cysteine side chains, thereby preventing disulfide bond formations without altering distances between the cysteines. In addition, there is no previous crystallography data for the Na^+ bound state of the transporter, and inconclusive crystallography data for the apo state (Boudker et al., 2007), due to the fragility of crystals in the absence of Na^+.

We here use double site-directed spin-labeling (DSDSL) electron paramagnetic resonance (EPR) spectroscopy to determine the extent and directionality of HP2 conformational changes relative to surrounding protein induced by Na^+ binding and by the binding of the substrate $_{L}$-aspartate or inhibitor $_{DL}$-TBOA. DSDSL-EPR provides the ability to examine small conformational changes (< 20-25 Å) by

estimating distances between spins based on the dipolar interactions between them. Briefly, two paramagnetic spins in close proximity interact via dipole-dipole interactions depending on the distance, r, between spins to the third power (r^3) (Liu et al., 2001). Compared to most fluorescence probes, the small size of spin labels enhances accuracy of distance estimates and minimizes influences on protein stability and secondary structure (Bolin et al., 1998; McHaourab et al., 1996). Most importantly, EPR experiments can be performed on membrane proteins in the native environment of a lipid bilayer.

Using DSDSL-EPR on the bacterial aspartate transporter Glt_{Ph}, as well as voltage clamp fluorometry experiments on the mammalian glutamate transporter EAAT3, we demonstrate a directional conformational change associated with the binding of Na^+ to the apo state of the transporter, while a conformational change in the opposite direction is associated with the binding of $_L$-aspartate /$_L$-glutamate. The data obtained from this work suggests that the role of Na^+ binding to the apo state of the transporter is to stabilize the open state of the extracellular gate, thereby promoting substrate binding to the transporter and providing an explanation for the tight coupling between Na^+ and substrate in glutamate transporters.

3. Results

3.1. Selection of Glt_{Ph} residues for cysteine substitution

Using Glt_{Ph} crystal structures, we selected pairs of residues likely to report distance changes measurable by DSDSL-EPR during HP2 movement.

Specifically, in the crystal structure obtained in the presence of $_{DL}$-TBOA, two residues on the tip of HP2 (Ala353 and Val355) are in close proximity with residues on TM4a (Pro129 and Leu130). However, in the crystal structure obtained in the presence of $_{L}$-aspartate these same two HP2 residues are located 5-10 Å further away from TM4a and are instead located closer to residues in TM2 (Val51) and HP1 (Ser279) (Fig. 1a,b). These different structures of HP2 obtained in $_{DL}$-TBOA and $_{L}$-aspartate are referred to as the open and closed states of the extracellular gate, respectively (Boudker et al., 2007). To test these closed and open models of HP2, we generated five cysteine pairs using the residues mentioned above, in a Glt_{Ph} background where the only native cysteine (C321) was replaced with alanine. Distances between ß-carbon atoms in the $_{DL}$-TBOA-bound states vs. $_{L}$-aspartate-bound states are listed in Fig. 1c.

Our strategy to measure distances using DSDSL-EPR was to obtain EPR spectra for each cysteine pair in maximally labeled protein (2 spin labels/pair of residues) to under labeled protein (approximately 1 spin label/pair of residues). To ensure that maximally labeled and under labeled proteins represented the same conformations, we utilized a mixture of 67% diamagnetic (N-acetylated MTSL analog) to 33% paramagnetic (MTSL) label for the under-labeled condition (Gross et al., 1999) (Fig. 1d). Dipole-dipole interactions were then determined using the Ω parameter (Perozo et al., 1998), calculated as the ratio of central peak heights of EPR spectra in underlabeled to maximally labeled protein,

Figure 1. Strategy for measuring conformational changes with EPR. (a) Models of Glt_{Ph} crystal structures obtained in the presence of $_{DL}$-TBOA and $_{L}$-aspartate showing the position of HP2 residues Val355 and Ala353 relative to TM4a residues Pro129 and Leu130. (b) Models of Glt_{Ph} crystal structures obtained in the presence of $_{DL}$-TBOA and $_{L}$-aspartate showing the position of HP2 residues Val355 and Ala353 relative to TM2 residue Val51, and HP1 residue Ser279. In both (a) and (b) dashed lines indicate cysteine pairs that were used for EPR measurements.

c

Mutants	+TBOA (Å)	+ASP (Å)
353C-130C	8	15
355C-130C	11	20
355C-129C	10	20
355C-279C	14	7
355C-51C	20	10

d MTSL Analog

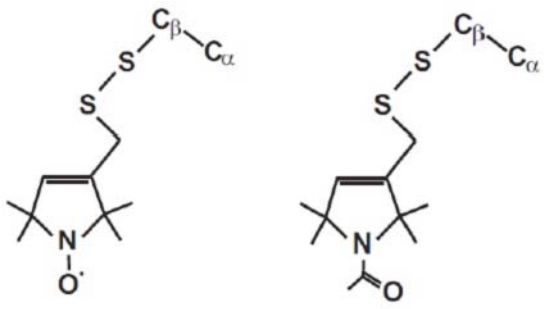

Figure 1. Strategy for measuring conformational changes with EPR. (c) Distances between ß-carbons for residue pairs in either $_{DL}$-TBOA or $_{L}$-aspartate (d) Structures of the paramagnetic (MTSL) and N-acetylated diamagnetic (Analog) labels used for EPR. MTSL and MTSL-analog are comparable in size and molecular volume to tryptophan residues.

normalized to the same number of spins. For interspin separations in the 8-25 Å range, Ω values increase as spins come closer to one another. This is due to the decrease in central peak height resulting from the dipole-dipole interactions.

3.2. Glt_{Ph} protein purification and spin-labeling

To measure spin-spin interactions using EPR, the spin labeling has to be carefully controlled. First, the protein to be labeled must be extremely pure so that the EPR spectral lineshapes are not distorted by labeling of cysteine residues in contaminating proteins. Secondly, because dipole-dipole interactions are established by comparing spectra from fully-labeled protein to under-labeled protein, it is imperative that the spin labeling is close to 100% (2 spin labels/pair of residues) in the fully-labeled condition and that double spin labeling in the under-labeled condition is minimized.

Using protocols previously developed (Yernool et al., 2004), we obtained highly purified protein (Fig. 2a). The purified protein was labeled with the probes (100% MTSL or 67% N-acetylated MTSL analog and 33% MTSL), and then re-purified using FPLC (Fig. 2b) to both isolate the trimeric protein and to remove any excess unreacted label. No EPR signal was detected from cysteine-less Glt_{Ph}-A (Fig. 2c), having been exposed to the same labeling protocol as that of the double mutants. This verifies the purity of our proteins and shows the lack of any spin label contamination from other cysteines or from free unreacted spin label. To confirm maximal labeling of our mutant proteins, the mass of labeled and unlabeled protein were determined by mass spectrometry (Fig. 2d).

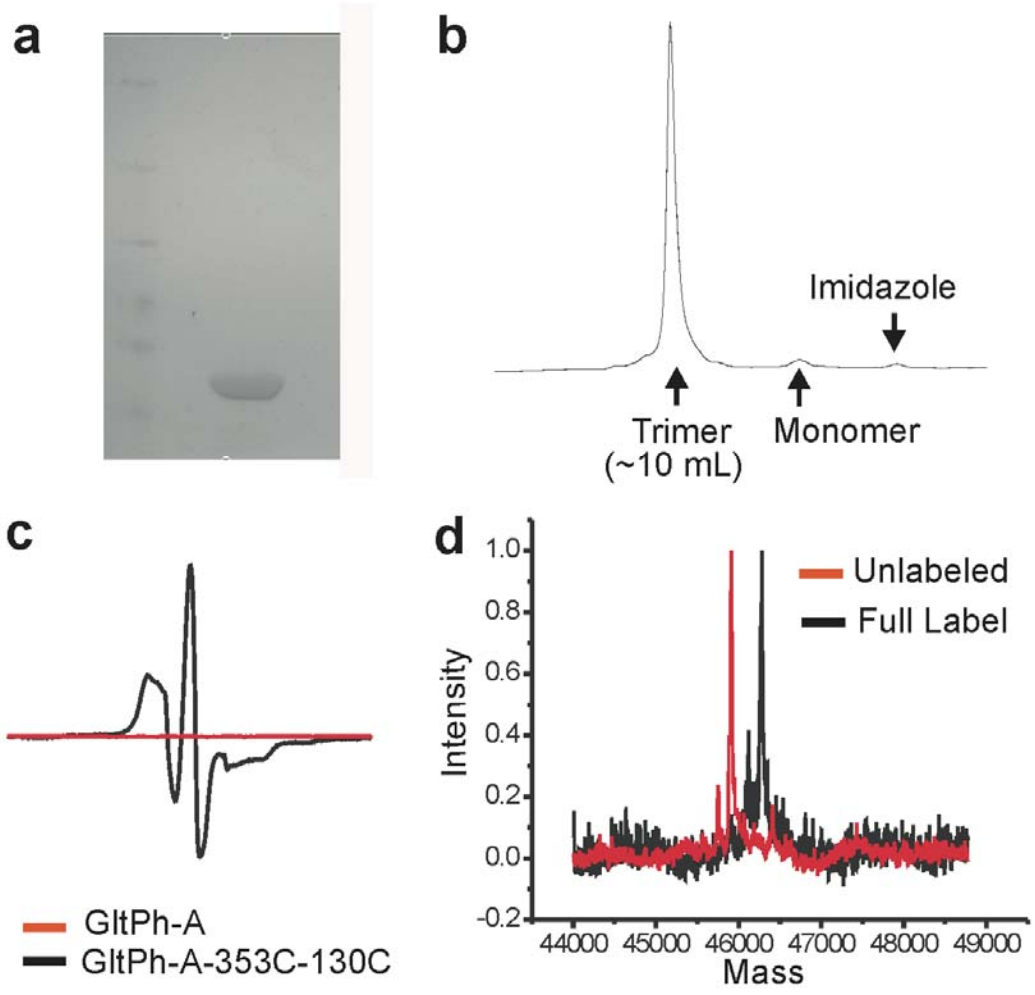

Figure 2. Protein purification and spin-labeling efficiency. (a) Representative example of SDS-PAGE analysis showing His-tagged Glt_{Ph} purified using Ni-NTA superflow. Denaturing conditions result in the detection of Glt_{Ph} monomer by Coomassie blue staining. (b) Gel-filtration chromatography of Glt_{Ph} used to simultaneously isolate functional trimeric transporters and remove excess spin-label. X-axis corresponds to elution volume. (c) No EPR signal is detected from the cysteine-less mutant Glt_{Ph}-A subjected to the same spin labeling conditions as Glt_{Ph}-A-353C-130C. EPR measurements were performed on purified, labeled proteins in n-dodecyl-β-D-maltopyranoside. (d) Electrospray mass spectrometry data showing a characteristc 372 dalton shift in molecular weight indicating fully labeled double mutant protein.

3.3. Structural and functional properties of spin-labeled Glt_{Ph} mutants

We next examined the functional properties of Glt_{Ph}-A (cys-less) as well as the single mutants Glt_{Ph}-A-353 and Glt_{Ph}-A-355 using radioactive uptake assays on proteins incorporated into preformed liposomes. The single mutants were utilized in these uptake assays because either residues 353 or 355 were to be used in all EPR experiments, therefore the functionality of the transporter spin-labeled at these residues was first examined. While substantial transport was observed in the cys-less mutant (Glt_{Ph}) (Fig. 3a), spin-labeling Glt_{Ph}-A-353 and Glt_{Ph}-A-355 reduced $_{L}$-aspartate uptake to background levels (Fig. 3a). Most likely, spin labeling of these residues in HP2 prevented transporters from continuously cycling through the substrate uptake cycle. Previous studies on mammalian transporters have shown that mutating and/or labeling of cysteines introduced in HP2 resulted in transporters that did not show significant uptake of radioactive substrates (Borre et al., 2002; Grunewald et al., 2002; Ryan and Vandenberg, 2002; Seal et al., 2001). However, these previous studies also demonstrated that mutating and/or labeling of cysteines introduced into HP2 did not prevent substrate binding or extracellular conformational changes in mammalian transporters. Using a scintillation proximity assay (Quick and Javitch, 2007), we verified that substrate and inhibitor binding remained intact in spin-labeled transporters (Fig. 3b). Because spin-labeling residues 353 and 355 did not affect substrate/inhibitor binding, but prevented continuous transporter cycling, we were able to monitor in isolation the separate conformational changes induced by the binding of Na^{+}, $_{L}$-aspartate, and $_{DL}$-TBOA.

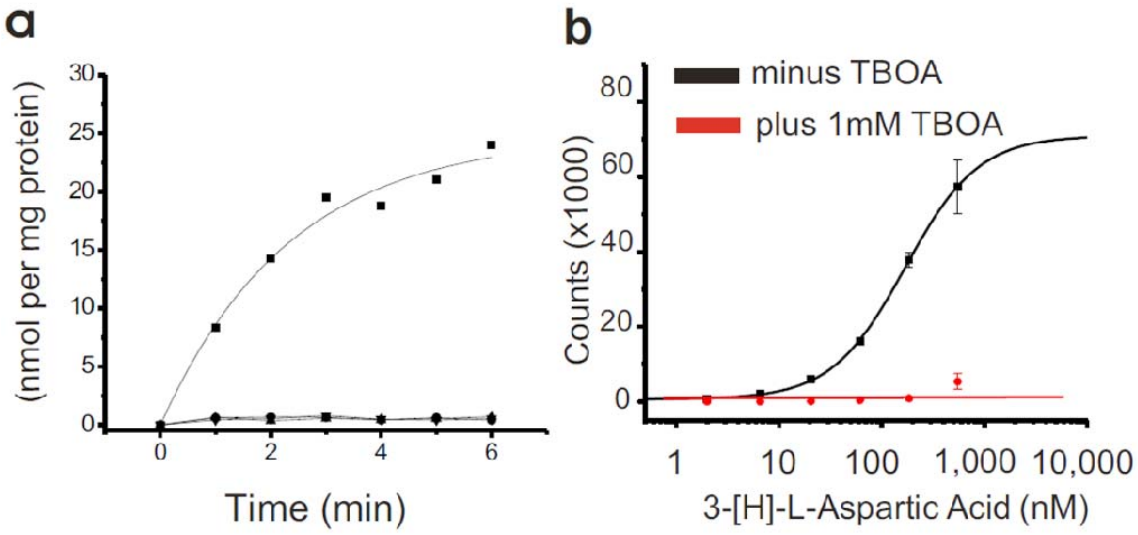

Figure 3. Spin-labeling HP2 residues disrupts transport but not substrate and inhibitor binding. (a) 3-[H]-$_{L}$-aspartic acid uptake in the presence of an inwardly directed Na^+ gradient remains intact in Glt_{Ph}-A proteoliposomes (squares), while spin labeling Glt_{Ph}-A-353C (upward triangles) and Glt_{Ph}-A-355C (circles) reduces uptake to background levels (downward triangles). Background was defined as the counts observed in the absence of a Na^+ gradient (100mM K^+ on both sides of the membrane). (b) Scintillation proximity assay (SPA) reveals 3-[H]-$_{L}$-aspartic acid binding and competitive inhibition by $_{DL}$-TBOA remains intact in spin-labeled double mutant transporters. Double mutant 355C-279C is shown as an example.

3.4. Opposite Glt_{Ph} HP2 movements in $_{DL}$-TBOA compared to $_{L}$-aspartate

We initially chose to examine omega interaction parameters under the two conditions used for the published crystal structures, in the presence of either inhibitor ($_{DL}$-TBOA) or substrate ($_{L}$-aspartate). Glt_{Ph} protein has been reported to incorporate equally effectively into liposomes with the cytosolic part of the protein facing the outside or the inside of the liposome (Ryan et al., 2009). Therefore, to achieve a homogenous population of a specific conformational state for the EPR measurements, we reconstituted purified, labeled protein into preformed liposomes in the presence of either $_{L}$-aspartate or $_{DL}$-TBOA on both sides of the liposome membrane (Fig. 4).

EPR spectra for all cysteine pairs showed differences in dipole-dipole interactions in the presence of the substrate $_{L}$-aspartate compared to inhibitor $_{DL}$-TBOA (Fig. 5). Comparing EPR spectra in under-labeled and maximally labeled transporters, a decrease in central peak height was observed in $_{DL}$-TBOA compared to $_{L}$-aspartate for three residue pairs (A353C-L130C, V355C-L130C and V355C-P129C) located on the tip of HP2 and TM4a (Fig. 5a**)**. In contrast, one residue pair (V355C-V51) on HP2 and TM2 and one residue pair (V355C-S279C) on HP2 and HP1 displayed decreased central peak heights in $_{L}$-aspartate compared to $_{DL}$-TBOA (Fig. 5a). Quantifying these changes using the Ω parameter revealed greater spin-spin interactions in $_{DL}$-TBOA than in $_{L}$-aspartate for three residue pairs (A353C-L130C, V355C-L130C, V355C-P129C), while for the other two residue pairs (V355C-S279C, V355C-V51C) there was greater spin-spin interaction in $_{L}$-aspartate than in $_{DL}$-TBOA (Fig. 5b). The pattern

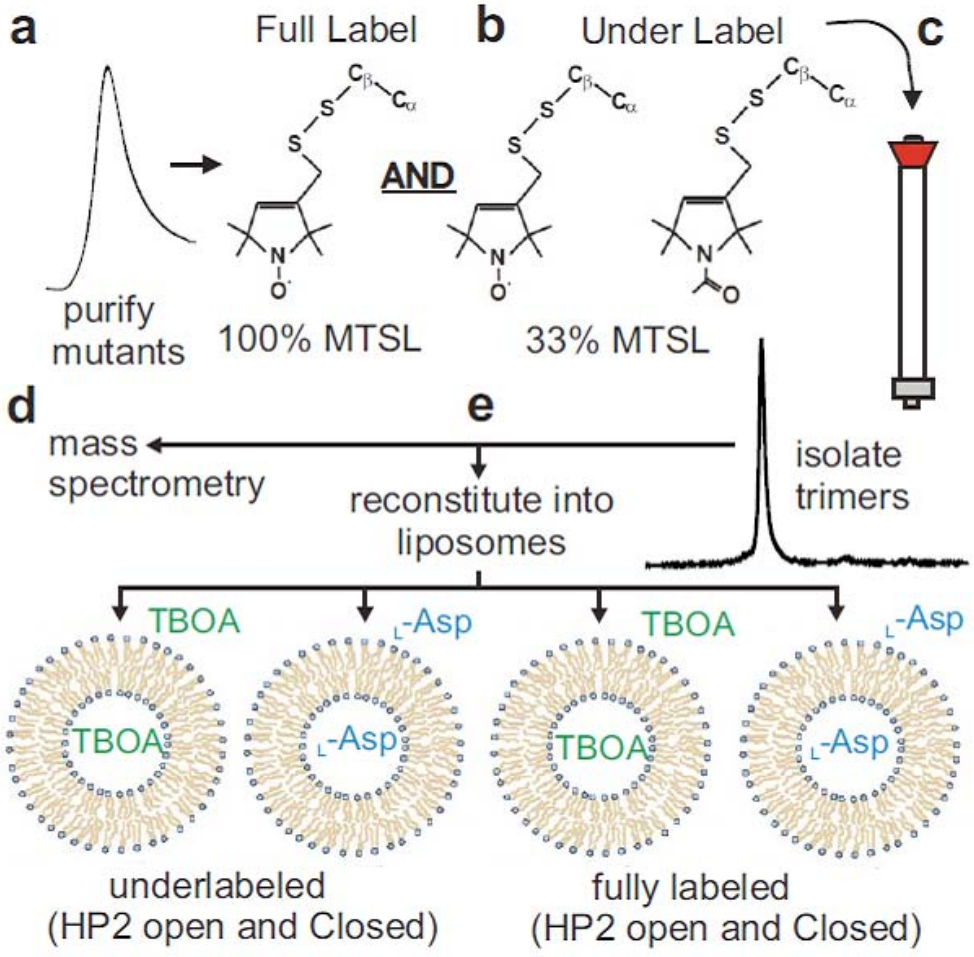

Figure 4. Experimental strategy to generate fully labeled and underlabeled proteoliposomes in presence of $_{DL}$-TBOA and $_{L}$-aspartate. Double-cysteine mutant Glt_{Ph} transporters were (a) purified, (b) labeled with MTSL or a mix of N-acetylated MTSL and MTSL and (c) repurified by FPLC. The spin-labeled Glt_{Ph} protein was (d) analyzed by mass spectroscopy to verify labeling efficiency and (e) reconstituted into liposomes in the presence of $_{DL}$-TBOA or $_{L}$-aspartate.

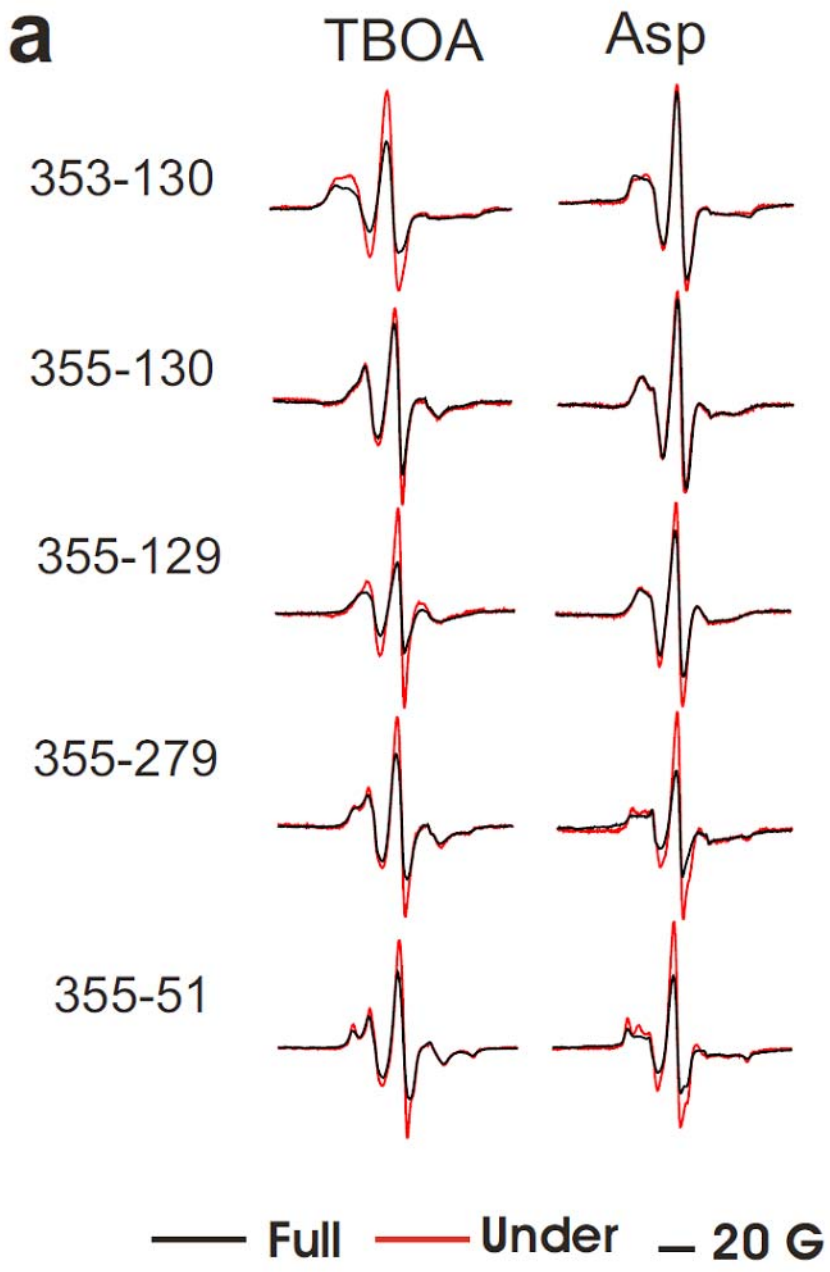

Figure 5. Changes in spin-spin interactions show movement of HP2. (a) EPR spectra in the presence of $_{DL}$-TBOA (left) and $_{L}$-aspartate (right) for under labeled (red lines) and maximally spin labeled (black lines) cysteine pairs, normalized to the same number of spins.

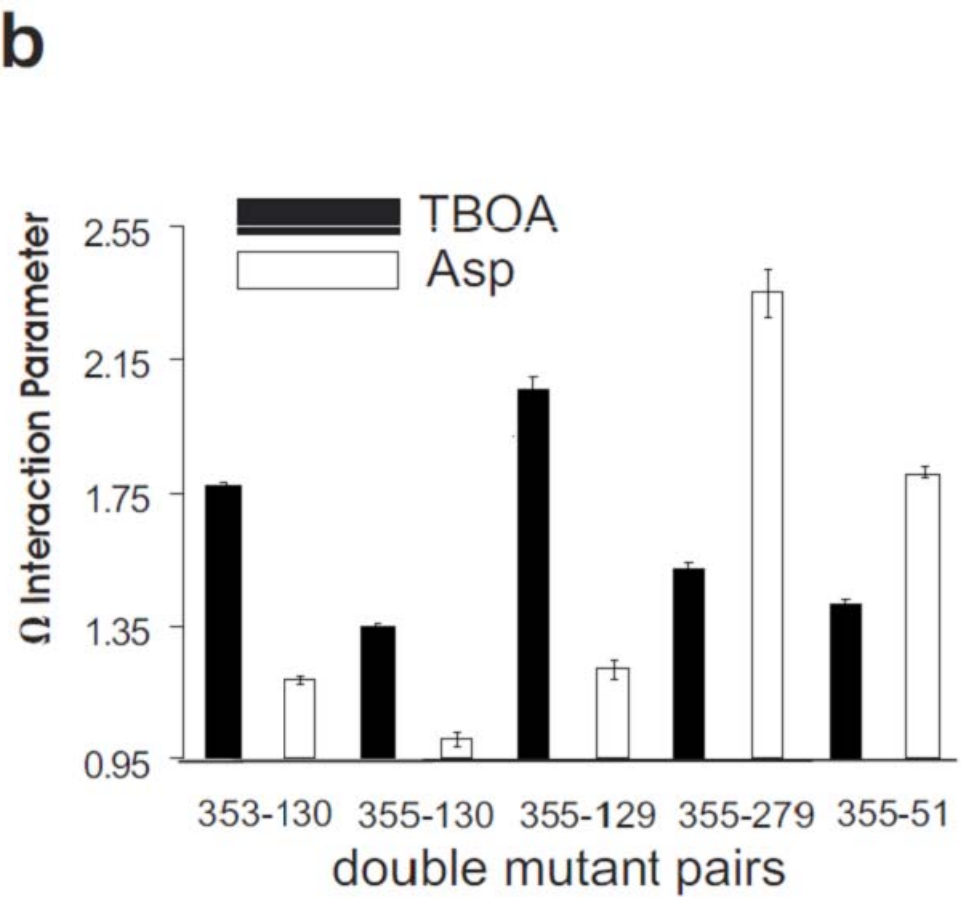

Figure 5. Changes in spin-spin interactions show movement of HP2. (b) Omega interaction parameters calculated for each pair of double cysteine mutants in $_{DL}$-TBOA (black bars) and in $_{L}$-aspartate (open bars). Error bars represent the standard deviation from three independent omega interaction parameter computations. Error bars represent the standard deviation from three independent omega interaction parameter computations performed on a single experiment.

of changes in the Ω parameter for all five pairs is best explained by a relative movement of the tip of HP2 away from TM4a and towards TM2 and HP1 upon $_{L}$-aspartate binding, as compared to the $_{DL}$-TBOA-bound state. The difference in omega factors obtained for residue pairs that, according to crystal structures, should be located at comparable distances, can be explained by the different rotameric states that the spin label may occupy. In this light, omega interaction parameters we obtained do not allow for direct comparison to β-carbon distances predicted from crystal structures (Fig. 1c), but again, this can be explained by rotamer conformation and will be discussed thoroughly in the supplementary information section of this thesis below.

3.5. HP2 movement upon Na^+-binding to the apo state in Glt_{Ph}

We next examined the pattern of dipole-dipole interaction between spin-labeled double mutants in the apo state (Na^+ and $_{L}$-aspartate-free) and the Na^+-only state. To conduct these experiments, proteins were first spin-labeled and then FPLC was used to simultaneously isolate trimeric proteins, remove excess spin-label, and allow on-column removal of glutamate/aspartate. Spin-labeled proteins in detergent buffer containing 100mM Na^+ were incorporated into liposomes pre-loaded with buffer containing 100mM Na^+. The use of Na^+ containing buffers served to ensure the stability of the trimeric protein during incorporation into liposomes (Boudker et al., 2007). Once the protein was in the more native environment of the liposomes, gramicidin A was incorporated into

the liposomes and the Na^+ buffer was exchanged through several rounds of centrifugation and resuspension of liposomes in Na^+-free buffer.

After the removal of Na^+, EPR spectra were recorded in the apo state. Na^+ was then added to the samples at a final concentration of 100 mM, and EPR spectra were recorded in the Na^+ bound state. After the addition of Na^+, the effect of extracellular GABA on the EPR spectra was tested, and spectra in the presence of $_L$-aspartate was again recorded (Fig. 6). Comparing all EPR spectra in underlabeled and maximally labeled transporters recorded under the apo, Na^+-bound, Na^+ plus GABA and Na^+ plus $_L$-aspartate-states, a characteristic pattern emerged. Three of the double mutants (353-130, 355-130, and 355-129) displayed a decreased central peak height in the presence of Na^+ compared to the apo state (Fig. 6a). For these three mutants, central peak heights were substantially increased above that seen in Na^+ upon the addition of $_L$-aspartate. Quantifying these changes using the Ω parameter revealed greater spin-spin interactions in the presence of Na^+ compared to the apo state and $_L$-aspartate-bound state, with the least interaction seen in the presence of $_L$-aspartate and an intermediate amount of interaction observed in the apo state (Fig. 6b). The two other double mutants we examined (355-279 and 355-51) revealed a different pattern of interaction. For these double mutants a decrease in central peak height was observed in aspartate, as compared to both the apo state and Na^+ only state (Fig. 6a). Quantifying these changes using the Ω interaction parameter for double mutant 355-279 revealed the least interaction in Na^+ and the greatest interaction in aspartate, with an intermediate interaction in the apo

Figure 6. HP2 movement towards TM4 upon Na^+-binding to the apo state. (a) EPR spectra in the presence of K^+, Na^+, GABA, and $_L$-aspartate for underlabeled (red lines) and maximally spin labeled (black lines) cysteine pairs, normalized to the same number of spins.

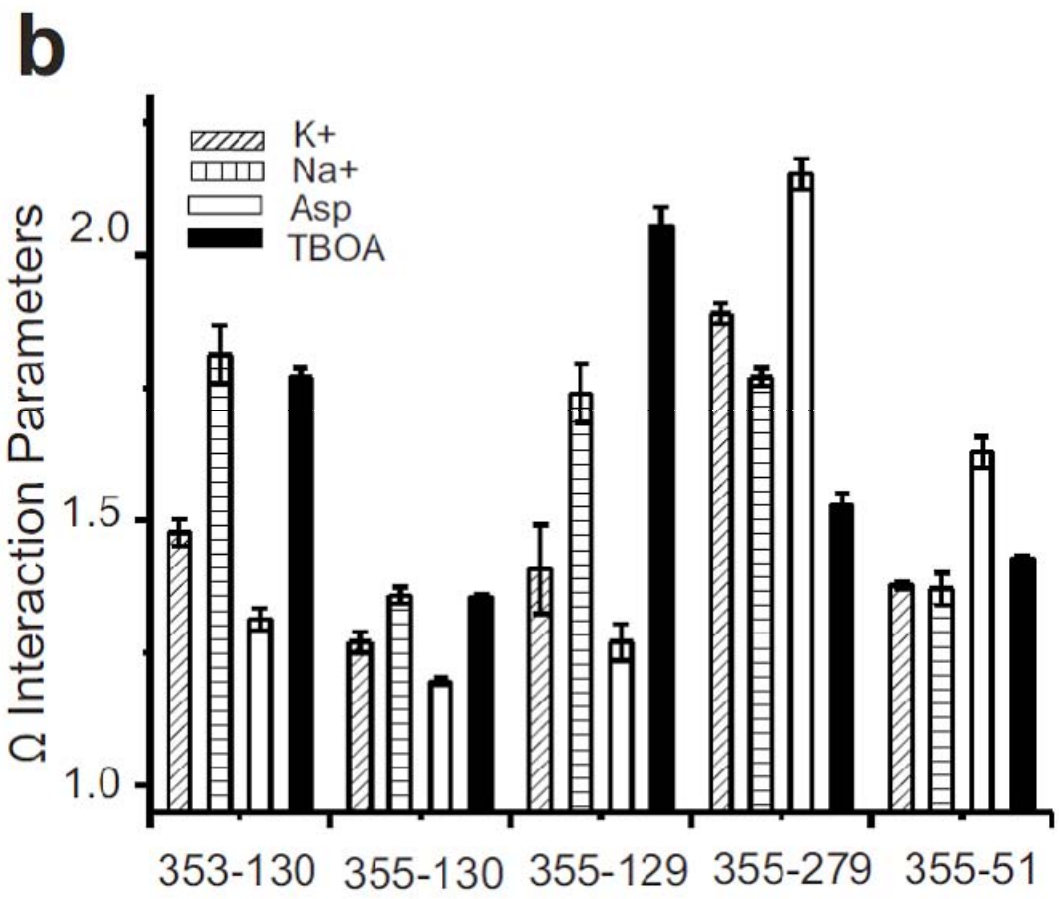

Figure 6. HP2 movement towards TM4 upon Na^+-binding to the apo state. (b) Omega interaction parameters calculated for each pair of double cysteine mutants in K^+ (diagonally hatched bars), Na^+ (horizontally hatched bars), and $_L$-aspartate (open bars). Also shown for comparison is the data obtained in Fig. 5 in $_{DL}$-TBOA (black bars). Error bars represent the standard deviation from three independent omega interaction parameter computations performed on a single experiment.

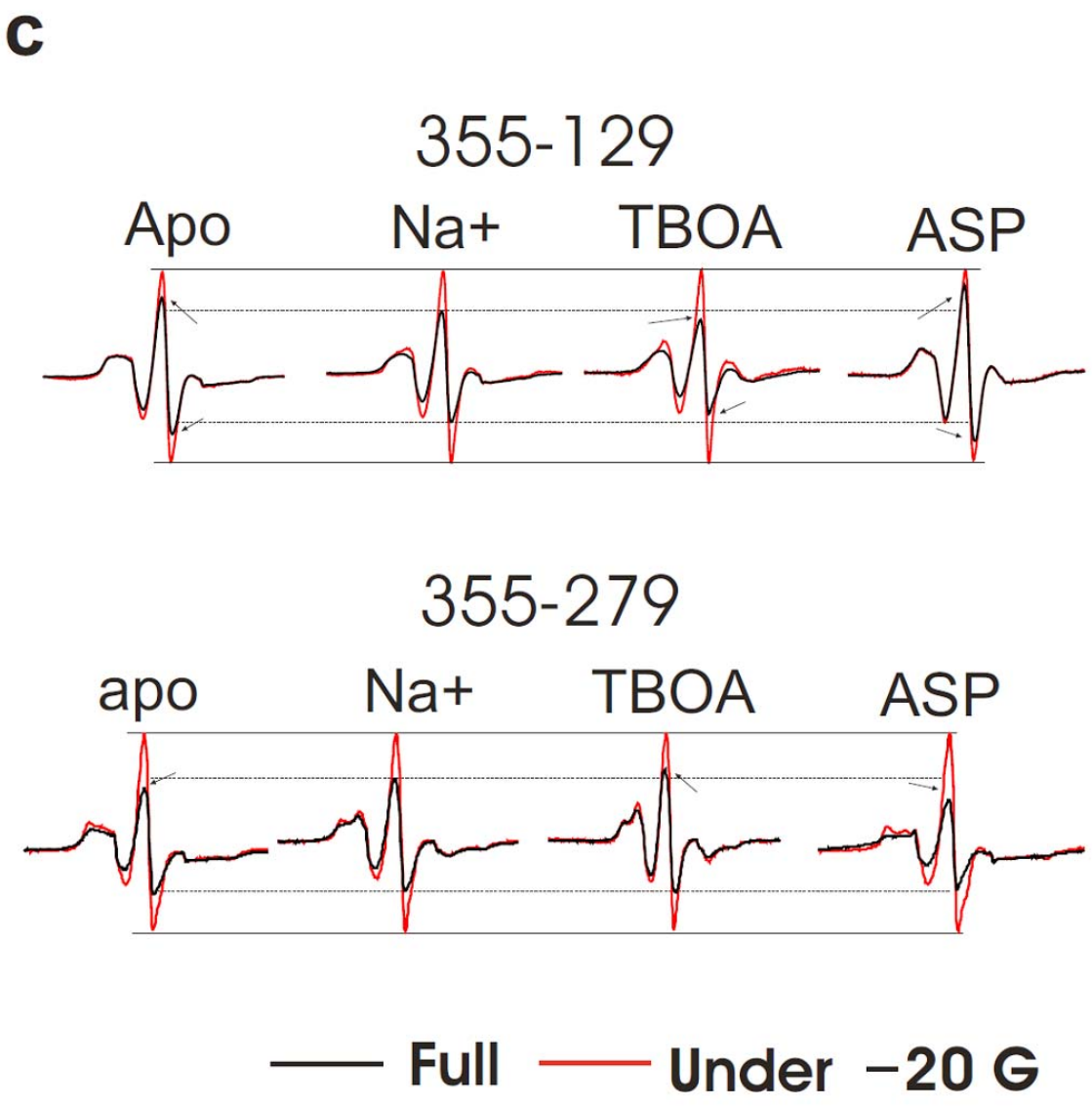

Figure 6. HP2 movement towards TM4 upon Na^+-binding to the apo state. (c) EPR spectra in the presence of K^+, Na^+, $_{DL}$-TBOA, and $_{L}$-aspartate for residue pair 355-129 and 355-279. Dotted lines in figure allow for comparison of K^+, $_{DL}$-TBOA, and $_{L}$-aspartate fully labeled central peak heights to that of Na^+. Solid lines allow for comparison of underlabeled central peak heights.

state (Fig. 6b). Ω interaction parameter calculations for double mutant 355-51 again revealed the greatest interaction in aspartate, but without a difference in interaction between the apo state and the Na^+-bound state (Fig. 6b, but also see Supplementary Fig. S2 and Supplementary information). In Fig. 6b, omega interaction parameters obtained in the presence of $_{DL}$-TBOA (from Fig. 5) are included in order to show the comparison between Na^+-bound states and $_{DL}$-TBOA-bound states. The differing extent of interaction seen in TBOA for residue pairs which, according to crystal structures should be located at similar distances from one another (353-130, 355-130, 355-129) can be explained by taking into account the different rotameric states that the spin label may occupy, discussed in the supplementary information section below. EPR spectra from 355-129 and 355-279 in the apo, Na^+, $_{DL}$-TBOA, and $_{L}$-aspartate-bound states are presented as examples in Fig. 6c to highlight the opposite changes in central peak heights induced by coligand, substrate, and inhibitor, for these two residue pairs.

Finally, no change in central peak heights or lineshapes were observed for any double mutant upon the addition of GABA (compare Na^+ to Na^+ plus GABA, Fig. 6a), further demonstrating that the conformational changes induced by Na^+, $_{L}$-aspartate, and $_{DL}$-TBOA are specific for ligands that interact with the transporter.

3.6. HP2 movement upon Na^+-binding to the apo state in EAAT3

The Ω interaction parameters in the presence of Na^+ are very similar to the values in the presence of $_{DL}$-TBOA, suggesting that the binding of Na^+ results in a movement of HP2 towards TM4, similar to the movement induced by the inhibitor

$_{DL}$-TBOA (Fig. 6b). We were interested to know if we could also detect this initial conformational change induced by Na^+ in the mammalian transporter EAAT3. Because we had previously generated a mutant in EAAT3 (413C) that was very close to the corresponding residues in Glt_{Ph} (residue 413 in EAAT3 is equivalent to residue 357 in Glt_{Ph}), we chose to examine whether Na+-binding similarly induced a conformational change of HP2 in EAAT3.

The 413C EAAT3 expressed in *Xenopus* oocytes was labeled with Alexa-546, and voltage clamp fluorometry was performed (Fig. 7). In voltage clamp fluorometry, changes in fluorescence are assumed to report on conformational changes that change the local environment around the attached fluorophore (Larsson et al., 2004; Mannuzzu et al., 1996).

In the absence of Na^+ (Na^+ substituted with choline$^+$), no voltage-dependent change in fluorescence was observed (Fig. 7a,d). The addition of Na^+ results in clear voltage-dependent fluorescence changes (Fig. 7b,d). At more hyperpolarized potentials, which promote the binding of Na^+ to the transporter (Larsson et al., 2004; Wadiche et al., 1995b), an increase in fluorescence is observed. The change in fluorescence suggests a movement of the tip of HP2 upon the binding of Na^+ to the apo state of the transporter. In contrast, the addition of $_L$-glutamate to Alexa-546-labeled 413C EAAT3 resulted in a decrease in fluorescence (Fig. 7c,d). At very depolarized potentials the fluorescence signals for the apo state, the Na^+-bound state, and the glutamate-bound states collapse to roughly the same levels due to that the voltage dependence of Na^+-binding to the transporter makes Na^+-binding less favorable at highly depolarized

potentials (Larsson et al., 2004; Wadiche et al., 1995b). The changes in fluorescence for 413C, with opposite polarities upon the binding of $_{L}$-glutamate compared to the binding of Na^{+}, are consistent with opposite movements of the tip of HP2 upon the binding of $_{L}$-aspartate and Na^{+} in mammalian EAATs, as shown above for HP2 in the bacterial transporter Glt_{Ph} using EPR.

4. Discussion

The omega interaction parameter data from the apo state, Na^{+}-bound state, $_{DL}$-TBOA-bound state, and the $_{L}$-aspartate-bound state lead us to the following conclusions about the movement of HP2 in the bacterial Glt_{Ph} transporter (Fig. 8). In the apo state (Fig. 8a), HP2 appears to adopt a conformation intermediate to that of the $_{L}$-aspartate-bound closed HP2 state (Fig. 8d) and the $_{DL}$-TBOA-bound open HP2 state (Fig. 8c). This could be because HP2 is static in this intermediate state, but could also indicate that the structure of HP2 is dynamic and instead is sampling both the open and closed conformations, leading to the observation in our experiments of an intermediate state. Upon the binding of Na^{+} to the apo state of the transporter, HP2 undergoes a movement that brings the tip of HP2 further away from TM2 and HP1 and closer in proximity to TM4a (Fig. 8b). This Na^{+}-bound state resembles the $_{DL}$-TBOA-bound open HP2 state (Fig. 8c), with slight differences. In $_{DL}$-TBOA (Fig. 8c), the tip of HP2 is more displaced toward TM4a than in the Na^{+}-bound state (see discussion below and Fig. 6b,c). Finally, upon binding of $_{L}$-aspartate to the Na^{+}-bound state of the transporter, HP2 undergoes a movement that brings the tip of HP2 away from TM4a and closer

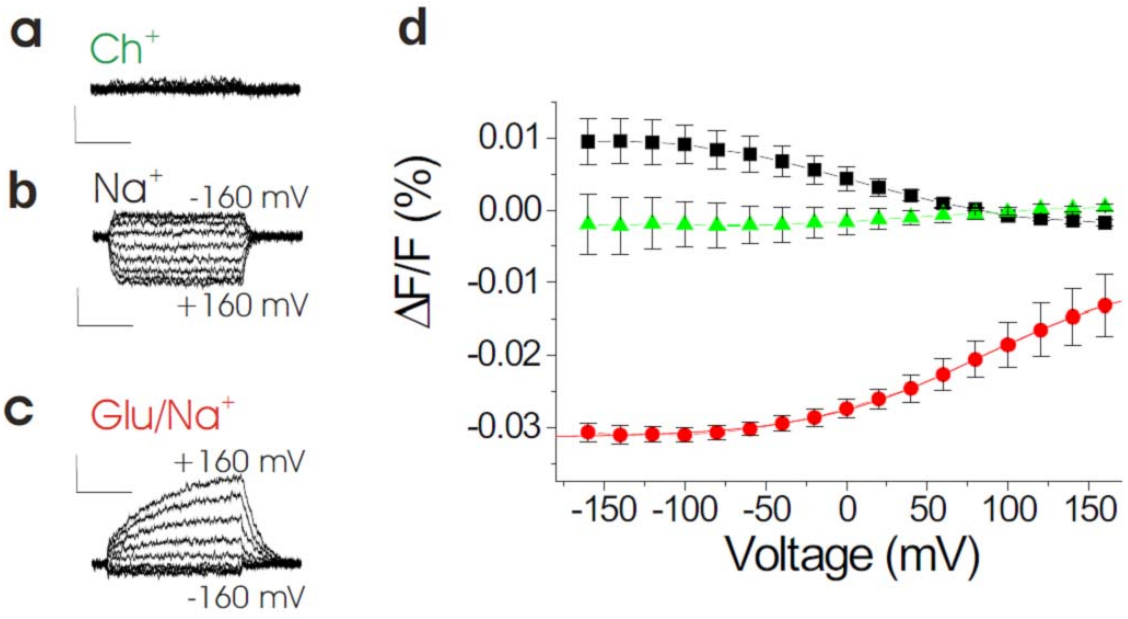

Figure 7. Opposite polarity of fluorescence changes upon the binding of $_L$-glutamate compared to the binding of Na^+. Voltage clamp fluorometry was performed on Alexa-546-labeled mammalian EAAT3-413C in (a) the apo state (Na^+ substituted for choline$^+$), (b) in the presence of Na^+, and (c) in the presence of Na^+ and $_L$-glutamate. (d) Changes in fluorescence are plotted as a function of membrane potential. Error bars in (d) represent the S.E.M from three independent experiments.

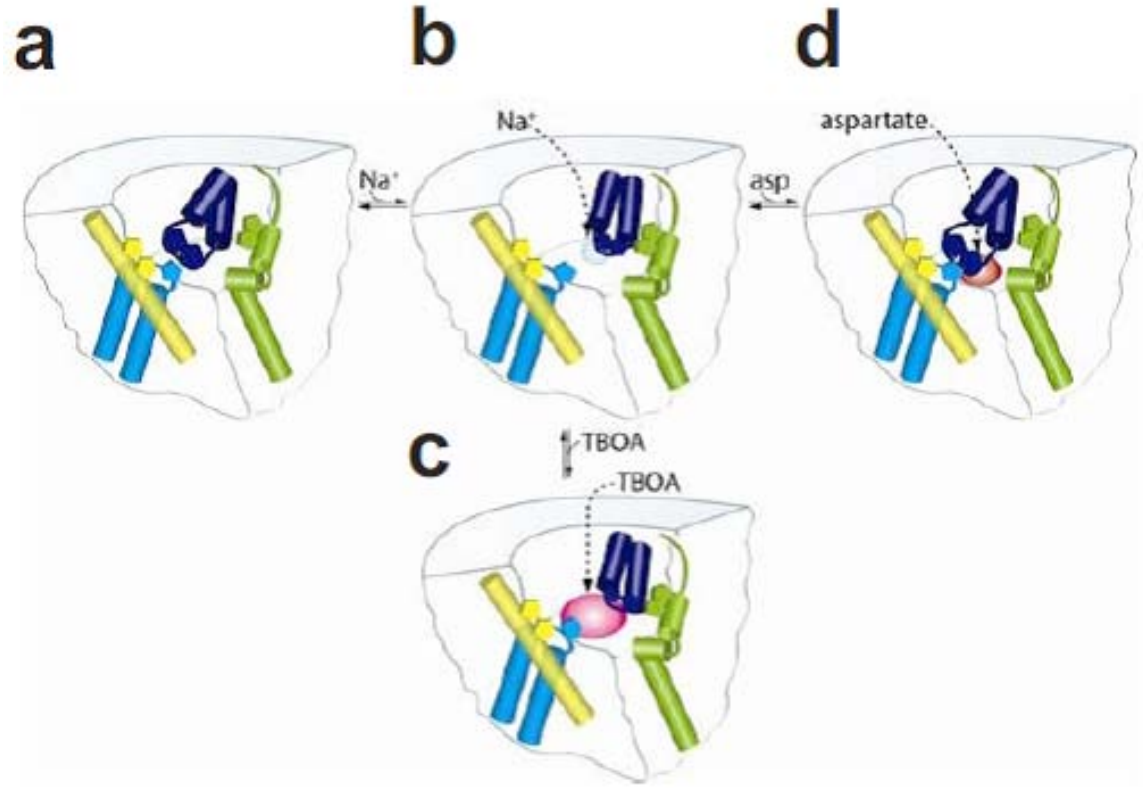

Figure 8. Model of HP2 positions illustrated for a single subunit. (a) In the apo state HP2 (dark blue) adopts a closed conformation, similar to the $_{L}$-aspartate-bound (d) state. The binding of Na^{+} (b) to the apo state stabilizes HP2 in an open-state, similar to that of the $_{DL}$-TBOA-bound (c) state. TM4 (green), TM2 (yellow), HP1 (light blue).

in proximity to TM2 and HP1, thereby closing the HP2 gate (Fig. 8d). Taken together, our EPR data shows that Na^+ and $_L$-aspartate induce opposite movements of HP2 in the bacterial Glt_{Ph}. Fluorescence measurements on the mammalian EAAT3 transporter are also consistent with the conclusion that the binding of the two co-substrates, Na^+ and amino acid substrate, induce opposite movements of HP2 in mammalian glutamate transporters.

While spin-label conformation and side-chain orientation influence our EPR measurements (see Supplementary information), nonetheless our EPR data on the $_L$-aspartate- and $_{DL}$-TBOA-bound states, the two states for which crystal structures exist, are consistent with the position of HP2 in these published crystal structures (Figs. 1a,b, Fig. 5, and see also supplementary Fig. S1). In $_{DL}$-TBOA, residues 355 and 353 on HP2 are close to TM4a (residues 129 and 130) and further away from HP1 (residue 279) and TM2 (residue 51). The dipole-dipole interactions for 355-51 in $_{DL}$-TBOA (Fig. 5b) are stronger than expected from the intrasubunit β-carbon distances in Fig. 1. However, upon closer examination, there are possible intersubunit spin-spin interactions in TBOA for spins attached to 355 and 51, that explains the larger than expected spin-spin interaction for this pair (see Supplementary information and Supplementary Fig. S2). In $_L$-aspartate, HP2 is closer to the center of the subunit: residues 355 and 353 have moved away from TM4a (residues 129 and 130) and moved closer to HP1 (residue 279), and TM2 (residue 51). The different extent of dipole-dipole interaction for residue pairs that in Figure 1a appear to be located at similar distances (for example 355-129 and 355-130) is due to differences in side-chain orientations and spin-label

conformations (see Supplementary information). For example, residues 355 and 130 point in opposite directions in the $_{DL}$-TBOA-bound state, which explains why the omega interaction parameters do not indicate that spin labels attached to these residues are in as close proximity to each other as suggested by Figure 1a. However, if the most likely side chain positions and rotameric states are assumed then our EPR data is consistent with the position of HP2 in the crystal structures in the presence of $_{L}$-aspartate and $_{DL}$-TBOA (see Supplementary information).

In the apo state (Fig. 8a) and the Na^{+}-bound state (Fig. 8b), two conformations of which there are no full crystal structures available (Boudker et al., 2007) our EPR data suggests that HP2 adopts two conformations that are intermediate to the $_{L}$-aspartate-bound closed HP2 conformation (Fig. 8d) and the $_{DL}$-TBOA-bound open HP2 conformation (Fig. 8c). In the apo state, for all residue pairs (expect for 355-51), the interaction parameter is intermediate to those in $_{L}$-aspartarte and in $_{DL}$-TBOA, but closer to the $_{L}$-aspartate values than to the $_{DL}$-TBOA values (Figs. 5, 6, 8 and also see Supplementary information for a discussion of 355-51). We therefore cautiously conclude that in the apo state HP2 adopts an intermediate state between the $_{DL}$-TBOA-bound and $_{L}$-aspartate-bound states, somewhat closer to the $_{L}$-aspartate-bound HP2 closed state (Figs. 5, 6, 8). We also are aware however, that what we interpret from our EPR experiments on the apo-state to be “intermediate” could also indicate that HP2 is dynamic and not rigid, sampling both the open and closed states. If this is the case, our omega interaction parameter data would reveal an intermediate state, when in fact HP2

is not in a static state. Future experiments are needed to resolve this question. In line with this, previous attempts to identify the apo state using crystallography were inconclusive. Boudker et al. (2007) prepared Na^+ and substrate-depleted crystals and examined threefold averaged electron density maps corresponding to the HP2 region. They found that HP2 could reside in an 'open' conformation, essentially indistinguishable from that seen in the $_{DL}$-TBOA-bound state. In unaveraged maps, however, they reported that subunits C and A showed density for HP2 in a more 'closed' conformation. As mentioned above, our EPR analysis suggests that in the apo-state HP2 resides in an intermediate position, closer to the $_{L}$-aspartate-bound HP2 closed state (Figs. 5, 6, 8), but could also indicate a dynamic structure sampling both the open and closed states.

Examination of the differences in omega interaction parameters obtained in going from the apo state of the transporter to the Na^+-bound state of the transporter suggests a movement of HP2 that brings residues in HP2 (353 and 355) closer in proximity to residues on TM4a (129 and 130). In three double-mutants (353-130, 355-130, and 355-129), the addition of Na^+ to the apo state of the transporter resulted in an increased omega interaction parameter and therefore an increased interaction between spins for these residue pairs (Figs. 6, 8b). Interestingly, in the Na^+-bound state, residues 355-279 are positioned closer to each other than they are in the $_{DL}$-TBOA-bound state, while residues 355-129 are further away from each other in the Na^+-bound state than they are in the $_{DL}$-TBOA-bound state (Fig. 6c, 8). This suggests that the tip of HP2 is more displaced toward TM4a in $_{DL}$-TBOA than in the Na^+-bound state. The simplest explanation for these results

is that steric restrictions of the aromatic ring of $_{DL}$-TBOA force the tip of HP2 (355) closer to residue 129 and further from residue 279 in the presence of $_{DL}$-TBOA as compared to Na^+ (Figs. 6, 8).

So what roles do the different conformations of HP2 play in the function of the transporter? As suggested from the crystal structures, the position of HP2 in the presence of $_{L}$-aspartate is most likely that of a closed gate, where extracellular access to the binding pocket is cut off. Again, our EPR data suggests that HP2 adopts a similar, but not completely closed, conformation in the apo state. We suggest that this conformation might restrict access for $_{L}$-aspartate, but not for Na^+, to the binding pocket or distort the binding pocket so that $_{L}$-aspartate cannot bind until Na^+ has bound. Previous crystal structures of Glt_{Ph} in which both substrate and ions were bound were deemed 'occluded' by showing that the substrates or ions were largely inaccessible to a 1.4 Å radius probe (Gouaux, 2008). Therefore, while the occluded state effectively closes off extracellular access to bound substrate, an intermediate state such as seen in our EPR analysis of the apo state could allow binding-site access to Na^+ while restricting access for the much larger $_{L}$-aspartate. Consistent with this hypothesis, it has earlier been shown by fluorescence and current measurements that aspartate/glutamate cannot bind to bacterial Glt_{Ph} or mammalian EAATs transporters in the absence of Na^+ (Boudker et al., 2007; Kanner and Bendahan, 1982; Larsson et al., 2004; Ryan et al., 2009; Wadiche et al., 1995b).

Upon the binding of Na^+ to the apo state of the transporter, our EPR data on Glt_{Ph} and our fluorescence data on EAAT3 suggest that the tip of HP2 undergoes

a movement that would open up the binding pocket, thereby allowing for amino acid substrate binding. Consistent with this, in a recent paper (in press) we have shown evidence that the backbone oxygens of residues 353 and 355 at the tip of HP2 actually contributes directly to one of the Na^+ binding sites in the apo state. Computer modeling further suggests that Na^+ bound to this Na^+-binding site contributes directly to the aspartate-binding site. Taken together, these data support a model whereby a cation-specific conformational change of HP2 creates and stabilizes the substrate-binding site. This in turn could explain the strict coupling of Na^+ transport to uptake of glutamate (Menaker et al., 2006).

The pattern of dipole-dipole interaction for all double mutant pairs clearly demonstrates that HP2 undergoes conformational changes that support the hypothesis (Boudker et al., 2007) that HP2 functions as the extracellular gate. This is the first direct measurement of the movement of HP2 for a transporter in a membrane environment. Using DSDSL-EPR spectroscopy on the bacterial glutamate transporter homolog Glt_{Ph}, combined with VCF experiments on the human glutamate transporter EAAT3, we have expanded on the available crystal structures by showing that the initial binding of Na^+ to the apo state of the transporter results in a directional conformational change associated with HP2. Our results suggest that this initial conformational change plays a role in stabilizing HP2 in an 'open to the outside' conformation, thereby exposing the substrate binding site.

5. Supplementary information

We developed the following analysis to facilitate a quantitative comparison of our omega interaction parameters to the calculated distances in the available crystal structures. This analysis serves as a control that our EPR results are consistent with the available crystal structures.

In conducting DSDSL-EPR studies, the accuracy or distance resolution obtained is often limited by the different rotameric states that the spin label may occupy. Recently, several reports have addressed the inherent distributions of the nitroxide, including development of a tether-in-a-cone model (Hustedt et al., 2006) for spin label distributions and the application of simulation methods to identify likely label configurations (Sale et al., 2005). Here we devised a simple *in silico* approach to obtain an estimate of the range of potential distances between spin labels for each pair of cysteines. Briefly, it is known that molecular rotations of the spin label side chain R1 are limited by a weak interaction that occurs between Sδ and Cα proton, making the molecular volume and conformations of R1 (MTSL side chain) similar to tryptophan side chains (Czogalla et al., 2007). Therefore, we mutated the Glt_{Ph} pairs of residues in DeepView (http://spdbv.vital-it.ch/) to tryptophans, and using stringent constraints for side-chain conformations, measured the range of potential distances between the outer tips of the tryptophan side chains.

We next plotted the omega interaction parameters we obtained from our experiments using $_{DL}$-TBOA and $_{L}$-aspartate against the expected distance estimates from our *in silico* measurements. Plotting our data in this fashion allowed us to correlate omega interaction parameters with actual distances.

Quantitatively, our Ω interaction parameter results (Supplementary Fig. S1) are consistent with our *in silico* measurements, as well as with previously published DSDSL-EPR experiments (Scoville et al., 2006).

Our analysis suggests that the different extent of dipole-dipole interaction for residue pairs that appear to be located at similar distances (for example 355-129 and 355-130) is due to differences in side-chain orientations and spin-label conformations (in this case for 129 and 130). We therefore next sought to determine whether we could use our omega interaction parameter data from all of our double mutant pairs for a particular state ($_{DL}$-TBOA or $_{L}$-aspartate-bound), in conjunction with the crystallography data, to constrain potential rotamer conformations to a best-fit for each residue. Our reasoning for doing this was to gain more information on the most likely conformation of each rotomer, and as well to verify that our data was consistent between residue pairs for given rotamer conformations. For example, constraining rotamer conformations to a best-fit for a given residue pair should not clash with omega interaction parameter data for other residue-pairs using the same constrained residue(s). Indeed, using Deepview we find very nice correlation and no clashes between all residue pairs when attempting to utilize omega interaction parameter data in conjunction with the tryptophan conformations. The results of this analysis will be discussed below for each residue pair in $_{DL}$-TBOA and $_{L}$-aspartate. Finally, we discuss this analysis in the context of our new data in the apo state and Na^{+}-bound states.

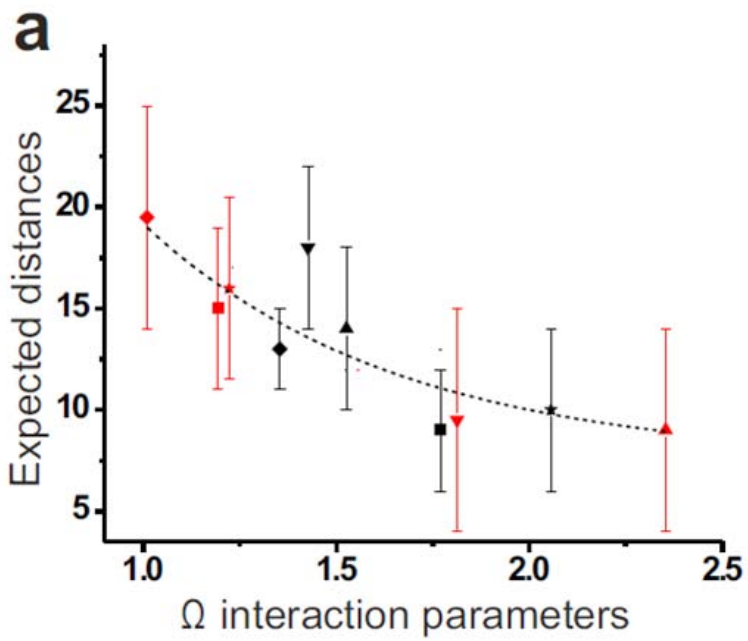

Supplementary Figure S1. Correlation of omega interaction parameters with expected distances. (a) Experimentally derived omega interaction parameters are plotted against the in silico-obtained (Deepview) range of potential distances between residue pairs. 353-130 (squares), 355-130 (diamonds), 355-129 (stars), 355-279 (upward triangles), 355-51 (downward triangles). The symbols are placed in the middle of the range of possible spin-spin distances for all likely rotamer combinations. Red symbols (aspartate) and black symbols (TBOA). The dashed line is a fit of the data to an exponential decay. Theoretically, the equation of this line should be able to predict an approximate distance between two residue pairs for which there is no crystal structure information, given an experimentally determined omega interaction parameter.

We begin the discussion with an analysis of all residue pairs in $_{DL}$-TBOA. Because residue 355 was used for all pairs except 353-130, we first attempted to constrain residue 355 to a best-fit corresponding to our omega interaction parameters. Fortunately, only two conformations of 355 were deemed acceptable by our stringent use of the Deepview program. Of those, both corresponded reasonably well with our omega interaction parameter data (355-130, 355-129, 355-279, 355-51), with one rotamer in particular providing the best-fit overall. Fixing residue 355 in this rotamer position, we find 355 can come within 6Å of residue 129. In this position for 355, interaction with 130 is limited to 11-16Å, consistent with our omega interaction parameter data. The same is true for 355-279 when 355 is constrained to this same position. Fixing residue 355 and examining rotamer conformations for 279 indicates that these residues can come within 11Å of each other, again consistent with our omega interaction parameter data. Also, using this analysis indicates that the spin-spin interactions seen for 355-51 in $_{DL}$-TBOA are due to intersubunit spin-spin interactions, with residue 355 on one subunit coming within 15Å of residue 51 on a different subunit (Supplementary Fig. S2).

We next examined whether our data was consistent for residue pair 353-130 in $_{DL}$-TBOA. For example, does it make sense that residue 353 comes into closer contact with residue 130 in $_{DL}$-TBOA than residue 355 does? Fortunately only two rotamers of 353 were deemed acceptable Deepview conformations, and in both cases 353 clearly comes into closer proximity with 130 than 355 in $_{DL}$-TBOA, interacting in a range of about 6-12Å.

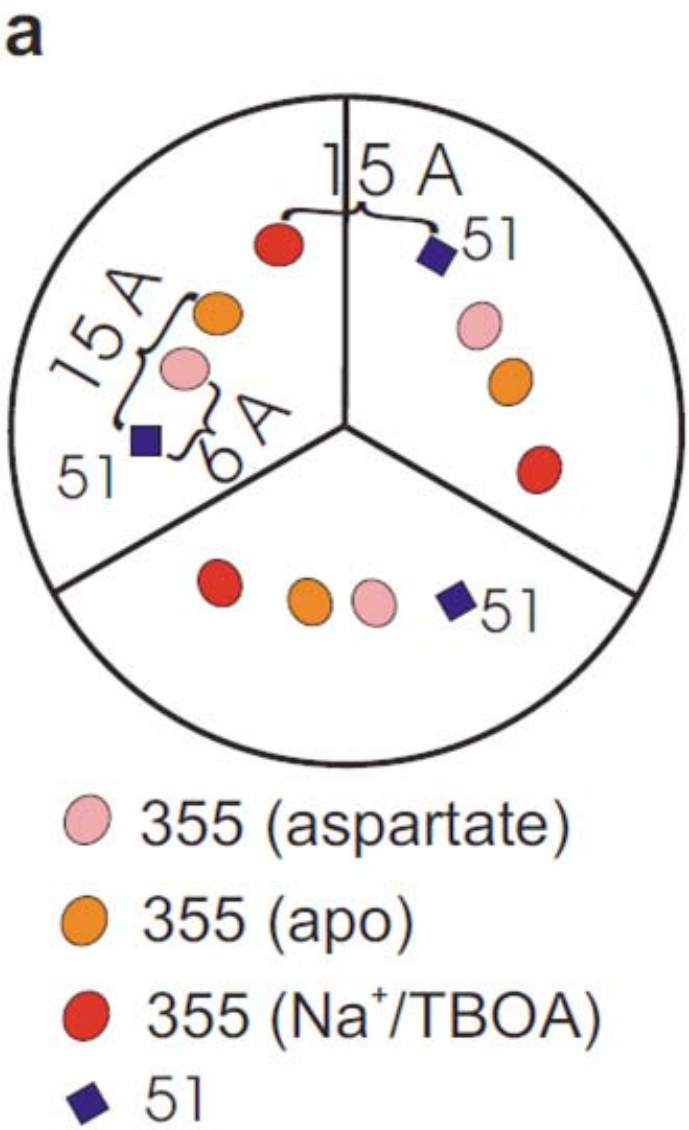

Supplementary Figure S2. Intra- and intersubunit interactions between residues 355 and 51. (a) Two-dimensional model depicting three Glt_{Ph} subunits. The position of residue 355 is shown for the apo, Na+/TBOA-bound, and $_L$-aspartate-bound states. Proximity to residue 51 is indicated for the three separate conformational positions of residue 355.

With our omega interaction parameters found to be consistent with the crystal structures and best-fit analysis using Deepview for $_{DL}$-TBOA, we next examined our data in the $_{L}$-aspartate-bound state. We again began by attempting to constrain residue 355 to a particular best-fit rotamer. In this case the analysis was slightly more complicated because 7 rotamers for 355 were all found to be acceptable conformations by Deepview parameters. However, upon filtering through all the data we again found a best fit for residue 355. For this particular rotamer, residue 355 comes into very close contact with residue 279, in the range of 5-9Å. Residue 51 is also in close contact with this 355 rotamer in the range of 8-12Å, slightly further away than 279, consistent with our omega interaction parameter data. Also for this 355 rotamer, residues 355-129 and 355-130 move considerably away from one another in $_{L}$-aspartate, with the distances between residues 355-129 slightly closer (15-20Å) than the distances between 355-130 (~18-20Å). Attempting to find a best-fit rotamer pair for 353-130 in $_{L}$-aspartate was complicated by the fact that 7 rotamers for 130, and 3 rotamers for 353 were considered acceptable in Deepview. Nonetheless, an examination of all rotamer combinations for this residue pair showed a range of 11-19Å, again consistent with our omega interaction parameter data and suggesting residues 353-130 move apart considerably upon the binding of $_{L}$-aspartate, as compared to $_{DL}$-TBOA.

In multimeric proteins with multiple spin labels per subunit (such as in our case), one has to consider the possibility of intersubunit spin-spin interactions. Our Deepview analysis found that this is important for residue pair 355-51. In $_{DL}$-

TBOA, the omega interaction parameter for 355-51 (Fig. 5B) is larger than expected from the β-carbon distances in Fig. 1. Also, for residue pair 355-51, we did not see much change in omega interaction parameters between the apo state, Na^+-bound state, and the $_{DL}$-TBOA-bound state (Fig 6a,b). However, using Deepview analysis in conjunction with our omega interaction parameter data, these observations can be explained by a combination of intra- and intersubunit spin-spin interactions (Supplementary Fig. S2). In $_L$-aspartate, residues 355 and 51 come into quite close intrasubunit contact resulting in a large omega interaction parameter. The larger than expected interaction parameters in the $_{DL}$-TBOA-bound state can be explained by an intersubunit spin-spin interaction between 51 and 355. Our Deepview analysis suggests that in Na^+ and $_{DL}$-TBOA, residues 355 and 51 interact via intersubunit interaction, while in the apo state 355-51 interact via intrasubunit interaction at a similar distance.

Due to the labeling protocol we used to ensure that maximally labeled and under labeled proteins were in the same conformations, the observed changes in the lineshapes and Ω interaction parameters induced by spin-spin interactions are most likely lower estimates because (1) in the under labeled conditions, some fraction of the subunits will still be double labeled and (2) in the maximally labeled conditions, we estimate from the mass spectroscopy data that spin labeling was in the 90-100% range. However, by using the available crystal structures as an internal calibration of the Ω interaction parameters (Supplementary Fig. S1), we conclude that the differences in the observed Ω interaction parameters between residues pairs are consistent with the positions

of HP2 in the crystal structures in $_{L}$-aspartate and $_{DL}$-TBOA. In addition, because the observed Ω interaction parameters in the apo state and in Na^{+} are intermediate to the Ω interaction parameters in $_{L}$-aspartate and $_{DL}$-TBOA, we conclude that the positions of HP2 in the apo and Na^{+}-bound states are intermediate to the positions of HP2 in $_{L}$-aspartate and $_{DL}$-TBOA (Fig. 8). By interpolation, using the calibrated Ω interaction parameters to distance relationship (Supplementary Fig. S1), we estimate the approximate positions of HP2 in the apo and Na^{+} bound states (Fig. 8).

In summary, by including intersubunit interactions and most likely side-chain orientations and rotameric state, the Ω parameters from all residues pairs are consistent with a relative movement of the tip of HP2 toward TM4a upon Na^{+} binding, as well as $_{DL}$-TBOA binding, and away from TM4a and towards TM2 and HP1 upon binding of $_{L}$-aspartate.

IV. Chapter 4

Summary and Conclusions

In this current work, we set out to develop the technique of DSDSL-EPR for use on the bacterial glutamate transporter homolog Glt_{Ph}. Our reasoning for this was two-fold. First, we reasoned that this technique would provide the necessary sensitivity to confirm that the small movements observed in the proposed extracellular gate (HP2) in crystal structures also occurred in the more native environment of a lipid bilayer. Using protocols developed and described in this thesis, we verified that indeed this is the case (See Fig. 5 in results). Secondly, we reasoned that development of this technique would enable future EPR experiments capable of elucidating many different aspects of the transport cycle. Our initial experiments suggest this to be true; by using our technique we were able to reveal the nature of small structural conformational changes in the extracellular gate (HP2) in response to the binding of Na^+ to the apo-state of the transporter (see Fig. 6, 7, 8 in results).

While our experiments were centered on elucidating small conformational changes in HP2 when the transporter is in the outward-facing state, the data we obtained has led us to propose a model for Glt_{Ph} transport (presented below).

Upon obtaining our data in the apo-state, we were initially perplexed as to why the extracellular gate would be primarily closed in the absence of ions and substrate. Fortunately, we believe the most recent crystal structures of Glt_{Ph}

have shed light on this question, leading us to speculate on the data we have presented in this thesis. In their most recent crystallography paper, the Boudker group (Reyes et al., 2009) proposed a model in which translocation of substrate and ion binding sites across the membrane requires both HP2, as well as HP1, to be in a closed conformation (see Fig. 17, Chapter 1). They proposed that subsequent movement of HP1 was next required for substrate and ion release to the cytosol, however what was not clear in this paper was what happens after HP1 is open to the inside. Indeed, in their paper the authors state "the structural re-arrangements within the transport domain, which would allow for closure of the extracellular and intracellular gates in the absence of bound substrate and ions, remain to be elucidated" (Reyes et al., 2009).

What is clear from our data is that in the apo-state HP2 is in a primarily closed conformation. Thus, we propose a model in which in the apo-state, both HP2 *and* HP1 are closed to allow for reorientation of the substrate and ion-binding sites (Fig. 1). This is consistent with the idea proposed by the Boudker group, namely that in order for the C-terminal vertical movement to occur (in the forward direction), both HP2 and HP1 must occupy a "closed" conformation.

So in our model (Fig. 1), it is thus the binding of Na+ to the apo-state that opens and stabilizes HP2, in effect creating a substrate-binding site (Fig. 1). Binding of substrate then closes HP2, and with both HP2 and HP1 in a closed conformation, translocation of the substrate and ion binding sites can occur. Further conformational change in HP1 thus results in the release of ions and substrate

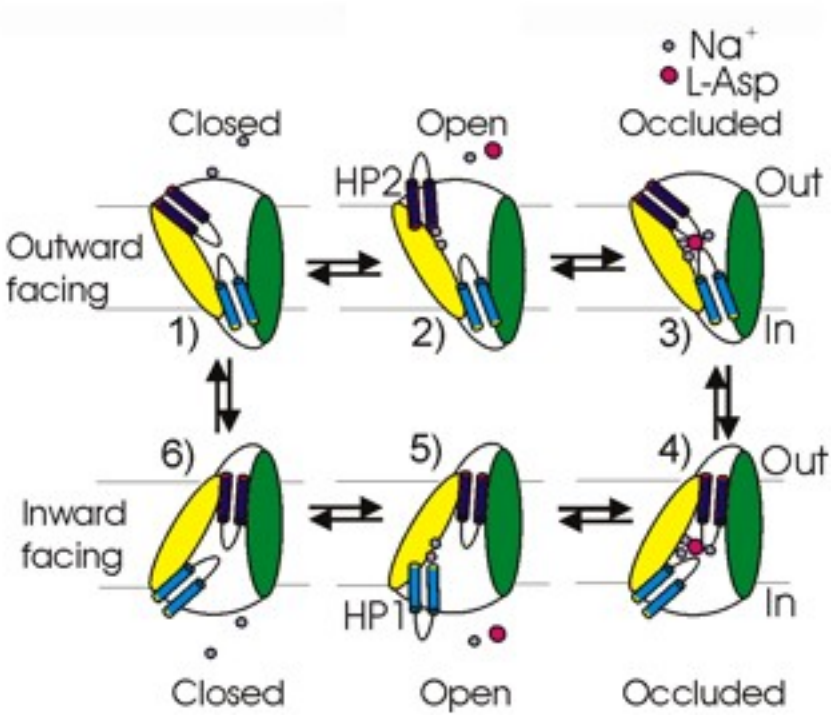

Figure 1. Transport model of Glt_{Ph}. In the apo-state, both HP2 (purple) and HP1 (blue) reside in a primarily closed conformation. This allows for the ability of HP2 and HP1 to slide vertically through the membrane (1 and 6), and reorient the binding sites. In the outward-facing apo-state, the binding of Na^+ results in a movement of HP2 that opens the extracellular gate (2). Subsequent binding of a second Na+ ion and an L-asp results in a closing of the extracellular gate (HP2) (3). At this point, with HP2 and HP1 in a closed conformation, HP2 and HP1 can again slide vertically through the membrane (3-4), to reorient the binding sites to the cytosol. Further conformation of HP1 is then required for the release of ions and substrate to the cytosol (5).

to the cytosol. Finally, in the apo-state, the most stable position of HP1 and HP2 is in a closed conformation, to allow for reorientation of the transporter.

At the end of the introduction to this thesis (Chapter 1), a conceptual overview of how mammalian glutamate transporters accomplish uptake was presented. Our model of the transport cycle in Glt_{Ph} shares many common features, yet there are many differences and unknowns.

First off, conformational change is seen in HP2 upon the binding of Na^+ to the apo-state in mammalian transporters, and as we have presented in this thesis, this too occurs in the bacterial transporter. We therefore suggest that the role of the binding of (most likely) the second Na^+ ion is to open and stabilize HP2, and thus create the substrate-binding site. In neurons, which are bathed in high extracellular Na^+ solution, this would mean that transporters predominantly occupy an "open to the outside" conformation, ready to bind glutamate. This is most likely an evolutionary adaptation from the bacterial transporters, as the bacterial species (*Pyrococcus horikoshii*) from which Glt_{Ph} is obtained lived in saltwater. According to this idea, the sodium ions serve to "ready" the transporter for glutamate binding.

Subsequent to substrate binding, it is unclear in the bacterial transporters whether another Na^+ ion binds, or whether the bacterial transporters are only coupled to two Na^+ ions. This remains to be elucidated. Nevertheless, it is likely, but not yet proven, that subsequent to substrate-binding a large vertical movement of the C-terminal region seen in the bacterial transporters also occurs in the mammalian transporters. This too needs further investigation in the

mammalian transporters. In the inward-facing state of the transport process, clearly ions and substrate are released to the cytosol in both mammalian transporters, as well as bacterial transporters. The movement of HP1 is proposed to be required for this to occur in both mammalian transporters as well as bacterial transporters, but this too is yet to be proven. This will likely remain an active area of research for many years to come.

Finally, a major difference between the mammalian transport cycle and the bacterial transport cycle is the fact that K^+ is not required for the reorientation step in the bacterial transporter. What then, is the evolutionary significance of the role of K^+ in the reorientation step in mammalian transporters? First off, in mammalian transporters the K^+ return step is coupled to transport, thus it serves to contribute to the thermodynamics of glutamate uptake against its concentration gradient. However, there is another role for the K^+ return step in mammals, and that is to speed up the transport cycle. The bacterial transport cycle at room temperature is exceedingly slow, on the order of minutes. However the mammalian transport cycle is much faster, on the order of tens of milliseconds. The K^+ return step is proposed to be the slowest step in the mammalian transport cycle, yet without it the cycle would never be completed. As mentioned above at the end of the introduction, two negative charges serve to counterbalance the positive charge on the K^+ ion in order to facilitate the return step, and therefore at negative potentials, this step becomes more rapid. In neurons, following a depolarization event, hyperpolarization of the neuron would serve to significantly speed up the transport cycle. In contrast, our work

suggests that in the *bacterial* transporters the most stable conformation of HP1 and HP2 are in a predominantly closed conformation in the absence of external factors, thus allowing for the reorientation of substrate and ions to the extracellular space. Nonetheless, it appears, but again is not proven, that the reorientation step in mammalian transporters as well as bacterial transporters requires HP1 and HP2 to reside in a closed conformation. This too will be important to resolve in future experiments.

In terms of future EPR experiments, the recent publication of crystal structures (Reyes et al., 2009) and modeling work (Crisman et al., 2009) (verified by disulfide-bond formation experiments) representing the inward-facing, occluded state provides a framework from which to conduct future EPR experiments to uncover conformational changes *not seen* in crystal structures, such as the proposed intracellular opening of HP1 (Boudker et al., 2007; Crisman et al., 2009; Reyes et al., 2009). That this recent crystal structure reveals the possibility of "locking" Glt_{Ph} in the inward-facing, occluded state is quite fortunate and beneficial for future EPR experiments for several reasons. First, in contrast to Glt_{Ph}, mammalian EAATs can be biased toward spending a larger fraction of time in the inward-facing state by adding extracellular potassium (Shlaifer and Kanner, 2007). Glt_{Ph} does not require K^+ to reorient (Ryan et al., 2009), thus adding extracellular potassium would not be expected to bias the transporter toward an inward-facing state. Second, adding extracellular Na^+ and glutamate to mammalian EAATs biases the transporters toward an inward-facing state

because the K^+ return step is slow (thus the transporter spends more time in an inward-facing state). In Glt_{Ph} this is not necessarily the case. Certainly the crystal structures do not suggest that adding extracellular Na^+ and substrate would bias the transporter toward an inward-facing state, as structures obtained in the presence of Na^+ and substrate represent the outward-facing, occluded state (Boudker et al., 2007; Yernool et al., 2004). Interestingly, both in membranes and detergent it was found that Glt_{Ph}(55C-364C) is more readily crosslinked by CuPhen in the absence of Na^+ and $_L$-asp, compared to the presence of Na^+ and $_L$-asp. While this is an intriguing finding and could represent a slight bias toward an inward-facing state in the absence of Na^+ and $_L$-asp, the fact that a large amount of protein remains un-crosslinked even after 15-30 minutes (Reyes et al., 2009) would complicate analysis of EPR experiments conducted on the inward-facing state. In contrast to CuPhen, $HgCl_2$ crosslinks Glt_{Ph}(55C/364C) in seconds, but does so in both the presence and absence of Na^+ and $_L$-asp, again complicating experimental design and analysis. Finally, even were there a way to bias Glt_{Ph} toward an inward-facing state, this too would be complicated by the fact that Glt_{Ph} is incorporated equally effectively into liposomes in both orientations (Ryan et al., 2009).

In the work described in this thesis, we made mutations that resulted in proteins unable to effectively transport substrate (Fig. 3, Chapter 3), thus locking the transporter in the outward-facing state. This was fortunate as it allowed us to make distance measurements using DSDSL-EPR on transporters that were not continuously cycling through the transport cycle. In a similar fashion, the ability

to crosslink Glt_{Ph}(55C-364C), thus locking the transporter in the inward-facing state, is also fortunate for our future EPR experiments. We propose using this to our advantage in similar ways to the experiments conducted in this thesis to obtain information on the conformational changes involved in the intracellular gate.

We can therefore make use of a similar experimental protocol we designed in this thesis, with modifications, for future experiments. We will again use DSDSL-EPR to make distance measurements, this time between residues located on HP1 and surrounding protein domains, in the apo-state, Na^+-only state, substrate and ion-bound states, and the inhibitor-bound state. We know from previous work that substrate (Boudker, 2009) and inhibitor (O. Boudker, unpublished observations) binds to the substrate-free Glt_{Ph}(55C-364C-$_{Hg}$) protein, validating the general methodology of this approach. The goal of these experiments will be to characterize movements of the intracellular gate with respect to surrounding protein domains. The recent publication of a modeling study (Chrisman 2009) in which TBOA is bound to Glt_{Ph} on the inside (when in an inward-facing state) will serve as a guide for which residues to choose. This approach will likely maximize our chances of finding residues on HP1 that move away from residues on other protein domains under different conditions.

Briefly, we propose an experimental protocol as follows. We will first crosslink Glt_{Ph}(55C-364C-$_{Hg}$) in the inward-facing, occluded state, and will then make distance measurements between residues on HP1 and residues on, for example, TM2 or TM5, under the conditions mentioned above. Making use of Glt_{Ph}(55C-

364C) will introduce complications not found in our work described in this thesis, namely the fact that cysteines must be introduced in which to cross-link the transporter, and additional cysteines must be introduced to conduct DSDSL-EPR distance measurements. This complication can be dealt with by designing our experimental protocol in the following way. First, we can take advantage of the fact that spin-spin interactions occur “through space”, and therefore interactions are not dependent on specific orientations (like those involved in disulfide-bond formation). We will therefore utilize the published inward-facing, occluded state crystal structure to select residues on HP1 and, for example, TM5 or TM2, to mutate to cysteines located close to each other, but which are not in a correct orientation to crosslink. That will be evaluated by purifying the double mutant, incubating with $HgCl_2$, and running on a gel, similar to the protocol utilized by Boudker (Reyes et al., 2009). Once we have determined a particular double cysteine mutant (we will call this construct “double cysteine EPR” mutant or “DC-EPR” mutant) will not crosslink, we can introduce sequentially 55C and 364C into our double-cysteine-EPR mutant. After verifying that no combination of triple cysteine mutants form a disulfide, we can then make the quadruple cysteine mutant, GltPh(55C-364C)-DC-EPR.

The quadruple mutant, or “QM-EPR”, will be purified and then crosslinked in the presence of $HgCl_2$ according to previously described protocols (Boudker 2009). Binding of Hg to the other thiols will also occur, but with much lower affinity. Hg bound to free thiols will be removed by running the crosslinked protein over a chromatography column under conditions that will reduce $HgCl_2$ to a

concentration which will 1) not prevent the high-affinity crosslinking of 55C-364C, but which will 2) remove the metal from single thiols. At this point, labeling of the free thiols with the sulfhydryl specific spin label MTSL will be done. Free label will again be removed by chromatography as was done in the work contained in this thesis, and protein will be reconstituted into liposomes.

Preparation of proteins in this fashion will provide us with Glt_{Ph} in the inward-facing state, with spin-labeled residues on HP1 and surrounding protein domains with which to make distance measurements under different "proposed" states of HP1. Similar to our findings presented in this thesis, we expect to find conformational changes associated with HP1 that will allow us to make conclusions on how ions and substrate are released into the cytoplasmic space, and how the transport domain returns to the outward-facing state. If the protocol described above proves too technically challenging, we could also attempt to find residues which, when labeled, simply lock the transporter in the inward-facing state, but which allow binding of substrate, ions, and inhibitors in a fashion similar to what we have described for the extracellular gate.

As we have discussed in this thesis, the accuracy of distance measurements obtained by DSDSL-EPR is limited by the rotameric states of the spin label. In our current work, we made use of advice provided by a previous study (Altenbach et al., 2001), namely that the accuracy of qualitative distance estimates is enhanced by making multiple measurements and thereby establishing a reproducible pattern of spin-spin interactions. In the future there are several ways to improve our distance measurements such that our estimates

are more quantitative. One way is to incorporate modeling strategies (Sale et al., 2005) that can account for the conformational flexibility of the spin-label, thus decreasing the uncertainty in the interpretation of spin-spin distance measurements. Another way is to incorporate the use of spin labels with greater side-chain rigidity (Columbus et al., 2001). The use of unnatural spin-labeled amino acids is also a possibility in the future. For example, expressed protein ligation (EPL) enables the ligation of a chemically synthesized protein domain, which can harbor an unnatural spin-labeled amino acid, with a recombinant protein domain purified from bacteria. The complication of this approach is that the folding process must be achieved in vitro, however successful folding of engineered ion channels has been described (Valiyaveetil et al., 2002), and could potentially work for Glt_{Ph} as well. Therefore, while the approach of DSDSL-EPR is complicated by the multiple rotameric states the spin label can occupy, future experimental procedures such as those described here are certain to improve the accuracy and reliability of distance measurements. DSDSL-EPR will therefore continue to be a valuable tool in the elucidation of conformational changes associated with substrate transport in Glt_{Ph}, as well as other soluble and membrane proteins.

In addition to distance measurements between two spin-labeled side chains, membrane protein accessibility studies can be conducted on spin-labeled proteins. Briefly, accessibility experiments are based on relaxation enhancement by another paramagnetic molecule in solution, for example molecular oxygen or various Ni(II) complexes. Collisions with the relaxing species allows more

microwave energy to be absorbed resulting in an increase in the power necessary for saturation, quantified by the power saturation parameter $P_{1/2}$. An increase of $P_{1/2}$ in the presence of the relaxing agent indicates an accessible region. By measuring $P_{1/2}$ in either molecular oxygen (hydrophobic) or Ni(II) (hydrophilic), the accessibility of the spin label to the relaxant is determined and interpreted as a location facing a hydrophilic region (aqueous phase) or a hydrophobic region (lipid phase or protein interior). Studies such as these will prove valuable for determining the precise pathway in Glt_{Ph} that substrate travels through from the extracellular to intracellular space. These experiments are again complicated by the fact that GltPh protein incorporates into the membrane equally effectively in both orientations (Ryan et al., 2009), but by carefully designing experiments and cautiously interpreting results, accessibility studies should prove a valuable technique for deciphering small conformational changes in Glt_{Ph}.

In summary, work contained in this thesis describes the development of DSDSL-EPR methodology for use on the bacterial glutamate transporter homolog Glt_{Ph}. We utilized our approach to first confirm the proposal that HP2 functions as the extracellular gate in glutamate transporters, and subsequently to elucidate small conformational changes that occur in HP2 upon the binding of Na^+ to the apo-state of the transporter. Using mammalian EAAT3 we confirmed that similar movements of HP2 also occur in mammalian glutamate transporters upon the binding of Na^+ to the apo-state of the transporter. This thus suggests that our use of DSDSL-EPR on the bacterial transporter Glt_{Ph} serves as a good model

system for predicting conformational changes that occur in mammalian glutamate transporters. Interestingly, the main difference between Glt_{Ph} and mammalian EAATs is the fact that Glt_{Ph} does not require K^+ to reorient the transporter from the inward-facing state to the outward-facing state (Ryan et al., 2009). Reyes et al., 2009, in their latest crystallography paper in which Glt_{Ph} is crystallized in the inward-facing conformation, state that "the structural rearrangements within the transport domain, which would allow for the closure of the extracellular and the intracellular gates in the absence of bound substrate and ions, remain to be elucidated". We believe that our EPR data shines light on these structural rearrangements, as in the apo-state we find that the extracellular gate (HP2) is in an essentially closed conformation. We therefore suggest that in the inward-facing state, subsequent to the release of ions and substrate to the cytosol, HP1 adopts a "closed" state similar to that observed for HP2 in the apo-state. It is at this point when both gates in the apo-state are mainly closed that the transporter reorients to the outside, where the binding of Na^+ then opens the extracellular gate and again readies the transporter for the binding of substrate. Why the return-step in the EAATs is then coupled to K^+ while the bacterial transporters are not remains to be revealed. The mechanistic details of this discrepancy are likely to provide interesting clues toward the understanding of the evolution of glutamate transporters.

The importance of further work and insight into the structural aspects of glutamate transporter function is highlighted by the numerous neurodegenerative and neuropsychiatric disorders in which EAAT dysfunction is implicated (Hinoi et

al., 2005). In this light, the recent discovery of a potentially neuroprotective compound, named Parawixin 1, from *Parawixia bistriata* spider venom is extremely intriguing. Parawixin 1 functions to enhance transport via a novel mechanism that appears due to Parawixin 1 acting allosterically to change the dynamics of the K^+ return step. That compounds such as Parawixin 1 function to enhance transport therefore suggests that rational drug design stemming from detailed knowledge of the structural aspects of the transport cycle could prove highly effective. Under conditions where increased concentrations of glutamate lead to excitotoxicity, such as during stroke and ischemia (Oechmichen and Meissner, 2006), a compound with the ability to enhance glutamate uptake could prove invaluable for limiting excitotoxic damage. There is therefore clearly a precedent for more work to be done on the biophysical aspects of glutamate transporters. Successful implementation of strategies aimed at manipulating and controlling extracellular levels of glutamate by specifically targeting glutamate transporters is a highly promising future goal.

References

Altenbach, C., Oh, K.J., Trabanino, R.J., Hideg, K., and Hubbell, W.L. (2001). Estimation of inter-residue distances in spin labeled proteins at physiological temperatures: experimental strategies and practical limitations. Biochemistry *40*, 15471-15482.

Aoki, M., Lin, C.L., Rothstein, J.D., Geller, B.A., Hosler, B.A., Munsat, T.L., Horvitz, H.R., and Brown, R.H., Jr. (1998). Mutations in the glutamate transporter EAAT2 gene do not cause abnormal EAAT2 transcripts in amyotrophic lateral sclerosis. Ann Neurol *43*, 645-653.

Armstrong, N., Sun, Y., Chen, G.Q., and Gouaux, E. (1998). Structure of a glutamate-receptor ligand-binding core in complex with kainate. Nature *395*, 913-917.

Arriza, J.L., Eliasof, S., Kavanaugh, M.P., and Amara, S.G. (1997). Excitatory amino acid transporter 5, a retinal glutamate transporter coupled to a chloride conductance. Proc Natl Acad Sci U S A *94*, 4155-4160.

Arriza, J.L., Fairman, W.A., Wadiche, J.I., Murdoch, G.H., Kavanaugh, M.P., and Amara, S.G. (1994). Functional comparisons of three glutamate transporter subtypes cloned from human motor cortex. J Neurosci *14*, 5559-5569.

Arriza, J.L., Kavanaugh, M.P., Fairman, W.A., Wu, Y.N., Murdoch, G.H., North, R.A., and Amara, S.G. (1993). Cloning and expression of a human neutral amino acid transporter with structural similarity to the glutamate transporter gene family. J Biol Chem *268*, 15329-15332.

Auger, C., and Attwell, D. (2000). Fast removal of synaptic glutamate by postsynaptic transporters. Neuron *28*, 547-558.

Austermuhle, M.I., Hall, J.A., Klug, C.S., and Davidson, A.L. (2004). Maltose-binding protein is open in the catalytic transition state for ATP hydrolysis during maltose transport. J Biol Chem *279*, 28243-28250.

Barbour, B., Brew, H., and Attwell, D. (1988). Electrogenic glutamate uptake in glial cells is activated by intracellular potassium. Nature *335*, 433-435.

Barish, M.E. (1983). A transient calcium-dependent chloride current in the immature Xenopus oocyte. J Physiol *342*, 309-325.

Baude, A., Nusser, Z., Roberts, J.D., Mulvihill, E., McIlhinney, R.A., and Somogyi, P. (1993). The metabotropic glutamate receptor (mGluR1 alpha) is concentrated at

perisynaptic membrane of neuronal subpopulations as detected by immunogold reaction. Neuron *11*, 771-787.

Ben-Ari, Y. (2002). Excitatory actions of gaba during development: the nature of the nurture. Nat Rev Neurosci *3*, 728-739.

Bendahan, A., Armon, A., Madani, N., Kavanaugh, M.P., and Kanner, B.I. (2000). Arginine 447 plays a pivotal role in substrate interactions in a neuronal glutamate transporter. J Biol Chem *275*, 37436-37442.

Bergles, D.E., Tzingounis, A.V., and Jahr, C.E. (2002). Comparison of coupled and uncoupled currents during glutamate uptake by GLT-1 transporters. J Neurosci *22*, 10153-10162.

Billups, B., and Attwell, D. (1996). Modulation of non-vesicular glutamate release by pH. Nature *379*, 171-174.

Billups, B., Rossi, D., and Attwell, D. (1996). Anion conductance behavior of the glutamate uptake carrier in salamander retinal glial cells. J Neurosci *16*, 6722-6731.

Bolin, K.A., Hanson, P., Wright, S.J., and Millhauser, G.L. (1998). An NMR investigation of the conformational effect of nitroxide spin labels on Ala-rich helical peptides. J Magn Reson *131*, 248-253.

Borre, L., and Kanner, B.I. (2001). Coupled, but not uncoupled, fluxes in a neuronal glutamate transporter can be activated by lithium ions. J Biol Chem *276*, 40396-40401.

Borre, L., Kavanaugh, M.P., and Kanner, B.I. (2002). Dynamic equilibrium between coupled and uncoupled modes of a neuronal glutamate transporter. J Biol Chem *277*, 13501-13507.

Boudker, O., Ryan, R.M., Yernool, D., Shimamoto, K., and Gouaux, E. (2007). Coupling substrate and ion binding to extracellular gate of a sodium-dependent aspartate transporter. Nature *445*, 387-393.

Bouvier, M., Szatkowski, M., Amato, A., and Attwell, D. (1992). The glial cell glutamate uptake carrier countertransports pH-changing anions. Nature *360*, 471-474.

Brasnjo, G., and Otis, T.S. (2004). Isolation of glutamate transport-coupled charge flux and estimation of glutamate uptake at the climbing fiber-Purkinje cell synapse. Proc Natl Acad Sci U S A *101*, 6273-6278.

Brocke, L., Bendahan, A., Grunewald, M., and Kanner, B.I. (2002). Proximity of two oppositely oriented reentrant loops in the glutamate transporter GLT-1 identified by paired cysteine mutagenesis. J Biol Chem *277*, 3985-3992.

Brown, R.H., Jr. (1995). Amyotrophic lateral sclerosis: recent insights from genetics and transgenic mice. Cell *80*, 687-692.

Chaudhry, F.A., Lehre, K.P., van Lookeren Campagne, M., Ottersen, O.P., Danbolt, N.C., and Storm-Mathisen, J. (1995). Glutamate transporters in glial plasma membranes: highly differentiated localizations revealed by quantitative ultrastructural immunocytochemistry. Neuron *15*, 711-720.

Chen, W., Mahadomrongkul, V., Berger, U.V., Bassan, M., DeSilva, T., Tanaka, K., Irwin, N., Aoki, C., and Rosenberg, P.A. (2004). The glutamate transporter GLT1a is expressed in excitatory axon terminals of mature hippocampal neurons. J Neurosci *24*, 1136-1148.

Chen, Y., and Swanson, R.A. (2003). The glutamate transporters EAAT2 and EAAT3 mediate cysteine uptake in cortical neuron cultures. J Neurochem *84*, 1332-1339.

Coco, S., Verderio, C., Trotti, D., Rothstein, J.D., Volterra, A., and Matteoli, M. (1997). Non-synaptic localization of the glutamate transporter EAAC1 in cultured hippocampal neurons. Eur J Neurosci *9*, 1902-1910.

Columbus, L., and Hubbell, W.L. (2002). A new spin on protein dynamics. Trends Biochem Sci *27*, 288-295.

Columbus, L., Kalai, T., Jeko, J., Hideg, K., and Hubbell, W.L. (2001). Molecular motion of spin labeled side chains in alpha-helices: analysis by variation of side chain structure. Biochemistry *40*, 3828-3846.

Conti, F., DeBiasi, S., Minelli, A., Rothstein, J.D., and Melone, M. (1998). EAAC1, a high-affinity glutamate tranporter, is localized to astrocytes and gabaergic neurons besides pyramidal cells in the rat cerebral cortex. Cereb Cortex *8*, 108-116.

Crisman, T.J., Qu, S., Kanner, B.I., and Forrest, L.R. (2009). Inward-facing conformation of glutamate transporters as revealed by their inverted-topology structural repeats. Proc Natl Acad Sci U S A.

Czogalla, A., Pieciul, A., Jezierski, A., and Sikorski, A.F. (2007). Attaching a spin to a protein -- site-directed spin labeling in structural biology. Acta Biochim Pol *54*, 235-244.

Danbolt, N.C. (2001). Glutamate uptake. Prog Neurobiol *65*, 1-105.

Danbolt, N.C., Storm-Mathisen, J., and Kanner, B.I. (1992). An [Na+ + K+]coupled L-glutamate transporter purified from rat brain is located in glial cell processes. Neuroscience *51*, 295-310.

Dehnes, Y., Chaudhry, F.A., Ullensvang, K., Lehre, K.P., Storm-Mathisen, J., and Danbolt, N.C. (1998). The glutamate transporter EAAT4 in rat cerebellar Purkinje cells: a

glutamate-gated chloride channel concentrated near the synapse in parts of the dendritic membrane facing astroglia. J Neurosci *18*, 3606-3619.
Derouiche, A., and Rauen, T. (1995). Coincidence of L-glutamate/L-aspartate transporter (GLAST) and glutamine synthetase (GS) immunoreactions in retinal glia: evidence for coupling of GLAST and GS in transmitter clearance. J Neurosci Res *42*, 131-143.

Dingledine, R., Borges, K., Bowie, D., and Traynelis, S.F. (1999). The glutamate receptor ion channels. Pharmacol Rev *51*, 7-61.

Dutzler, R., Campbell, E.B., Cadene, M., Chait, B.T., and MacKinnon, R. (2002). X-ray structure of a ClC chloride channel at 3.0 A reveals the molecular basis of anion selectivity. Nature *415*, 287-294.

Edman, P. (1949). A method for the determination of amino acid sequence in peptides. Arch Biochem *22*, 475.

Eliasof, S., and Jahr, C.E. (1996). Retinal glial cell glutamate transporter is coupled to an anionic conductance. Proc Natl Acad Sci U S A *93*, 4153-4158.

Eliasof, S., and Werblin, F. (1993). Characterization of the glutamate transporter in retinal cones of the tiger salamander. J Neurosci *13*, 402-411.

Erecinska, M., Wantorsky, D., and Wilson, D.F. (1983). Aspartate transport in synaptosomes from rat brain. J Biol Chem *258*, 9069-9077.

Eskandari, S., Kreman, M., Kavanaugh, M.P., Wright, E.M., and Zampighi, G.A. (2000). Pentameric assembly of a neuronal glutamate transporter. Proc Natl Acad Sci U S A *97*, 8641-8646.

Fairman, W.A., Vandenberg, R.J., Arriza, J.L., Kavanaugh, M.P., and Amara, S.G. (1995). An excitatory amino-acid transporter with properties of a ligand-gated chloride channel. Nature *375*, 599-603.

Farrens, D.L., Altenbach, C., Yang, K., Hubbell, W.K., Khorana, H.G. (1996). Requirement of a rigid-body motion of transmembrane helices for light activation of rhodopsin. Science *274*, 768-70.

Fanucci, G.E., and Cafiso, D.S. (2006). Recent advances and applications of site-directed spin labeling. Curr Opin Struct Biol *16*, 644-53.

Forrest, L.R., Zhang, Y.W., Jacobs, M.T., Gesmonde, J., Xie, L., Honig, B.H., and Rudnick, G. (2008). Mechanism for alternating access in neurotransmitter transporters. Proc Natl Acad Sci U S A *105*, 10338-10343.

Franciolini, F., and Nonner, W. (1987). Anion and cation permeability of a chloride channel in rat hippocampal neurons. J Gen Physiol *90*, 453-478.

Franciolini, F., and Nonner, W. (1994). Anion-cation interactions in the pore of neuronal background chloride channels. J Gen Physiol *104*, 711-723.

Furness, D.N., and Lehre, K.P. (1997). Immunocytochemical localization of a high-affinity glutamate-aspartate transporter, GLAST, in the rat and guinea-pig cochlea. Eur J Neurosci *9*, 1961-1969.

Furuta, A., Martin, L.J., Lin, C.L., Dykes-Hoberg, M., and Rothstein, J.D. (1997). Cellular and synaptic localization of the neuronal glutamate transporters excitatory amino acid transporter 3 and 4. Neuroscience *81*, 1031-1042.

Gouaux, E. (2008). The molecular logic of sodium-coupled neurotransmitter transporters. Phil. Trans. R. Soc. B *364*, 149-154.

Grant, G.B., and Dowling, J.E. (1995). A glutamate-activated chloride current in cone-driven ON bipolar cells of the white perch retina. J Neurosci *15*, 3852-3862.

Grant, G.B., and Werblin, F.S. (1996). A glutamate-elicited chloride current with transporter-like properties in rod photoreceptors of the tiger salamander. Vis Neurosci *13*, 135-144.

Grewer, C., Balani, P., Weidenfeller, C., Bartusel, T., Tao, Z., and Rauen, T. (2005). Individual subunits of the glutamate transporter EAAC1 homotrimer function independently of each other. Biochemistry *44*, 11913-11923.

Grewer, C., Watzke, N., Rauen, T., and Bicho, A. (2003). Is the glutamate residue Glu-373 the proton acceptor of the excitatory amino acid carrier 1? J Biol Chem *278*, 2585-2592.

Gross, A., Columbus, L., Hideg, K., Altenbach, C., and Hubbell, W.L. (1999). Structure of the KcsA potassium channel from Streptomyces lividans: a site-directed spin labeling study of the second transmembrane segment. Biochemistry *38*, 10324-10335.

Grunewald, M., Bendahan, A., and Kanner, B.I. (1998). Biotinylation of single cysteine mutants of the glutamate transporter GLT-1 from rat brain reveals its unusual topology. Neuron *21*, 623-632.

Grunewald, M., and Kanner, B. (1995). Conformational changes monitored on the glutamate transporter GLT-1 indicate the existence of two neurotransmitter-bound states. J Biol Chem *270*, 17017-17024.

Grunewald, M., and Kanner, B.I. (2000). The accessibility of a novel reentrant loop of the glutamate transporter GLT-1 is restricted by its substrate. J Biol Chem *275*, 9684-9689.

Grunewald, M., Menaker, D., and Kanner, B.I. (2002). Cysteine-scanning mutagenesis reveals a conformationally sensitive reentrant pore-loop in the glutamate transporter GLT-1. J Biol Chem *277*, 26074-26080.

Guillet, B.A., Velly, L.J., Canolle, B., Masmejean, F.M., Nieoullon, A.L., and Pisano, P. (2005). Differential regulation by protein kinases of activity and cell surface expression of glutamate transporters in neuron-enriched cultures. Neurochem Int *46*, 337-346.

Hakuba, N., Gyo, K., Yanagihara, N., Mitani, A., and Kataoka, K. (1997). Efflux of glutamate into the perilymph of the cochlea following transient ischemia in the gerbil. Neurosci Lett *230*, 69-71.

Hakuba, N., Koga, K., Gyo, K., Usami, S.I., and Tanaka, K. (2000). Exacerbation of noise-induced hearing loss in mice lacking the glutamate transporter GLAST. J Neurosci *20*, 8750-8753.

Harada, T., Harada, C., Watanabe, M., Inoue, Y., Sakagawa, T., Nakayama, N., Sasaki, S., Okuyama, S., Watase, K., Wada, K., *et al.* (1998). Functions of the two glutamate transporters GLAST and GLT-1 in the retina. Proc Natl Acad Sci U S A *95*, 4663-4666.

He, Y., Janssen, W.G., Rothstein, J.D., and Morrison, J.H. (2000). Differential synaptic localization of the glutamate transporter EAAC1 and glutamate receptor subunit GluR2 in the rat hippocampus. J Comp Neurol *418*, 255-269.

Herman, M.A., and Jahr, C.E. (2007). Extracellular glutamate concentration in hippocampal slice. J Neurosci *27*, 9736-9741.

Himi, T., Ikeda, M., Yasuhara, T., Nishida, M., and Morita, I. (2003). Role of neuronal glutamate transporter in the cysteine uptake and intracellular glutathione levels in cultured cortical neurons. J Neural Transm *110*, 1337-1348.

Hinoi, E., Takarada, T., Tsuchihashi, Y., and Yoneda, Y. (2005). Glutamate transporters as drug targets. Curr Drug Targets CNS Neurol Disord *4*, 211-220.

Huang, Z., and Tajkhorshid, E. (2008). Dynamics of the extracellular gate and ion-substrate coupling in the glutamate transporter. Biophys J *95*, 2292-2300.

Hustedt, E.J., and Beth, A.H. (1999). Nitroxide spin-spin interactions: applications to protein structure and dynamics. Annu Rev Biophys Biomol Struct *28*, 129-153.

Hustedt, E.J., Smirnov, A.I., Laub, C.F., Cobb, C.E., and Beth, A.H. (1997). Molecular distances from dipolar coupled spin-labels: the global analysis of multifrequency continuous wave electron paramagnetic resonance data. Biophys J *72*, 1861-1877.

Hustedt, E.J., Stein, R.A., Sethaphong, L., Brandon, S., Zhou, Z., and Desensi, S.C. (2006). Dipolar coupling between nitroxide spin labels: the development and application of a tether-in-a-cone model. Biophys J *90*, 340-356.

Inanami, O., Hashida, S., Iizuka, D., Horiuchi, M., Hiraoka, W., Shimoyama, Y., Nakamura, H., Inagaki, F., and Kuwabara, M. (2005). Conformational change in full-length mouse prion: a site-directed spin-labeling study. Biochem Biophys Res Commun *335*, 785-792.

Jain, A., Martensson, J., Stole, E., Auld, P.A., and Meister, A. (1991). Glutathione deficiency leads to mitochondrial damage in brain. Proc Natl Acad Sci U S A *88*, 1913-1917.

Jardetzky, O. (1966). Simple allosteric model for membrane pumps. Nature *211*, 969-970.

Kanai, Y., and Hediger, M.A. (1992). Primary structure and functional characterization of a high-affinity glutamate transporter. Nature *360*, 467-471.

Kanai, Y., and Hediger, M.A. (2004). The glutamate/neutral amino acid transporter family SLC1: molecular, physiological and pharmacological aspects. Pflugers Arch *447*, 469-479.

Kanai, Y., Nussberger, S., Romero, M.F., Boron, W.F., Hebert, S.C., and Hediger, M.A. (1995). Electrogenic properties of the epithelial and neuronal high affinity glutamate transporter. J Biol Chem *270*, 16561-16568.

Kanai, Y., Smith, C.P., and Hediger, M.A. (1993). A new family of neurotransmitter transporters: the high-affinity glutamate transporters. FASEB J *7*, 1450-1459.

Kanner, B.I. (2006). Structure and function of sodium-coupled GABA and glutamate transporters. J Membr Biol *213*, 89-100.

Kanner, B.I., and Bendahan, A. (1982). Binding order of substrates to the sodium and potassium ion coupled L-glutamic acid transporter from rat brain. Biochemistry *21*, 6327-6330.

Kanner, B.I., Kavanaugh, M.P., and Bendahan, A. (2001). Molecular characterization of substrate-binding sites in the glutamate transporter family. Biochem Soc Trans *29*, 707-710.

Kanner, B.I., and Sharon, I. (1978). Active transport of L-glutamate by membrane vesicles isolated from rat brain. Biochemistry *17*, 3949-3953.

Kavanaugh, M.P., Bendahan, A., Zerangue, N., Zhang, Y., and Kanner, B.I. (1997). Mutation of an amino acid residue influencing potassium coupling in the glutamate transporter GLT-1 induces obligate exchange. J Biol Chem *272*, 1703-1708.

Kekuda, R., Prasad, P.D., Fei, Y.J., Torres-Zamorano, V., Sinha, S., Yang-Feng, T.L., Leibach, F.H., and Ganapathy, V. (1996). Cloning of the sodium-dependent, broad-scope, neutral amino acid transporter Bo from a human placental choriocarcinoma cell line. J Biol Chem *271*, 18657-18661.

Klug, C.S., and Feix, J.B. (2008). Methods and applications of site-directed spin labeling EPR spectroscopy. Methods Cell Biol *84*, 617-658.

Koch, H.P., Brown, R.L., and Larsson, H.P. (2007a). The glutamate-activated anion conductance in excitatory amino acid transporters is gated independently by the individual subunits. J Neurosci *27*, 2943-2947.

Koch, H.P., Hubbard, J.M., and Larsson, H.P. (2007b). Voltage-independent sodium-binding events reported by the 4B-4C loop in the human glutamate transporter excitatory amino acid transporter 3. J Biol Chem *282*, 24547-24553.

Koch, H.P., and Larsson, H.P. (2005). Small-scale molecular motions accomplish glutamate uptake in human glutamate transporters. J Neurosci *25*, 1730-1736.

Kugler, P., and Schmitt, A. (1999). Glutamate transporter EAAC1 is expressed in neurons and glial cells in the rat nervous system. Glia *27*, 129-142.

Larsson, H.P., Picaud, S.A., Werblin, F.S., and Lecar, H. (1996). Noise analysis of the glutamate-activated current in photoreceptors. Biophys J *70*, 733-742.

Larsson, H.P., Tzingounis, A.V., Koch, H.P., and Kavanaugh, M.P. (2004). Fluorometric measurements of conformational changes in glutamate transporters. Proc Natl Acad Sci U S A *101*, 3951-3956.

Lehre, K.P., and Danbolt, N.C. (1998). The number of glutamate transporter subtype molecules at glutamatergic synapses: chemical and stereological quantification in young adult rat brain. J Neurosci *18*, 8751-8757.

Lehre, K.P., Levy, L.M., Ottersen, O.P., Storm-Mathisen, J., and Danbolt, N.C. (1995). Differential expression of two glial glutamate transporters in the rat brain: quantitative and immunocytochemical observations. J Neurosci *15*, 1835-1853.

Leighton, B.H., Seal, R.P., Shimamoto, K., and Amara, S.G. (2002). A hydrophobic domain in glutamate transporters forms an extracellular helix associated with the permeation pathway for substrates. J Biol Chem *277*, 29847-29855.

Leighton, B.H., Seal, R.P., Watts, S.D., Skyba, M.O., and Amara, S.G. (2006). Structural rearrangements at the translocation pore of the human glutamate transporter, EAAT1. J Biol Chem *281*, 29788-29796.

Levy, L.M., Warr, O., and Attwell, D. (1998). Stoichiometry of the glial glutamate transporter GLT-1 expressed inducibly in a Chinese hamster ovary cell line selected for low endogenous Na+-dependent glutamate uptake. J Neurosci *18*, 9620-9628.

Lin, C.L., Bristol, L.A., Jin, L., Dykes-Hoberg, M., Crawford, T., Clawson, L., and Rothstein, J.D. (1998). Aberrant RNA processing in a neurodegenerative disease: the cause for absent EAAT2, a glutamate transporter, in amyotrophic lateral sclerosis. Neuron *20*, 589-602.

Liu, Y.S., Sompornpisut, P., and Perozo, E. (2001). Structure of the KcsA channel intracellular gate in the open state. Nat Struct Biol *8*, 883-887.

Malmberg, N.J., and Falke, J.J. (2005). Use of EPR power saturation to analyze the membrane-docking geometries of peripheral proteins: applications to C2 domains. Annu Rev Biophys Biomol Struct *34*, 71-90.

Mannuzzu, L.M., Moronne, M.M., and Isacoff, E.Y. (1996). Direct physical measure of conformational rearrangement underlying potassium channel gating. Science *271*, 213-216.

Massie, A., Vandesande, F., and Arckens, L. (2001). Expression of the high-affinity glutamate transporter EAAT4 in mammalian cerebral cortex. Neuroreport *12*, 393-397.

Mayer, M.L., and Westbrook, G.L. (1987). The physiology of excitatory amino acids in the vertebrate central nervous system. Prog Neurobiol *28*, 197-276.

McHaourab, H.S., Kalai, T., Hideg, K., and Hubbell, W.L. (1999). Motion of spin-labeled side chains in T4 lysozyme: effect of side chain structure. Biochemistry *38*, 2947-2955.

McHaourab, H.S., Lietzow, M.A., Hideg, K., and Hubbell, W.L. (1996). Motion of spin-labeled side chains in T4 lysozyme. Correlation with protein structure and dynamics. Biochemistry *35*, 7692-7704.

McHaourab, H.S., Oh, K.J., Fang, C.J., and Hubbell, W.L. (1997). Conformation of T4 lysozyme in solution. Hinge-bending motion and the substrate-induced conformational transition studied by site-directed spin labeling. Biochemistry *36*, 307-316.

Mehboob, S., Luo, B.H., Fu, W., Johnson, M.E., and Fung, L.W. (2005). Conformational studies of the tetramerization site of human erythroid spectrin by cysteine-scanning spin-labeling EPR methods. Biochemistry *44*, 15898-15905.

Menaker, D., Bendahan, A., and Kanner, B.I. (2006). The substrate specificity of a neuronal glutamate transporter is determined by the nature of the coupling ion. J Neurochem *99*, 20-28.

Mim, C., Tao, Z., and Grewer, C. (2007). Two conformational changes are associated with glutamate translocation by the glutamate transporter EAAC1. Biochemistry *46*, 9007-9018.

Nelson, P.J., Dean, G.E., Aronson, P.S., and Rudnick, G. (1983). Hydrogen ion cotransport by the renal brush border glutamate transporter. Biochemistry *22*, 5459-5463.

Nieoullon, A., Canolle, B., Masmejean, F., Guillet, B., Pisano, P., and Lortet, S. (2006). The neuronal excitatory amino acid transporter EAAC1/EAAT3: does it represent a major actor at the brain excitatory synapse? J Neurochem *98*, 1007-1018.

Nikkuni, O., Takayasu, Y., Iino, M., Tanaka, K., and Ozawa, S. (2007). Facilitated activation of metabotropic glutamate receptors in cerebellar Purkinje cells in glutamate transporter EAAT4-deficient mice. Neurosci Res *59*, 296-303.

Oechmichen, M., and Meissner, C. (2006). Cerebral hypoxia and ischemia: the forensic point of view: a review. J Forensic Sci *51*, 880-887.

Oh, K.J., Altenbach, C., Collier, R.J., and Hubbell, W.L. (2000). Site-directed spin labeling of proteins. Applications to diphtheria toxin. Methods Mol Biol *145*, 147-169.

Olney, J.W., and Sharpe, L.G. (1969). Brain lesions in an infant rhesus monkey treated with monsodium glutamate. Science *166*, 386-388.

Otis, T.S., and Jahr, C.E. (1998). Anion currents and predicted glutamate flux through a neuronal glutamate transporter. J Neurosci *18*, 7099-7110.

Ottersen, O.P., Takumi, Y., Matsubara, A., Landsend, A.S., Laake, J.H., and Usami, S. (1998). Molecular organization of a type of peripheral glutamate synapse: the afferent synapses of hair cells in the inner ear. Prog Neurobiol *54*, 127-148.

Pedersen, W.A., Fu, W., Keller, J.N., Markesbery, W.R., Appel, S., Smith, R.G., Kasarskis, E., and Mattson, M.P. (1998). Protein modification by the lipid peroxidation product 4-hydroxynonenal in the spinal cords of amyotrophic lateral sclerosis patients. Ann Neurol *44*, 819-824.

Perozo, E., Cortes, D.M., and Cuello, L.G. (1998). Three-dimensional architecture and gating mechanism of a K+ channel studied by EPR spectroscopy. Nat Struct Biol *5*, 459-469.

Perozo, E., Cortes, D.M., Sompornpisut, P., Kloda, A., and Martinac, B. (2002). Open channel structure of MscL and the gating mechanism of mechanosensitive channels. Nature *418*, 942-948.

Perozo, E., Kloda, A., Cortes, D.M., and Martinac, B. (2001). Site-directed spin-labeling analysis of reconstituted Mscl in the closed state. J Gen Physiol *118*, 193-206.

Pfeiffer, M., Rink, T., Gerwert, K., Oesterhelt, D., and Steinhoff, H.J. (1999). Site-directed spin-labeling reveals the orientation of the amino acid side-chains in the E-F loop of bacteriorhodopsin. J Mol Biol *287*, 163-171.

Picaud, S., Larsson, H.P., Wellis, D.P., Lecar, H., and Werblin, F. (1995a). Cone photoreceptors respond to their own glutamate release in the tiger salamander. Proc Natl Acad Sci U S A *92*, 9417-9421.

Picaud, S.A., Larsson, H.P., Grant, G.B., Lecar, H., and Werblin, F.S. (1995b). Glutamate-gated chloride channel with glutamate-transporter-like properties in cone photoreceptors of the tiger salamander. J Neurophysiol *74*, 1760-1771.

Pines, G., Danbolt, N.C., Bjoras, M., Zhang, Y., Bendahan, A., Eide, L., Koepsell, H., Storm-Mathisen, J., Seeberg, E., and Kanner, B.I. (1992). Cloning and expression of a rat brain L-glutamate transporter. Nature *360*, 464-467.

Pines, G., and Kanner, B.I. (1990). Counterflow of L-glutamate in plasma membrane vesicles and reconstituted preparations from rat brain. Biochemistry *29*, 11209-11214.

Pow, D.V., and Barnett, N.L. (2000). Developmental expression of excitatory amino acid transporter 5: a photoreceptor and bipolar cell glutamate transporter in rat retina. Neurosci Lett *280*, 21-24.

Pow, D.V., Barnett, N.L., and Penfold, P. (2000). Are neuronal transporters relevant in retinal glutamate homeostasis? Neurochem Int *37*, 191-198.
Puel, J.L. (1995). Chemical synaptic transmission in the cochlea. Prog Neurobiol *47*, 449-476.

Puel, J.L., Pujol, R., Ladrech, S., and Eybalin, M. (1991). Alpha-amino-3-hydroxy-5-methyl-4-isoxazole propionic acid electrophysiological and neurotoxic effects in the guinea-pig cochlea. Neuroscience *45*, 63-72.

Qu, S., and Kanner, B.I. (2008). Substrates and non-transportable analogues induce structural rearrangements at the extracellular entrance of the glial glutamate transporter GLT-1/EAAT2. J Biol Chem *283*, 26391-26400.

Quick, M., and Javitch, J.A. (2007). Monitoring the function of membrane transport proteins in detergent-solubilized form. Proc Natl Acad Sci U S A *104*, 3603-3608.

Rabenstein, M.D., and Shin, Y.K. (1995). Determination of the distance between two spin labels attached to a macromolecule. Proc Natl Acad Sci U S A *92*, 8239-8243.

Rao, V.L., Baskaya, M.K., Dogan, A., Rothstein, J.D., and Dempsey, R.J. (1998). Traumatic brain injury down-regulates glial glutamate transporter (GLT-1 and GLAST) proteins in rat brain. J Neurochem *70*, 2020-2027.

Rauen, T., and Kanner, B.I. (1994). Localization of the glutamate transporter GLT-1 in rat and macaque monkey retinae. Neurosci Lett *169*, 137-140.

Rauen, T., Rothstein, J.D., and Wassle, H. (1996). Differential expression of three glutamate transporter subtypes in the rat retina. Cell Tissue Res *286*, 325-336.

Rauen, T., Taylor, W.R., Kuhlbrodt, K., and Wiessner, M. (1998). High-affinity glutamate transporters in the rat retina: a major role of the glial glutamate transporter GLAST-1 in transmitter clearance. Cell Tissue Res *291*, 19-31.

Represa, A., and Ben-Ari, Y. (2005). Trophic actions of GABA on neuronal development. Trends Neurosci *28*, 278-283.

Reyes, N., Ginter, C., and Boudker, O. (2009). Transport mechanism of a bacterial homologue of glutamate transporters. Nature.

Rink, T., Riesle, J., Oesterhelt, D., Gerwert, K., and Steinhoff, H.J. (1997). Spin-labeling studies of the conformational changes in the vicinity of D36, D38, T46, and E161 of bacteriorhodopsin during the photocycle. Biophys J *73*, 983-993.

Robberecht, W., Sapp, P., Viaene, M.K., Rosen, D., McKenna-Yasek, D., Haines, J., Horvitz, R., Theys, P., and Brown, R., Jr. (1994). Cu/Zn superoxide dismutase activity in familial and sporadic amyotrophic lateral sclerosis. J Neurochem *62*, 384-387.

Rogawski, M.A., Thurkauf, A., Yamaguchi, S., Rice, K.C., Jacobson, A.E., and Mattson, M.V. (1989). Anticonvulsant activities of 1-phenylcyclohexylamine and its conformationally restricted analog 1,1-pentamethylenetetrahydroisoquinoline. J Pharmacol Exp Ther *249*, 708-712.

Rosen, D.R., Bowling, A.C., Patterson, D., Usdin, T.B., Sapp, P., Mezey, E., McKenna-Yasek, D., O'Regan, J., Rahmani, Z., Ferrante, R.J., *et al.* (1994). A frequent ala 4 to val superoxide dismutase-1 mutation is associated with a rapidly progressive familial amyotrophic lateral sclerosis. Hum Mol Genet *3*, 981-987.

Rothstein, J.D., Martin, L., Levey, A.I., Dykes-Hoberg, M., Jin, L., Wu, D., Nash, N., and Kuncl, R.W. (1994). Localization of neuronal and glial glutamate transporters. Neuron *13*, 713-725.

Rothstein, J.D., Martin, L.J., and Kuncl, R.W. (1992). Decreased glutamate transport by the brain and spinal cord in amyotrophic lateral sclerosis. N Engl J Med *326*, 1464-1468.

Rothstein, J.D., Van Kammen, M., Levey, A.I., Martin, L.J., and Kuncl, R.W. (1995). Selective loss of glial glutamate transporter GLT-1 in amyotrophic lateral sclerosis. Ann Neurol *38*, 73-84.

Ryan, R.M., Compton, E.L., and Mindell, J.A. (2009). Functional characterization of a Na+-dependent aspartate transporter from Pyrococcus horikoshii. J Biol Chem *284*, 17540-17548.

Ryan, R.M., and Mindell, J.A. (2007). The uncoupled chloride conductance of a bacterial glutamate transporter homolog. Nat Struct Mol Biol *14*, 365-371.

Ryan, R.M., Mitrovic, A.D., and Vandenberg, R.J. (2004). The chloride permeation pathway of a glutamate transporter and its proximity to the glutamate translocation pathway. J Biol Chem *279*, 20742-20751.

Ryan, R.M., and Vandenberg, R.J. (2002). Distinct conformational states mediate the transport and anion channel properties of the glutamate transporter EAAT-1. J Biol Chem *277*, 13494-13500.

Sale, K., Song, L., Liu, Y.S., Perozo, E., and Fajer, P. (2005). Explicit treatment of spin labels in modeling of distance constraints from dipolar EPR and DEER. J Am Chem Soc *127*, 9334-9335.

Schmitt, A., Asan, E., Puschel, B., and Kugler, P. (1997). Cellular and regional distribution of the glutamate transporter GLAST in the CNS of rats: nonradioactive in situ hybridization and comparative immunocytochemistry. J Neurosci *17*, 1-10.

Schulz, J.B., Lindenau, J., Seyfried, J., and Dichgans, J. (2000). Glutathione, oxidative stress and neurodegeneration. Eur J Biochem *267*, 4904-4911.

Scoville, D., Stamm, J.D., Toledo-Warshaviak, D., Altenbach, C., Phillips, M., Shvetsov, A., Rubenstein, P.A., Hubbell, W.L., and Reisler, E. (2006). Hydrophobic loop dynamics and actin filament stability. Biochemistry *45*, 13576-13584.

Seal, R.P., and Amara, S.G. (1998). A reentrant loop domain in the glutamate carrier EAAT1 participates in substrate binding and translocation. Neuron *21*, 1487-1498.

Seal, R.P., Leighton, B.H., and Amara, S.G. (2000). A model for the topology of excitatory amino acid transporters determined by the extracellular accessibility of substituted cysteines. Neuron *25*, 695-706.

Seal, R.P., Shigeri, Y., Eliasof, S., Leighton, B.H., and Amara, S.G. (2001). Sulfhydryl modification of V449C in the glutamate transporter EAAT1 abolishes substrate transport

but not the substrate-gated anion conductance. Proc Natl Acad Sci U S A *98*, 15324-15329.

Selvin, P.R. (1995). Fluorescence resonance energy transfer. Methods Enzymol *246*, 300-334.

Shafqat, S., Tamarappoo, B.K., Kilberg, M.S., Puranam, R.S., McNamara, J.O., Guadano-Ferraz, A., and Fremeau, R.T., Jr. (1993). Cloning and expression of a novel Na(+)-dependent neutral amino acid transporter structurally related to mammalian Na+/glutamate cotransporters. J Biol Chem *268*, 15351-15355.

Shashidharan, P., Huntley, G.W., Murray, J.M., Buku, A., Moran, T., Walsh, M.J., Morrison, J.H., and Plaitakis, A. (1997). Immunohistochemical localization of the neuron-specific glutamate transporter EAAC1 (EAAT3) in rat brain and spinal cord revealed by a novel monoclonal antibody. Brain Res *773*, 139-148.

Sheng, M. (1996). PDZs and receptor/channel clustering: rounding up the latest suspects. Neuron *17*, 575-578.

Shimamoto, K., Lebrun, B., Yasuda-Kamatani, Y., Sakaitani, M., Shigeri, Y., Yumoto, N., and Nakajima, T. (1998). DL-threo-beta-benzyloxyaspartate, a potent blocker of excitatory amino acid transporters. Mol Pharmacol *53*, 195-201.

Shlaifer, I., and Kanner, B.I. (2007). Conformationally sensitive reactivity to permeant sulfhydryl reagents of cysteine residues engineered into helical hairpin 1 of the glutamate transporter GLT-1. Mol Pharmacol *71*, 1341-1348.

Shrivastava, I.H., Jiang, J., Amara, S.G., and Bahar, I. (2008). Time-resolved mechanism of extracellular gate opening and substrate binding in a glutamate transporter. J Biol Chem *283*, 28680-28690.

Sims, K.D., and Robinson, M.B. (1999). Expression patterns and regulation of glutamate transporters in the developing and adult nervous system. Crit Rev Neurobiol *13*, 169-197.

Slotboom, D.J., Konings, W.N., and Lolkema, J.S. (2001). Cysteine-scanning mutagenesis reveals a highly amphipathic, pore-lining membrane-spanning helix in the glutamate transporter GltT. J Biol Chem *276*, 10775-10781.

Slotboom, D.J., Sobczak, I., Konings, W.N., and Lolkema, J.S. (1999). A conserved serine-rich stretch in the glutamate transporter family forms a substrate-sensitive reentrant loop. Proc Natl Acad Sci U S A *96*, 14282-14287.

Smith, S.S., Steinle, E.D., Meyerhoff, M.E., and Dawson, D.C. (1999). Cystic fibrosis transmembrane conductance regulator. Physical basis for lyotropic anion selectivity patterns. J Gen Physiol *114*, 799-818.

Steinhoff, H.J. (2004). Inter- and intra-molecular distances determined by EPR spectroscopy and site-directed spin labeling reveal protein-protein and protein-oligonucleotide interaction. Biol Chem *385*, 913-920.

Storck, T., Schulte, S., Hofmann, K., and Stoffel, W. (1992). Structure, expression, and functional analysis of a Na(+)-dependent glutamate/aspartate transporter from rat brain. Proc Natl Acad Sci U S A *89*, 10955-10959.

Stryer, L., and Haugland, R.P. (1967). Energy transfer: a spectroscopic ruler. Proc Natl Acad Sci U S A *58*, 719-726.

Szatkowski, M., Barbour, B., and Attwell, D. (1990). Non-vesicular release of glutamate from glial cells by reversed electrogenic glutamate uptake. Nature *348*, 443-446.

Takayasu, Y., Iino, M., Kakegawa, W., Maeno, H., Watase, K., Wada, K., Yanagihara, D., Miyazaki, T., Komine, O., Watanabe, M., *et al.* (2005). Differential roles of glial and neuronal glutamate transporters in Purkinje cell synapses. J Neurosci *25*, 8788-8793.

Takayasu, Y., Iino, M., Takatsuru, Y., Tanaka, K., and Ozawa, S. (2009). Functions of glutamate transporters in cerebellar Purkinje cell synapses. Acta Physiol (Oxf) *197*, 1-12.

Takumi, Y., Matsubara, A., Danbolt, N.C., Laake, J.H., Storm-Mathisen, J., Usami, S., Shinkawa, H., and Ottersen, O.P. (1997). Discrete cellular and subcellular localization of glutamine synthetase and the glutamate transporter GLAST in the rat vestibular end organ. Neuroscience *79*, 1137-1144.

Tanaka, J., Ichikawa, R., Watanabe, M., Tanaka, K., and Inoue, Y. (1997a). Extra-junctional localization of glutamate transporter EAAT4 at excitatory Purkinje cell synapses. Neuroreport *8*, 2461-2464.

Tanaka, K., Watase, K., Manabe, T., Yamada, K., Watanabe, M., Takahashi, K., Iwama, H., Nishikawa, T., Ichihara, N., Kikuchi, T., *et al.* (1997b). Epilepsy and exacerbation of brain injury in mice lacking the glutamate transporter GLT-1. Science *276*, 1699-1702.

Tao, Z., Gameiro, A., and Grewer, C. (2008). Thallium ions can replace both sodium and potassium ions in the glutamate transporter excitatory amino acid carrier 1. Biochemistry *47*, 12923-12930.

Tao, Z., and Grewer, C. (2007). Cooperation of the conserved aspartate 439 and bound amino acid substrate is important for high-affinity Na+ binding to the glutamate transporter EAAC1. J Gen Physiol *129*, 331-344.

Tao, Z., Zhang, Z., and Grewer, C. (2006). Neutralization of the aspartic acid residue Asp-367, but not Asp-454, inhibits binding of Na+ to the glutamate-free form and cycling of the glutamate transporter EAAC1. J Biol Chem *281*, 10263-10272.

Teichman, S., Qu, S., and Kanner, B.I. (2009). The equivalent of a thallium binding residue from an archeal homolog controls cation interactions in brain glutamate transporters. Proc Natl Acad Sci U S A *106*, 14297-14302.

Torp, R., Danbolt, N.C., Babaie, E., Bjoras, M., Seeberg, E., Storm-Mathisen, J., and Ottersen, O.P. (1994). Differential expression of two glial glutamate transporters in the rat brain: an in situ hybridization study. Eur J Neurosci *6*, 936-942.

Torp, R., Lekieffre, D., Levy, L.M., Haug, F.M., Danbolt, N.C., Meldrum, B.S., and Ottersen, O.P. (1995). Reduced postischemic expression of a glial glutamate transporter, GLT1, in the rat hippocampus. Exp Brain Res *103*, 51-58.

Trotti, D., Rolfs, A., Danbolt, N.C., Brown, R.H., Jr., and Hediger, M.A. (1999). SOD1 mutants linked to amyotrophic lateral sclerosis selectively inactivate a glial glutamate transporter. Nat Neurosci *2*, 427-433.

Utsunomiya-Tate, N., Endou, H., and Kanai, Y. (1996). Cloning and functional characterization of a system ASC-like Na+-dependent neutral amino acid transporter. J Biol Chem *271*, 14883-14890.

Valiyaveetil, F.I., MacKinnon, R., and Muir, T.W. (2002). Semisynthesis and folding of the potassium channel KcsA. J Am Chem Soc *124*, 9113-9120.

Wadiche, J.I., Amara, S.G., and Kavanaugh, M.P. (1995a). Ion fluxes associated with excitatory amino acid transport. Neuron *15*, 721-728.

Wadiche, J.I., Arriza, J.L., Amara, S.G., and Kavanaugh, M.P. (1995b). Kinetics of a human glutamate transporter. Neuron *14*, 1019-1027.

Wadiche, J.I., and Jahr, C.E. (2001). Multivesicular release at climbing fiber-Purkinje cell synapses. Neuron *32*, 301-313.

Wadiche, J.I., and Kavanaugh, M.P. (1998). Macroscopic and microscopic properties of a cloned glutamate transporter/chloride channel. J Neurosci *18*, 7650-7661.

Watase, K., Hashimoto, K., Kano, M., Yamada, K., Watanabe, M., Inoue, Y., Okuyama, S., Sakagawa, T., Ogawa, S., Kawashima, N., *et al.* (1998). Motor discoordination and increased susceptibility to cerebellar injury in GLAST mutant mice. Eur J Neurosci *10*, 976-988.

Watzke, N., Bamberg, E., and Grewer, C. (2001). Early intermediates in the transport cycle of the neuronal excitatory amino acid carrier EAAC1. J Gen Physiol *117*, 547-562.

Watzke, N., Rauen, T., Bamberg, E., and Grewer, C. (2000). On the mechanism of proton transport by the neuronal excitatory amino acid carrier 1. J Gen Physiol *116*, 609-622.

Wersinger, E., Schwab, Y., Sahel, J.A., Rendon, A., Pow, D.V., Picaud, S., and Roux, M.J. (2006). The glutamate transporter EAAT5 works as a presynaptic receptor in mouse rod bipolar cells. J Physiol *577*, 221-234.

Xu, M., and Akabas, M.H. (1996). Identification of channel-lining residues in the M2 membrane-spanning segment of the GABA(A) receptor alpha1 subunit. J Gen Physiol *107*, 195-205.

Yamada, K., Watanabe, M., Shibata, T., Tanaka, K., Wada, K., and Inoue, Y. (1996). EAAT4 is a post-synaptic glutamate transporter at Purkinje cell synapses. Neuroreport *7*, 2013-2017.

Yang, W., and Kilberg, M.S. (2002). Biosynthesis, intracellular targeting, and degradation of the EAAC1 glutamate/aspartate transporter in C6 glioma cells. J Biol Chem *277*, 38350-38357.

Yernool, D., Boudker, O., Jin, Y., and Gouaux, E. (2004). Structure of a glutamate transporter homologue from Pyrococcus horikoshii. Nature *431*, 811-818.

Zarbiv, R., Grunewald, M., Kavanaugh, M.P., and Kanner, B.I. (1998). Cysteine scanning of the surroundings of an alkali-ion binding site of the glutamate transporter GLT-1 reveals a conformationally sensitive residue. J Biol Chem *273*, 14231-14237.

Zerangue, N., and Kavanaugh, M.P. (1996). Flux coupling in a neuronal glutamate transporter. Nature *383*, 634-637.

Zhang, Y., Bendahan, A., Zarbiv, R., Kavanaugh, M.P., and Kanner, B.I. (1998). Molecular determinant of ion selectivity of a (Na+ + K+)-coupled rat brain glutamate transporter. Proc Natl Acad Sci U S A *95*, 751-755.

Zhang, Y., and Kanner, B.I. (1999). Two serine residues of the glutamate transporter GLT-1 are crucial for coupling the fluxes of sodium and the neurotransmitter. Proc Natl Acad Sci U S A *96*, 1710-1715.